12-14-2017

Ion Channel SUMOylation: a Novel Role for SUMO in Homeostatic Regulation of Multiple Ionic Conductances

Anna Parker

ION CHANNEL SUMOYLATION: A NOVEL ROLE FOR SUMO IN HOMEOSTATIC REGULATION OF MULTIPLE IONIC CONDUCTANCES

by

ANNA R. PARKER

Under the Direction of Deborah J. Baro, PhD

ABSTRACT

Neurons can adjust their ionic currents to maintain a stable output. The homeostatic mechanisms that produce compensatory changes in ionic currents operate over multiple time scales. The rapid mechanisms that act over minutes are mostly unknown. We have been characterizing a fast homeostatic mechanism that stabilizes activity phase in the rhythmically active lateral pyloric neuron (LP) of the crustacean stomatogastric ganglion. LP activity phase is invariant. It is determined, in part, by the balance between the hyperpolarization-activated current (I_h) and the transient potassium current (I_A). When LP I_A is experimentally decreased, activity phase is initially disrupted, but then it recovers over minutes. This is because the decrease in I_A modifies LP activity, which in turn alters cytosolic Ca^{2+} levels. Ca-dependent

enzymes then mediate a reduction in LP I_h to restore the balance between the two conductances. We have been studying the molecular mechanisms that correlate LP I_A and I_h in an activity-dependent fashion. We have found that neuronal activity adjusts the level of ion channel post-translational modification by Small Ubiquitin-like Modifier (SUMO), a peptide which when conjugated to target proteins alters their protein-protein interactions. Using a heterologous expression system, we showed that enhancing SUMOylation of HCN or Kv4 ion channels that mediate I_h and I_A, respectively, produced opposite effects on the amplitudes of I_h and I_A. We also demonstrated that a given change in activity produced the opposite effect on SUMOylation levels associated with each current. Thus, activity-dependent regulation of ion channel SUMOylation specified a positive correlation between the two currents. We have also demonstrated that activity-dependent regulation of ion channel SUMOylation is conditional; it only occurs in the presence of the appropriate modulatory tone. We showed this is because modulators, like dopamine, specify the targets of the SUMOylation machinery. In sum, we have discovered a novel mechanism that acts over minutes to correlate ionic conductances and thereby stabilize neuronal output.

INDEX WORDS: SUMOylation, Dopamine, Activity-Dependent, Ion Channel, HCN, Kv4, Homeostatic Regulation, Stomatogastric

ION CHANNEL SUMOYLATION: A NOVEL ROLE FOR SUMO IN HOMEOSTATIC REGULATION OF MULTIPLE IONIC CONDUCTANCES

by

ANNA R. PARKER

A Dissertation Submitted in Partial Fulfillment of the Requirements for the Degree of

Doctor of Philosophy

in the College of Arts and Sciences

Georgia State University

2017

ION CHANNEL SUMOYLATION: A NOVEL ROLE FOR SUMO IN HOMEOSTATIC REGULATION OF MULTIPLE IONIC CONDUCTANCES

by

ANNA R. PARKER

Committee Chair: Deborah J. Baro

Committee: Chun Jiang

Aaron Roseberry

Astrid Prinz

Electronic Version Approved:

Office of Graduate Studies

College of Arts and Sciences

Georgia State University

Dec 2017

DEDICATION

I would like to dedicate my dissertation to my family. My parents, Calvin and Mendy Huff, have always encouraged me to strive for my dreams (no matter how many years it takes). It is because they nurtured and supported my love of science that I chose to pursue my Ph.D. and a career doing what I love. They have loved me and supported through the many ups and downs that have come with graduate school, and there aren't enough words to express how grateful I am for them. My husband, Christian Parker, whom I met and married while I was in graduate school, has been a daily source of encouragement and inspiration for me. He has been incredibly patient with my late hours, long weekends of work, and occasional bouts of neurotic stress. I can't wait to close this chapter and start the next one with him and the family we plan to start. My two older brothers, Bradley and Kelly Huff, and my sister-in-law, Jana Huff, have always been a significant source of support for me, without their love, encouragement, and shared moments of much-needed laughter during times of stress, I would not have been able to accomplish what I have. My aunt and uncle, Harry and Rachel Kelly, have been wonderfully supportive and have never missed an opportunity to tell me how proud they are of me. Thank you so much.

ACKNOWLEDGEMENTS

First, I would like to thank my Ph.D. advisor, Dr. Deborah Baro. She has not only helped to mold me as a successful researcher but has encouraged to become a more confident woman. Dr. Baro nurtured my scientific curiosity and thanks to her I have learned more about research and hard work than I ever could have asked for and I couldn't be more grateful!

Second, I would like to thank the members of my committee, Dr. Chun Jiang, Dr. Aaron Roseberry, and Dr. Astrid Prinz. They have provided me with much-needed guidance and support as I progressed towards obtaining my Ph.D. I would also like to thank Dr. Vincent Rehder for his advice during my qualifying exams and his continued support following the completion of my exam. Thank you to Dr. David Blaustein and Nancy Russell along with the professors that I worked with as a teaching assistant, Dr. Paul Ulrich, and Dr. Rebekah Chapman, for providing me with a wonderful experience as a teaching assistant. Also, a sincere thank you to all of the professors that have taught and supported me in my graduate career; Dr. Paul Katz, Dr. Sarah Pallas, Dr. Donald Edwards, and Dr. Anne Murphy. Thank you also to the Brains and Behavior Fellowship Program for the support it has been an honor to be a fellow.

Next, I would like to thank all of the students I have worked with over the years in the Baro lab, for their friendship, the help they provided me with my project and the opportunity many provided me to develop my skills as a teacher and mentor. They include but are in no way limited to Meghyn Welch, Lori Forster, Saline Atlas, Leslie-Anne Jansen, Janhavi Dubhashi, Sarah Tasneem, Kristin Jackson, Sasha Guillory, Melissa Issa-Boube, and Ayisha Mcintyre. Also, I would like to express my appreciation for Dr. Wulf-Dieter Christian Krenz, Dr. Edmond Rodgers, and Tim Dever, who worked in the lab when I first started graduate school and played a significant role in helping me to get my bearings and begin my research. Here I would also like

to give special thanks to Meghyn Welch, you have not only helped me immensely in accomplishing what I have with my research, but you have become a real friend.

Finally, I would like to thank the many members of other labs. A special thank you to Liana Artinian from the Rehder Lab and Dr. Ningren Cui of the Jiang Lab for their help in establishing our patch clamping rig. Thank you to the members of the Roseberry lab, Anna Dunigan, and Katherine Stuhrman, for the help and advice you provided. Thank you to the Jiang lab, Dr. Weiwei Zhong, Dr. Max Oginsky, Dr. Shuang Zhang and Christopher Johnson, for letting us the technical help you gave and the use your equipment when we were in need.

TABLE OF CONTENTS

LIST OF TABLES

LIST OF FIGURES

LIST OF ABBREVIATIONS

ADHD	Attention Deficit Hyperactivity Disorder
cAMP	Cyclic adenosine monophosphate
CNBD	Cyclic Nucleotide Binding Domain
CRMP	Collapsin Response Mediator Proteins
DA	Dopamine
HCN	Hyperpolarization-Activated Cyclic Nucleotide-Gated Channel
Hek Cells	Human Embryonic Kidney Cells
I_A	Transient Potassium Current
I_h	Hyperpolarization-Activated Current
LP	Lateral Pyloric Neuron
LTD	Long-Term Depression
LTP	Long-Term Potentiation
NMDA	*N*-methyl-D-aspartate
PIR	Post-Inhibitory Rebound
PKA	Protein Kinase A
SENP	Sentrin Specific Protease
SIM	SUMO-Interaction Motif
STDP	Spike Timing-Dependent Plasticity
STG	Stomatogastric Ganglion
STNS	Stomatogastric Nervous System
SUMO	Small Ubiquitin like Modifier

1 INTRODUCTION

Rhythmically active networks drive such functions as walking, swallowing, breathing, and swimming. These types of networks require that the precise timing of component neuron firing remain stable while still being flexible enough to respond to external stimuli. Thus, a mechanism is needed to stabilize neuronal excitability and maintain activity within a specific range. In the rhythmically active pyloric network of the spiny lobster, the timing of network neuron firing (phase) is maintained within a narrow range across individual animals (Bucher, Prinz et al. 2005, Goaillard, Taylor et al. 2009). Maintenance of pyloric neuron phase has been attributed to multiple cellular and synaptic parameters including the correlation of specific ionic conductances (Soofi, Archila et al. 2012, Zhao and Golowasch 2012). Researchers have described a long-term mechanism that acts through transcription and translation to maintain these correlations. However, we have published evidence that alterations in phase can be restored over minutes in the presence of tonic Dopamine (DA) (Krenz, Rodgers et al. 2015), indicating that a fast activity-dependent mechanism also exists to maintain phase. This dissertation will investigate a novel role for Small Ubiquitin-like Modifier (SUMO) in the rapid coregulation of the transient potassium current (I_A) and the hyperpolarization-activated current (I_h). We will also begin to characterize the involvement of tonic DA in the SUMO-mediated activity-dependent regulation of ionic conductances.

1.1 Stomatogastric Nervous System

The crustacean Stomatogastric Ganglion (STG) is a component of the Stomatogastric Nervous System (STNS), a well-characterized central pattern generator that drives the rhythmic contraction of the gut and foregut of the spiny lobster. The STG has long been an ideal model system for studying motor pattern generation and the effects of neuromodulation on a neural

circuit. Modulatory input is sent to the STG via descending inputs through the *stn* (Fig 1.2A; CoG), as well as being present in the hemolymph that is continuously bathing the ganglion (Oginsky, Rodgers et al. 2010, Hedrich, Diehl et al. 2011). Our work will focus on the pyloric circuit of the STG, a 14-neuron recurrent inhibitory circuit that drives the rhythmic contraction of the foregut (Fig 1.2C). The pyloric circuit produces a triphasic rhythm, that can be observed *in vivo* and *in situ*, through the patterned bursting of six different cell types. Each neuron fires in a particular phase relative to the other neurons. The firing pattern is set by the electrically coupled pacemaker kernel, composed of the anterior burster (AB) and the two pyloric dilator (PD) neurons, which simultaneously inhibit follower neurons (LP, PY, IC, and VD) (Fig 1.2C) (Marder and Bucher 2007). Through post-inhibitory rebound (PIR) the follower neurons repolarize and fire a burst of action potentials. The varying rates of PIR together with the synaptic architecture determine the order and timing of each follower neuron's burst. The lateral pyloric (LP) and inferior cardiac (IC) neurons recover first following pacemaker inhibition. Next the pyloric (PY) and ventricular dilator (VD) neurons fire to complete the triphasic cycle (Fig1.2B).

The LP neuron will be the primary focus of our research. LP functions in the circuit to slow increasing cycle frequencies. It sets an upper limit on cycle frequency by inhibiting PD. The timing of LP inhibition is critical because it maintains the narrow range of frequencies the network experiences. Without LP feedback on the pacemaker, frequencies could increase outside of that range and disrupt network activity (Weaver and Hooper 2003). The timing of LP inhibition is determined by its PIR (Johnson, Brown et al. 2011). The ratio of two opposing ionic conductances, I_A and I_h, regulates the rate of PIR (Harris-Warrick, Coniglio et al. 1995). Hyperpolarized potentials remove I_A inactivation, and activate I_h, depolarizing the cell (He, Chen

et al. 2014). Upon depolarization I_A is activated, producing an inward current that slows depolarization (Tierney and Harris-Warrick 1992, Birnbaum, Varga et al. 2004). In part, it is the balance between these two currents, one depolarizing the cell, the other slowing that depolarization, in part regulate the time at which the neuron fires its burst of action potentials.

The distribution, function, and regulation of I_A and I_h have been extensively studied in the STG. In the pyloric network, I_A plays an important role in determining neuron firing phase, cycle frequency, and spike frequency (Tierney and Harris-Warrick 1992, Harris-Warrick, Coniglio et al. 1995). The shal channel that mediates I_A undergoes extensive alternative splicing with the biophysical properties of the different spliceforms showing significant variability (Baro, Levini et al. 1997, Baro, Ayali et al. 2000, Baro, Quinones et al. 2001). Shal channels are primarily localized to the somatic membrane, primary neurites, and the neuropil of STG neurons (Baro, Ayali et al. 2000). I_h plays a critical role in neuronal excitability, rhythmic activity, and synaptic function (Robinson and Siegelbaum 2003, Goeritz, Ouyang et al. 2011, Kase and Imoto 2012). The Hyperpolarization-activated Cyclic Nucleotide-gated (HCN) channel that mediates I_h in the STG is also subject to alternative splicing, and the identified spliceforms show large variability in activation kinetic and voltage dependences (Ouyang, Goeritz et al. 2007). HCN channels primarily localize to the fine neural in the STG, in close proximity to synapses (Goeritz, Ouyang et al. 2011). Researchers have overexpressed shal in identified pyloric neurons and observed a corresponding increase in expression of I_h that prevented any significant changes in network activity (MacLean, Zhang et al. 2003, MacLean, Zhang et al. 2005). Interestingly, when the reciprocal experiment was performed, overexpressing I_h did not lead to a corresponding increase in I_A expression (Zhang, Oliva et al. 2003). However, additional studies have also demonstrated correlated expression of I_A and I_h and have underscored its importance in maintaining stable

network activity (Khorkova and Golowasch 2007, Hudson and Prinz 2010, Temporal, Desai et al. 2012, Zhao and Golowasch 2012, Golowasch 2014).

Phase refers to the timing of network neuron firing relative to the other network components. We study LP-on phase, which refers to the timing of LP firing relative to the pacemaker, and is calculated by dividing the LP-on delay by the cycle period (Fig 1.2B; b÷a) (Rodgers, Fu et al. 2011). Despite there being several-fold variability in conductance levels and synaptic strengths across individuals, phase and the I_A:I_h ratio are both highly conserved, underscoring their importance (Bucher, Prinz et al. 2005, Goaillard, Taylor et al. 2009). Maintaining I_A:I_h requires a regulatory mechanism or homeostat (MacLean, Zhang et al. 2003, MacLean, Zhang et al. 2005), and recent evidence indicates that tonic DA modulation may be part of that mechanism (Rodgers, Fu et al. 2011, Krenz, Hooper et al. 2013, Krenz, Parker et al. 2015).

1.2 Dopamine

DA is a neuromodulator that plays an essential role in many neurological processes such as motor control, reward, and motivation. Dysfunction of the dopaminergic system can result in a variety of conditions including Parkinson's Disease, Schizophrenia, Restless Leg Syndrome, and Attention Deficit Disorder (ADHD)(Schultz 2007). DA is released from dopaminergic neurons through volume transmission in many model systems, including the STNS (Oginsky, Rodgers et al. 2010). As opposed to a classical synapse where receptors are located within the synaptic cleft, directly adjacent to where the neuromodulator is being released, DA releases far away from its receptor and diffuses to reach them or reach distant reuptake mechanisms (Schultz 2007). Tonically active DA neurons produce a constant presence of DA at nanomolar (nM) levels, referred to as tonic DA (Schultz 2007, Owesson-White, Roitman et al. 2012, Nirogi, Komarneni

et al. 2013). Upon stimulation, dopaminergic neurons will release DA in bursts. This produces a transient increase in DA concentration that can reach micromolar (μM) to millimolar (mM) levels near the dopaminergic neuron at the time of release, and is referred to as phasic DA (Justice 1993, Goto, Otani et al. 2007, Rice, Patel et al. 2011). DA receptors can be present in either a high or low-affinity states. Tonic DA will activate high-affinity receptors, while phasic DA will activate low-affinity DA receptors, producing different responses in the target neuron. Tonic DA plays an enabling role and is known to enable motor, cognitive, and motivational processes (Bilder, Volavka et al. 2004, Krenz, Hooper et al. 2013, Krenz, Rodgers et al. 2015). On the other hand, phasic DA modifies these processes and many others (Schultz 2007, Bromberg-Martin, Matsumoto et al. 2010, Lisman, Grace et al. 2011). DA activates either type-1 or type-2 receptors (D1R and D2R respectively). Both receptors couple with G proteins and activation of these receptors have opposing effects. D1R's, acting through G_s increase adenylyl cyclase activity while D2R's acting through $G_{i/o}$ decrease it (Clark and Baro 2006, Clark, Khan et al. 2008). LP exclusively expresses D1Rs, therefore, the work presented here will focus on the canonical D1R pathway.

1.3 Dopamine in the STG

In the STG, phasic and tonic DA can affect many aspects of the network including rhythmic activity, the firing properties of specific neurons, synaptic strengths, and ionic conductances. Bath applying phasic DA to the STG alters the firing properties of each pyloric neuron differently (Harris-Warrick, Johnson et al. 1998). Since these early findings, additional studies have characterized the specific effects of DA on network output, synaptic strengths, and specific ionic conductances. In a study that examined the effects of phasic DA on the cycle frequencies of isolated pyloric neurons and the complete pyloric network, they found that phasic

concentrations of DA slightly decreased the cycle frequency of the pyloric rhythm (Ayali and Harris-Warrick 1999). This overall decrease in cycle frequency closely resembled the DA modulated decrease in the isolated AB-2xPD pacemaker kernel, resulting from the combination of an increase in AB frequency paired with a decrease in the frequencies of both PD neurons. Researchers have also characterized the pre- and postsynaptic effects of DA modulation at many of the pyloric synapses. As was mentioned before the synapse between LP and PD is particularly important because LP directly inhibits the pacemaker and can function to slow the network rhythm. DA modulation enhances LP pre-synaptic transmitter release through an increase in calcium levels at the presynaptic terminals and decreases the PD post-synaptic responsiveness to the transmitter (Johnson, Peck et al. 1995, Cleland and Selverston 1997, Johnson and Harris-Warrick 1997, Johnson, Kloppenburg et al. 2003, Kloppenburg, Zipfel et al. 2007, Johnson, Brown et al. 2011). The net outcome of these opposing effects is an overall enhancement of the inhibitory LP/PD synapse. Common among many pyloric neurons is DA modulation of I_A and I_h, although the directionality of this modulation can differ between neuron types. For instance, phasic concentrations of DA reduce I_A in the AB, PY, and IC neurons (Peck, Nakanishi et al. 2001), while it increases I_A in the PD neuron (Kloppenburg, Levini et al. 1999). Phasic DA significantly shifted the voltage of activation in the depolarized direction without changing G_{max} in LP, AB, PY, and VD neurons, with no effect on PD and IC I_h (Harris-Warrick, Coniglio et al. 1995, Peck, Gaier et al. 2006).

Our work focuses on the mechanisms that regulate LP neuron activity, and bath application of phasic µM DA decreases LP I_A, disrupting the LP I_A:I_h ratio and producing an advance in LP-on phase (Rodgers, Fu et al. 2011). The phase advance is accompanied by an increase in network cycle frequency and a decrease in LP burst duration. With persistent

exposure to phasic μM levels of DA, LP phase recovers while cycle frequency and burst duration remained altered (Rodgers, Fu et al. 2011, Krenz, Hooper et al. 2013). Additional studies have begun to describe both long and short-term mechanisms that regulate I_A and I_h and the role of tonic DA in this regulation.

To date, studies examining the correlation between I_h and I_A have focused long-term mechanisms that coregulate the two conductances through transcription and translation (Schulz, Goaillard et al. 2007, Temporal, Desai et al. 2012). We have demonstrated that tonic DA can regulate both LP I_A and I_h over the long-term through transcription and translation. Tonic DA persistently increases LP I_A G_{max} through a translation-dependent mechanism (Rodgers, Krenz et al. 2011, Rodgers, Krenz et al. 2013). We also showed that when LP-on phase is advanced in a manner that is thought to be mediated by an increase in I_A, phase can recover in the presence of tonic DA over the course of an hour (Rodgers, Fu et al. 2011). When changes in LP I_h were prevented phase recovery was no longer observed in the presence of tonic DA (Rodgers, Fu et al. 2011, Krenz, Hooper et al. 2013). These findings indicate that tonic DA may stabilize network activity through translation-dependent long-term regulation of LP I_A and I_h, likely to maintain the previously described I_A:I_h.

Although a majority of the literature examining the coregulation of ionic conductances describes a long-term mechanism acting over hours, logic would dictate that a short-term mechanism may also exist to restore conductance correlations and maintain stable network activity rapidly. Our recent findings have begun to describe an activity-dependent mechanism that can regulate ionic currents over minutes to restore LP-on phase. Rapid recovery of LP-on phase was demonstrated by pharmacologically decreasing I_A, advancing LP-on phase after only 1min (Krenz, Rodgers et al. 2015). LP-on phase recovered after only 20 mins, in the presence but

not the absence of tonic DA. Additional experiments that prevented changes in LP I_h with Cs showed that phase was no longer recovered in the presence of tonic (Krenz, Hooper et al. 2013, Krenz, Rodgers et al. 2015). We found that in fact tonic DA LP I_h G_{max} to be bidirectionally regulated by changes in duty cycle.

In the presence but not the absence of tonic DA (5nM), bidirectional changes in LP duty cycle (LP burst duration ÷ cycle period) produce corresponding bidirectional changes in LP I_h G_{max} (Krenz, Rodgers et al. 2015). In these experiments, the STG was superfused with saline containing or lacking (control) 5nM DA and slow wave and spike activity were blocked with TTX. LP activity, measured before TTX application, was used to construct a voltage step protocol to mimic the slow wave oscillations of LP. This voltage step protocol was then used to increase or decrease LP duty cycle and I_h was measured before and 10min after applying the voltage protocol. When the change in LP I_h G_{max} (I_h G_{max} after voltage protocol ÷ LP I_h G_{max} before voltage protocol) was plotted against the change in LP duty cycle, we observed that LP I_h G_{max} changed bidirectionally with changes in duty cycle (Krenz, Rodgers et al. 2015). Note that activity-dependent changes in LP I_h were only observed in the presence of tonic DA and that in the absence of DA there is no change in LP I_h G_{max} regardless of activity.

These experiments were followed by experiments that would begin to uncover the mechanism mediating LP I_h G_{max} activity-dependent regulation (Krenz, Rodgers et al. 2015). We found that tonic DA acting through D1Rs activates PKA which has two simultaneous effects; 1- PKA produces an activity-<u>independent</u> increase in LP I_h G_{max}, 2 – PKA permits calcineurin to decrease LP I_h G_{max} in an activity-<u>dependent</u> manner (Krenz, Rodgers et al. 2015). The specific mechanisms that mediate these processes remain uncharacterized. The work presented here will

examine SUMO mediated activity-dependent coregulation of LP I_h and I_A and the role of tonic DA in selecting the ionic conductance target of SUMOylation.

1.4 SUMOylation mediates activity-dependent regulation of ion channels

SUMO is a small peptide that is post-translationally added to target proteins, altering the properties of the modified protein in diverse ways. SUMOylation was first described over 20 years ago for its role in regulating the cell cycle and was thought to be restricted to the nucleus (Matunis, Coutavas et al. 1996, Mahajan, Delphin et al. 1997). Since then SUMO substrates have been identified throughout the cell and have been shown to regulate a wide variety of processes including DNA repair, transcription, protein trafficking, cell migration (Hay 2005). Recent studies have implicated SUMOylation in the regulation of neuronal proteins with functional consequences that include the regulation of synaptic plasticity, and altering the biophysical properties and trafficking of ion channels (Flotho and Melchior 2013).

There are four SUMO homologs in mammals (SUMO1-4). SUMO2 and 3 share ~97% homology and are often referred to as SUMO2/3 because they are not readily distinguishable by commercially available antibodies. Despite SUMO1 sharing only ~50% sequence identity with SUMO2/3 there is significant overlap in target proteins between SUMO1-3. The distribution and function of SUMO4 remains widely uncharacterized (Henley, Craig et al. 2014). SUMO is reversibly conjugated to the lysine residue of a target protein through an enzymatic cascade that closely resembles that of ubiquitin. Precursor SUMO requires proteolytic processing by a member of the sentrin protease (SENP) family to exposed the C-terminal diglycine motif before SUMO can be conjugated to a target protein. Mature SUMO is then activated through the formation of a thioester bond with the E1 SUMO-activating enzyme (SAE1/SAE2) (Fig 1.1). SUMO is then transferred to the single E2 SUMO-conjugating enzyme (Ubc9), which catalyzes

the formation of an isopeptide bond between the C-terminal diglycine of SUMO and the lysine of a target protein (Fig1.1). In some cases, SUMO conjugation by Ubc9 is facilitated by the presence of an E3 SUMO-ligase (Flotho and Melchior 2013). In most, but not all cases, SUMOylation occurs at a SUMO consensus sequence, ΨKXE (Ψ is a large hydrophobic residue and X can be any residue), that can be recognized by Ubc9. Conjugated SUMO can be cleaved from a target protein by SENP (Fig 1.1). Members of the SENP family of proteases differ in their affinity for different SUMO homologs as well as their ability to perform both hydrolase (maturing of precursor SUMO) and isopeptidase (deSUMOylation) functions (Mukhopadhyay and Dasso 2007, Nayak and Muller 2014).

Once conjugated to a target protein, SUMO acts like a docking station, promoting interaction between the SUMOylated protein and other proteins that contain a SUMO Interacting Motif (SIM) domain (Hay 2013). By promoting protein-protein interactions, SUMO can coordinately regulate functionally related proteins. In neurons, SUMO is emerging as an important regulator of activity and modulator-dependent processes (Lu, Liu et al. 2009, Loriol, Khayachi et al. 2013, Loriol, Casse et al. 2014). Numerous reports have described SUMOylation as being necessary for the regulation of different ion channels, including Na^+ channels (Dustrude, Wilson et al. 2013, Dustrude, Moutal et al. 2016, Plant, Marks et al. 2016), K^+ channels (Benson, Li et al. 2007, Dai, Kolic et al. 2009, Plant, Dowdell et al. 2011, Qi, Wang et al. 2014), and multiple glutamate receptors subunits (O'Brien, Kamboj et al. 1998, Konopacki, Jaafari et al. 2011, Chamberlain, Gonzalez-Gonzalez et al. 2012, Jaafari, Konopacki et al. 2013, Choi, Park et al. 2016). SUMO regulation can alter the biophysical properties or trafficking of ion channels. SUMO-mediated regulation of these channels plays an important role in neuronal excitability (Dustrude, Wilson et al. 2013, Qi, Wang et al. 2014, Dustrude, Moutal et al. 2016),

neuronal homeostasis (Craig, Jaafari et al. 2012), LTP (Jaafari, Konopacki et al. 2013, Nair, Patil et al. 2017), and LTD (Chamberlain, Gonzalez-Gonzalez et al. 2012, Luo, Ashikaga et al. 2013). SUMO has also been implicated in several neuronal disease states including seizures (Qi, Wang et al. 2014), Parkinson's Disease (Eckermann 2013, Guerra de Souza, Prediger et al. 2016), Alzheimer's Disease (Lee, Dale et al. 2014, Hoppe, Salbego et al. 2015), Huntington's Disease (Ochaba, Monteys et al. 2016), and Down Syndrome (Schorova and Martin 2016). Ion channels can be regulated by SUMO through either direct modification of the channel or indirect modification of an interacting protein. For example, direct modification of the Nav1.2 channel results in a shift of voltage-dependence of activation to a more negative voltage (Plant, Marks et al. 2016). On the other hand, indirect SUMOylation of CRMP2 promotes CRMP2 interaction with NaV1.7 leading to an increase in channel externalization (Dustrude, Wilson et al. 2013, Dustrude, Moutal et al. 2016).

1.5 Hypothesis

The work presented here will seek to address the question, "what are the mechanisms that mediate fast activity-dependent regulation of correlated ionic conductances?" We hypothesize that SUMOylation mediates fast activity-dependent regulation of correlated ionic conductances. We test this hypothesis by first characterizing SUMO regulation of the HCN channel, that mediates I_h, using a heterologous expression system. Next, we will then look to see if SUMO mediates activity-dependent regulation of LP I_h G_{max} in a similar manner to what was observed in the heterologous expression system. Finally, we will characterize activity-dependent regulation of LP I_A and the role of SUMO in mediating activity-dependence.

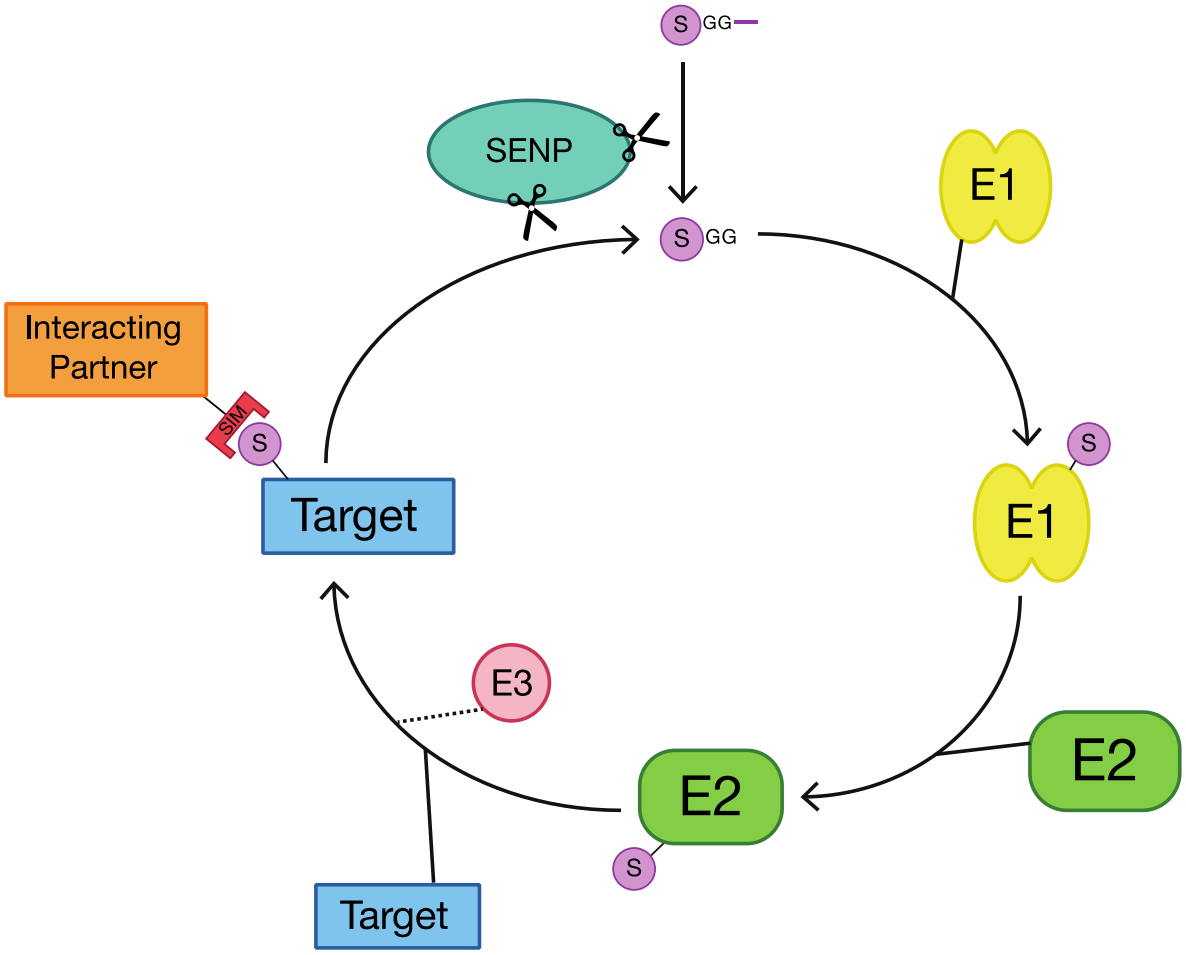

Figure 1.1 SUMOylation

The SUMO precursor protein is cleaved by SENP to expose its C-terminal diglycine motif (top). The mature SUMO is then conjugated to the SUMO activating enzyme (E1; SAE1/SAE2) through the formation of a thioester bond. SUMO is then passed to the SUMO conjugating enzyme (E2; Ubc9) which can then conjugate SUMO to a target protein through a process that may be facilitated by the presence of a SUMO ligase (E3). Once conjugated to a target protein SUMO acts as a docking site for proteins that possess a SIM domain, thus promoting protein-protein interactions. SUMO can be deconjugated from a target protein by SENP

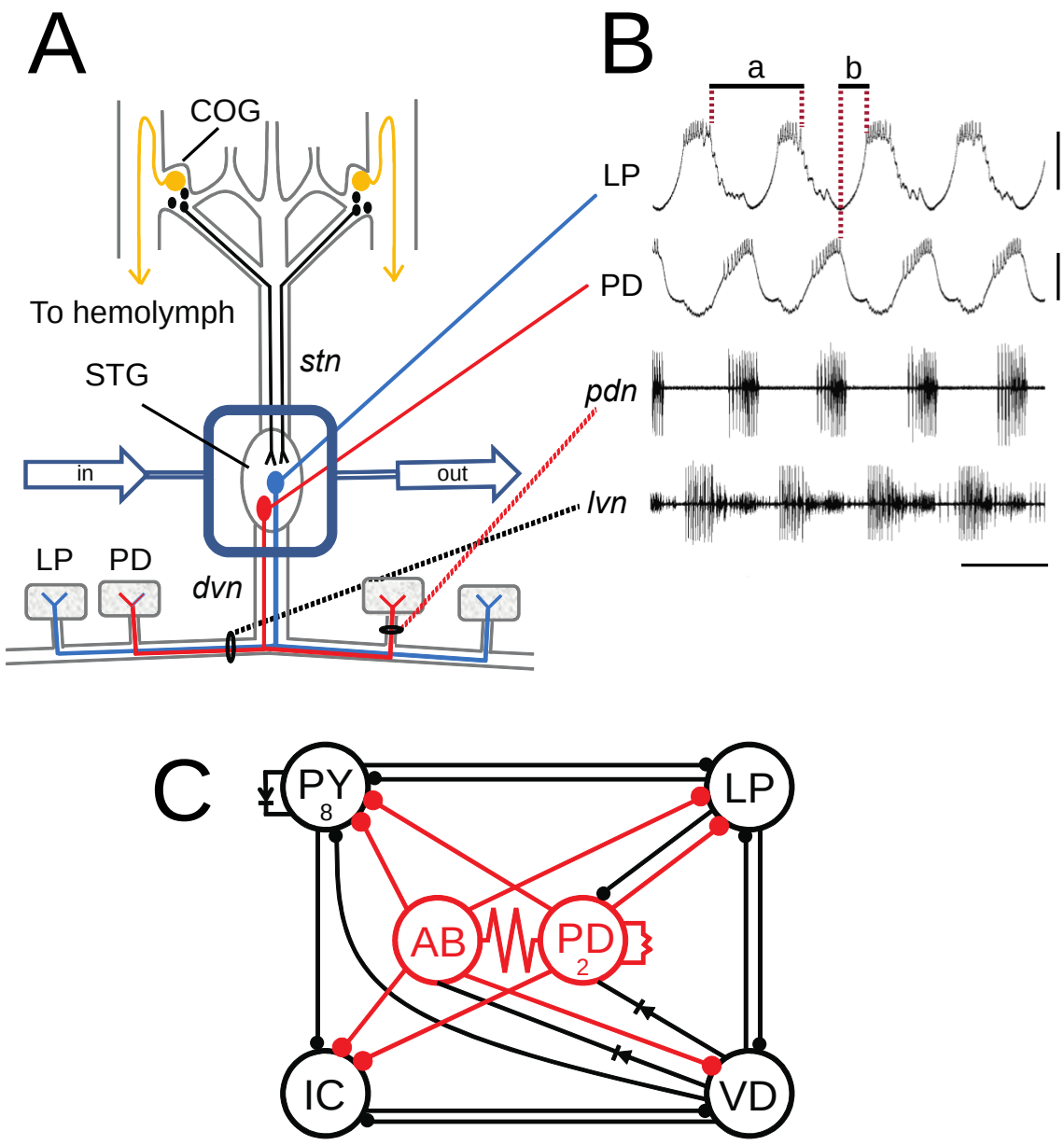

Figure 1.2 The Pyloric Network

(A) The STNS is dissected and pinned into a dish. A Vaseline well is used to enclose the STG (blue box). Saline is continuously superfused through the well (blue arrows). The commissural ganglia (CoGs) contain DA neurons that project through the *stn* to the STG. Two of the 14 STG neurons are depicted here, PD (red) and LP (blue). PD and LP axons project through the *dvn* and *lvn* to reach their target muscles. **(B)** Extracellular recordings were taken from the *lvn* and *pdn* using pin electrodes. Intracellular recordings were also taken from LP and PD using micropipettes. LP on-phase is defined as LP on-delay (b) divided by cycle period (a). **(C)** The pyloric network: the 6 types of pyloric neurons (open circles) and their connectivity are

diagrammed. Closed circles represent inhibitory synapses. Red connections show inhibition from the pacemaker kernel, and resistor/diode connection between AB and PD depicts electrical coupling

2 DETAILED MATERIALS AND METHODS

2.1 Hek cells

2.1.1 Tissue Culture

Cells were maintained in EMEM media (Corning; cat#10-009-CV) supplemented with 10% Fetal Bovine Serum (Sigma Aldrich; cat#F6178) and 1% Penecillin Streptomycin (Sigma Aldrich; cat#P4333) at 37℃ and 5%CO_2. For plates that needed to be split and passaged, media was aspirated and 1-2ml (for 100mm plates) of Trypsin-EDTA 0.25% (Gibco; cat#25200-056) was added to the plate and incubated for 2-3min, monitoring for cell detachment from the plate. Using a Pasteur pipette, any cells still attached to the plate were gently washed into one corner of the dish and the trypsin/cells suspension was transferred to of 15ml tube containing 5ml of complete media. Cells were gently pelleted at 2,000rpm for 2-3min. The liquid was aspirated from the cell pellet, the cells were gently resuspended in 1ml of complete media, an appropriate number of cells were dropped on a plate containing fresh media and gently swirled to distribute the cells evenly. Plates were returned to the 37℃ and 5%CO_2 incubator. If a specific number of cells needed to be plated a hemocytometer was used to determine a cell count. Briefly, suspended cells were diluted in 500µl of complete media (1:25), 100µl of Trypan blue was added, gently mixed and incubated for 5min at room temperature. Cells were then pipetted into the hemocytometer and counted according to the instructions included with the hemocytometer.

2.1.2 Cryopreservation

For long-term storage of Hek cells, a confluent 100mm plate was trypsinized, cells were pelleted and resuspended in 1ml of complete media. Hek cell suspension was transferred to a

cryotube (Thermo Fisher; cat#368632) containing 75ul (7.5%) DMSO, inverted to mix and quickly placed in a styrofoam box inside of a -80℃ freezer. Once frozen, usually 24hr later, the cryotube was transferred to a dewar filled with liquid nitrogen.

2.2 Calcium Phosphate Transfection

Approximately 24hr before transfection, enough cells were seeded onto a 60mm culture dish to obtain ~60% confluence the next day (~$1.9x10^6$ cells). The next day, the media was changed 1hr before transfecting. For a 60mm plate, 25µg total of plasmid DNA (divided equally for co-transfections) was combined with TE Buffer (10mM Tris-HCl, 1mM EDTA) to obtain a total volume of 440µl. Next, 60µl of 2M $CaCl_2$ was added drop wise to the DNA mixture, while gently flicking the tube. Next, 500µl of 2xHBS (275mM NaCl, 10mM KCl, 12mM dextrose, 1.4mM Na_2HPO_4, 40mM HEPES, pH 7.05-7.10, sterile filtered) that had been slowly thawed at room temperature was added dropwise while mixing. DNA mixture was immediately added to the cells by carefully dropping it evenly over the plate and gently rocking the plate to distribute the DNA. Plates were returned to the incubator for 4hr, and then the media was changed. The transfection efficiency was checked 48hr later, and only plates with >80% efficiencies were used for western blotting experiments.

2.3 GFP Immunoprecipitation

2.3.1 Hek Cell Lysates

To obtain a lysate, media was aspirated from a 100mm plate, and the plate was gently washed twice with cold PBS (137mM NaCl, 2.7mM KCl, 10mM Na_2HPO_4, 1.8mM KH_2PO_4, pH 7.4). Cells were lysed by adding 1ml of RIPA Buffer (50mM Tris-HCl pH7.4, 150mM NaCl, 0.1% SDS, 0.5% Deoxycholate, 1% NP-40, 20mM EDTA, 20mM *N*-Ethylmaleimide, 1:100 protease inhibitor cocktail) to the plate and incubating for 30min on ice, rocking the plate

occasionally. A cell scraper was used to scrape the contents of the plate into one corner where it could be collected and transferred to a microcentrifuge tube. Cell debris was pelleted at 14,000rpm at 4℃ for 10min, and the supernatant (cell lysate) was transferred to a clean microcentrifuge tube. Protein concentration was determined by BCA Assay. Briefly, 25µl of lysate (diluted 1:1, 1:5, and 1:10) and Bovine Serum Albumin standards (0, 125, 250, 500, 750, 1000, 1500, and 2000µg/ml) were added to the wells of a 96 well plate, noting of the order of the samples, 200µl of Reagent A:B (50:1) was added to each well, the plate was covered with plastic wrap and incubated at 37℃ for 30min. The absorbance was measured at 562nm on a plate reader and used with the standard concentrations to construct an xy-plot that was fit with a linear trendline. The equation for the trendline was then used to calculate the concentration of the lysate samples.

2.3.2 Co-Immunoprecipitation

Co-immunoprecipitation experiments of Hek cell lysates were performed using the Pierce Classic Magnetic IP & Co-IP Kit (Thermo Scientific cat# 88804). For GFP Co-IPs, 1mg of protein was combined with 2µl of an anti-GFP antibody (Abcam, cat# ab290) in a microcentrifuge tube with Pierce IP Lysis/Wash Buffer to a total volume of 500µl. Antibody/antigen complex was incubated together overnight at 4℃ with agitation. Magnetic beads were prepared by combining 25µl of the beads with 175µl of Pierce IP Lysis/Wash Buffer, collecting the beads on a magnetic stand, removing the supernatant, and repeating the wash with an additional 500µl of Pierce IP Lysis/Wash Buffer. The antigen/antibody complex was then added to the washed beads and incubated for 1hr at room temperature with agitation. The beads were then collected and washed twice with Pierce IP Lysis/Wash Buffer. To elute the immunoprecipitated product, 100µl of Elution Buffer was incubated with the beads for 10min at

room temperature, the beads were then collected, and the eluate was retained and neutralized with 10µl of Neutralization Buffer.

2.4 Biotinylation

Hek cells on 60mm plates were washed twice with 1ml of cold PBS-CM (PBS - 137mM NaCl, 2.7mM KCl, 10mM Na_2HPO_4, 1.8mM KH_2PO_4, pH 7.4 supplemented with 0.2mM $CaCl_2$ and 1.5mM $MgCl_2$). Biotin was added to the plate (2ml of 1mg/ml in PBS-CM; Thermo Fisher; cat#21331) and incubated for 30min at 4℃. Cells were washed twice with ice cold PBS-CM, and then 2ml of Quench Buffer (PBS-CM, 1.5mM $MgCl_2$, 0.2mM $CaCl_2$, 100mM Glycine) was added to the plate and incubated for 15min at 4℃. Next, the cells were lysed in 500µl RIPA Buffer (1% NP40, 50mM Tris pH 7.4, 150mM NaCl, 0.1% SDS, 0.5% DOC, 2mM EDTA, protease inhibitor cocktail at 1:100) for 30min on ice, occasionally rocking the plate. Contents of the plate were scraped into one corner using a cell scraper (Thermo Fisher; cat#08100241), the lysate was transferred to 1.5ml microcentrifuge tube, and the cell debris was pelleted by centrifuging for 10min at 14,000rpm at 4℃. NeutrAvidin beads (Thermo Fisher; cat#29201) were prepared by adding 100µl of NeutrAvidin slurry to a spin column (Thermo Fisher; cat#69725) and washing three times with 500µl of PBS, centrifuging for 1min at 500xg between each wash. The bottom of the spin column was capped, and the cleared lysate was then incubated with the beads for 2hr at 4℃ with agitation. Columns were uncapped and centrifuged for 2min at 1000xg; flow-through was retained as "intracellular fraction". Beads were washed 3 times with 500µl of Wash Buffer 1 (PBS supplemented with 1% NP40, and 0.1% SDS), 3 times with 500µl of Wash Buffer 2 (PBS supplemented with 0.1% NP40 and 0.5M NaCl), and then the tube was capped and 50µl of SDS Buffer (50mM Tris-HCl pH 6.8, 100mM DTT, 2% SDS, 0.1% Bromophenol blue, 10% glycerol) was added and incubated for 1hr at room temperature to elute

extracellular protein. Eluted protein (extracellular fraction) was centrifuged from the column into a clean tube at 1000xg for 2min.

Intracellular and Extracellular fractions were run together on a western blot, and the blot was cut just above the 50kDa ladder marker. The portion of the blot containing proteins >50kDa was dually probed with anti-GFP (Santa Cruz Biotechnology; cat#sc-8334; rabbit polyclonal; 1:2000) and anti-Na/K Pump (Abcam; cat#ab7671; mouse monoclonal; 1:3000) antibodies; with expected bands corresponding to GFP-HCN2 being ~150-250kDa and Na/K Pump being ~100kDa. The portion of the blot containing proteins <50kDa was probed with an anti-Actin antibody (Santa-Cruz Biotechnology; cat#sc-1616-R; rabbit polyclonal; 1:2000) to confirm no intracellular contamination was present in extracellular samples.

2.5 Whole Cell Patch Clamping of Hek Cells

Poly-L-Lysine coated cover slips were prepared as follows: 20mm round glass coverslips (Fisher Scientific; cat#12-546-2) were sterilized with ethanol and placed in the wells of 8 well dishes (Thermo Fisher; cat#267062) to air-dry; enough 50µg/ml Poly-L-Lysine (Sigma Aldrich; cat#P1524; prepared at 1mg/ml and sterile filtered) was added to each well to cover the coverslips; coverslips were incubated with Poly-L-Lysine for 1hr at 37℃; Poly-L-Lysine was aspirated; coverslips were washed once with dH_2O; allowed to air-dry and stored at 4℃. For whole-cell patch clamping, ~$7x10^4$ cells were seeded onto each coverslip 24-48hr before recording. Coverslips containing cells were perfused with extracellular saline (138mM NaCl, 5.6mM KCl, 2.6mM $CaCl_2$, 1.2mM $MgCl_2$, 10mM HEPES, 10mM Glucose, pH 7.4). Fire polished patch pipettes (Sutter Instruments; cat#B120-69-15; 5-8MΩ) were filled with intracellular saline (10mM NaCl, 145mM KCl, 1mM $MgCl_2$, 5mM HEPES, pH 7.2) and connected to the amplifier. To obtain a whole cell patch, a gentle negative pressure was used to

form a ≥1GΩ seal between the cell membrane and the opening of the micropipette. Suction was used to rupture the cell membrane and recordings were taken from cells that maintained a seal ≥700 MΩ following rupture. PClamp software implemented voltage protocols that were used to elicit the current being studied.

2.6 Tat-SUMO Peptide

2.6.1 Tat-SUMO Construct

Activated Panulirus interruptus SUMO (ending in diglycine) cDNA was obtained by PCR using specific primers that included EcoRI restriction sites on the 5' and 3' ends. Briefly, lobster cDNA was amplified using SUMO Forward (5'-TTTTGAATTCGATGTCCGAGGAAG CCAAGAA-3') and SUMO Reverse Primers (5'-GGGGGAATTCTCACCCACCAGTTTGCTG CTGGAACAC-3') with the following cycling parameters: 1cycle – 95℃ for 1min; 35℃ cycles – 95℃ for 30sec, 61℃ for 1min, 68℃ for 1min; 1 cycle – 68℃ for 5min. The ~275bp PCR product was gel isolated, and both the SUMO cDNA and pcDNA3 Tat HA vector (a gift from Matija Peterlin (Cujec, Okamoto et al. 1997); Addgene plasmid #14654) were cut with EcoRI (1ug of DNA to 1U of enzyme). The exposed ends of the cut Tat-HA vector were dephosphorylated using Calf Intestine Phosphatase (CIP), then the SUMO cDNA and Tat-HA vector were ligated at a 1:1, insert to vector ratio. The ligation product was transformed into competent cells, and the presence of colonies containing Tat-SUMO was identified by PCR using Tat vector-specific primers (For: 5'-GGGGGAATTCTCACCCACCAGTTTGCTGCTGG AACAC-3'). DNA from colonies containing Tat-SUMO were sequenced to confirm proper orientation of the insert.

2.6.2 Tat-SUMO Peptide Synthesis

To synthesize the Tat-SUMO peptide, the plasmid was transformed into BL21-CodonPlus (DE3)-RIPL E. coli (Agilent; cat#230280) and plated on NYZ agar plates. A single isolated colony was grown overnight in 200ml of NYZ broth containing ampicillin (100µg/ml) at 37°C with agitation. The 200ml overnight culture was then added to 1L of broth containing 500µM IPTG to induce expression of the peptide, and further incubated for 5hr. Cells were divided among 250ml autoclaved bottles and pelleted at 8,000rmp for 10min at 4°C, and the pellet was washed with cold PBS (137mM NaCl, 2.7mM KCl, 10mM Na_2HPO_4, 1.8mM KH_2PO_4, pH7.4). Pelleted cells were resuspended in 20ml of Buffer Z (8M Urea, 100mM NaCl, 20mM HEPES, pH8), transferred to autoclaved 50ml centrifuge tubes and sonicated on ice using a 10sec "on" 30sec "off" protocol at 15% amplitude for a total of 10min. Sonicate was cleared by centrifuging at 12,000rpm for 10mins at 4°C. The supernatant was transferred to a clean tube and the cleared sonicate was equilibrated with 10mM imidazole. Next, 10ml of Ni-NTA agarose resin (Qiagen; cat#1018244) was equilibrated with Buffer Z containing 10mM imidazole and then incubated with the sonicate at 4°C for 1hr. The resin mixture was added to a chromatography column (Bio-Rad; cat#7372512) and washed with 100ml of Buffer Z with 10mM imidazole. The peptide was eluted with incrementally increasing concentrations of imidazole (100, 250, 500mM, and 1M; 10ml each) and the buffer was exchanged for PBS with 10% glycerol using PD-10 desalting columns (GE Healthcare; cat#17085101). Peptide concentration was determined by BCA assay (as described in 2.5.1).

3 CHAPTER 1: SUMOYLATION OF THE HYPERPOLARIZATION-ACTIVATED CYCLIC NUCLEOTIDE-GATED CHANNEL 2 INCREASES SURFACE EXPRESSION AND THE MAXIMAL CONDUCTANCE OF THE HYPERPOLARIZATION-ACTIVATED CURRENT

Publication: **Parker, A. R.**, M. A. Welch, L. A. Forster, S. M. Tasneem, J. A. Dubhashi and D. J. Baro (2016). "SUMOylation of the Hyperpolarization-Activated Cyclic Nucleotide-Gated Channel 2 Increases Surface Expression and the Maximal Conductance of the Hyperpolarization-Activated Current." Front Mol Neurosci **9**: 168.

Contribution Disclosure: Authors A. Parker and D. Baro were responsible for the conception and design of the research presented here. Authors A. Parker, M. Welch, L. Forster, S. Tasneem, J. Dubhashi, and D. Baro provided substantial contribution to the acquisition and analysis of the data presented here. All authors also provided input during the drafting and revision of the manuscript.

3.1 Abstract

SUMO is a ~10kDa peptide that can be post-translationally added to a lysine (K) on a target protein to facilitate protein-protein interactions. Recent studies have found that SUMOylation can be regulated in an activity-dependent manner and that ion channel SUMOylation can alter the biophysical properties and surface expression of the channel. HCN channel surface expression can be regulated in an activity-dependent manner through unknown processes. We hypothesized that SUMOylation might influence the surface expression of HCN2 channels. In this manuscript, we show that HCN2 channels are SUMOylated in the mouse brain. Baseline levels of SUMOylation were also observed for a GFP-tagged HCN2 channel stably expressed in Hek cells. Elevating GFP-HCN2 channel SUMOylation above baseline in Hek cells led to an increase in surface expression that augmented I_h, mediated by these channels. Increased SUMOylation did not alter I_h voltage-dependence or kinetics of activation. There are five predicted intracellular SUMOylation sites on HCN2. Site-directed mutagenesis indicated that more than one K on the GFP-HCN2 channel was SUMOylated. Enhancing SUMOylation at one of the five predicted sites, K669, led to the increase in surface expression and I_h G_{max}. The role of SUMOylation at additional sites is currently unknown. The SUMOylation site at K669 is also conserved in HCN1 channels. Aberrant SUMOylation has been linked to neurological diseases that also display alterations in HCN1 and HCN2 channel expression, such as seizures and Parkinson's Disease. This work is the first report that HCN channels can be SUMOylated and that this can regulate surface expression and I_h.

3.2 Introduction

Post-translational modifications can rapidly regulate proteins. SUMOylation is one such modification that is essential for most organisms (Flotho and Melchior 2013). SUMO (a.k.a. Sentrin) is a ~100 amino acid peptide that is covalently added to a lysine (K) residue on a target protein. The addition involves several steps. First, the immature SUMO protein is cleaved by a SENP, exposing a C-terminal diglycine (Mukhopadhyay and Dasso 2007). The SUMO E1 activating enzyme then transfers the mature SUMO peptide to the E2 conjugating enzyme, Ubc9, which will then add SUMO to the target protein (Desterro, Thomson et al. 1997). SUMO can also be deconjugated from a target protein by SENP (Hickey, Wilson et al. 2012). In mammals, SUMO is encoded by a family of four genes, termed SUMO1-4 (Flotho and Melchior 2013). SUMO2 and SUMO3 proteins are ~97% identical and are not readily distinguishable in most experiments. SUMO 1 and SUMO2/3 proteins share ~46% identity, and their sets of targets greatly overlap. SUMO4 cannot be cleaved into the mature form by Ubc9, and its function is unclear.

Modification by SUMO is subject to numerous forms of regulation. The availability of the SUMOylation site on a target protein can be regulated by the presence of other post-translational modifications. For example, phosphorylation near the SUMOylation site can either inhibit or enhance SUMOylation (Bossis and Melchior 2006, Konopacki, Jaafari et al. 2011). SUMOylation can also be regulated by the availability of SUMO and/or SUMOylation enzymes (Loriol, Khayachi et al. 2013).

SUMOylation mediates protein-protein interactions (Makhnevych, Sydorskyy et al. 2009, Flotho and Melchior 2013). As such, SUMO can coordinately regulate many diverse cellular processes ranging from DNA repair in the nucleus to signal transduction at the plasma

membrane (Hickey, Wilson et al. 2012). The effects of SUMO are observed throughout the neuron (Henley, Craig et al. 2014). SUMOylation can influence neuronal transcription by controlling the stability of transcription factors; for example, BMAL1 ubiquitination and degradation is enhanced when it is SUMOylated (Lee, Lee et al. 2008). SUMO can also regulate synaptic release. SUMOylation of the synaptic vesicle protein, RIM1α, promotes its direct interaction with $Ca_v2.1$ channels, causing them to form clusters, which leads to rapid exocytosis of synaptic vesicles (Girach, Craig et al. 2013). In addition, SUMOylation plays a role in the trafficking of integral membrane proteins such as kainate receptors. SUMOylation of GluK2 is required for agonist-induced internalization of the kainate receptor, likely by facilitating its interaction with scaffolding and/or trafficking proteins (Konopacki, Jaafari et al. 2011, Chamberlain, Gonzalez-Gonzalez et al. 2012). However, the distinct interaction that leads to GluK2 internalization is still unknown. Voltage-gated ion channels are fundamental constituents of the neuronal membrane. Their trafficking is complex and highly regulated. The functions of SUMOylation in voltage-gated ion channel trafficking are largely unknown. We are interested in the role of SUMOylation in the regulated trafficking of Hyperpolarization-activated Cyclic Nucleotide gated (HCN) ion channels.

HCN channels play a pivotal role in shaping neuronal excitability and synaptic integration by influencing several neuronal activity features including membrane potential, firing threshold, resonance frequency, temporal summation and synaptic strength (Hutcheon and Yarom 2000, Wahl-Schott and Biel 2009, Shah 2014). The mammalian HCN1-4 gene family encodes distinct channel isoforms (He, Chen et al. 2014). All isoforms are permeable to K^+ and Na^+, activate upon hyperpolarization, and mediate a slowly depolarizing current termed the hyperpolarization-activated current (I_h). Besides being activated at hyperpolarized potentials,

HCN channels can also be gated by the binding of cyclic nucleotides to the C-terminal CNBD found in all isoforms (Robinson and Siegelbaum 2003, He, Chen et al. 2014).

HCN isoforms differ in their biophysical properties and modulation by cAMP. Under basal conditions, the CNBD inhibits hyperpolarization-gating to a different extent in each isoform due to its isoform-specific interactions with the core transmembrane domain and the C-linker that connects the CNBD to the transmembrane domain (Wang, Chen et al. 2001). This variable inhibition results in isoform-specific steady-state activation curves. For example, the steady-state activation curve of HCN2 channels is 20mV more hyperpolarized compared with HCN1 channels. Binding of cAMP to the CNBD relieves its inhibition on hyperpolarization-gating. Because of the isoform-specific interactions between the CNBD and the C-linker, the effect of cAMP binding will vary with the isoform (Wang, Chen et al. 2001). For example, binding of cAMP to the CNBD of HCN2 and HCN1 channels shifts their respective activation curves to more positive potentials, but HCN2 channels display a 17mV shift while HCN1 channels display a 4mV shift. Maximal effects of cAMP binding are observed for HCN2 and HCN4 isoforms. The activation kinetics also varies between isoforms with HCN1 and HCN4 having the fastest and slowest activation kinetics, respectively.

In addition to their distinct biophysical properties and cAMP modulation, each of the four isoforms also displays a unique expression pattern in the nervous system (He, Chen et al. 2014). HCN1 is highly enriched in the neocortex, hippocampus, cerebellar cortex and brainstem. HCN2 is widely expressed in most brain regions, while HCN3 has low expression levels in the nervous system. HCN4 expression mirrors HCN1 and is also selectively expressed in several thalamic nuclei and neuronal populations in the basal ganglia and habenular cortex. The formation of heteromeric channels further enhances the complexity of I_h function and modulation *in vivo*.

HCN channel surface expression throughout the nervous system can be adjusted over several time courses (Zha, Brewster et al. 2008, Shah 2014, Furst and D'Avanzo 2015, Smith, Al Otaibi et al. 2015, Brennan, Baram et al. 2016). Regulated SUMOylation could play a role in the trafficking of HCN channels. Since the trafficking of HCN2 channels has been fairly well studied (see Discussion), here we examine SUMOylation of HCN2 channels.

3.3 Methods

3.3.1 Drugs

All drugs were obtained from Sigma-Aldrich with the exception of Tween 20 (Fisher Scientific).

3.3.2 Mouse Brain Membrane Preparations

Nondenaturing: A single mouse forebrain was homogenized on ice in homogenization buffer (5mM NaH_2PO_4 buffer, 0.32M sucrose) supplemented with protease inhibitor cocktail (1:100, Sigma cat. #P8340) and 20mM N-Ethylmaleimide (NEM) to prevent SUMO deconjugation (Suzuki, Ichiyama et al. 1999). Cell debris was pelleted at 5,000rpm for 10min at 4°C, and the supernatant was retained and further centrifuged at 40,000rpm for 90min at 4°C to pellet membrane-bound proteins. The supernatant was removed and the pellet containing intracellular and extracellular membrane bound proteins was resuspended in 1ml of resuspension buffer (0.5% SDS, 5nM NaH_2PO_4, protease inhibitor cocktail at 1:100) followed by shaking at 4°C for 1hr. *Denaturing:* Tissue homogenization and centrifugation were the same as for the nondenaturing preparation. The membrane pellet was resuspended in 100µl of denaturing buffer (2% SDS, 50mM Tris-HCl pH7.5, 5mM DTT) followed by shaking at 4°C for 1hr. The preparation was then diluted to 1ml total volume with dH_2O and boiled for 10min. In all cases protein concentration was determined with a bicinchoninic acid assay (BCA Assay, Pierce BCA

Protein Assay Kit). Mouse brain membrane fractions were obtained from whole mouse forebrain tissue generously provided by Dr. Chun Jiang. All animal procedures were conducted in compliance with the regulation of the Institutional Animal Care and Use Committee of Georgia State University.

3.3.3 Plasmids and Antibodies

A previously described mouse GFP-HCN2 fusion plasmid (Santoro, Wainger et al. 2004) was generously provided by Dr. Bina Santoro's Lab. Plasmids for transient transfection include the following: mCherry2-C1 was a gift from Michael Davidson (Addgene plasmid #54563), Ubc9 (Yasugi and Howley 1996) was a gift from Peter Howley (Addgene plasmid #14438), SENP1 (Cheng, Kang et al. 2007) was a gift from Edward Yeh (Addgene plasmid #17357), and SUMO2 (Kamitani, Nguyen et al. 1998) was a gift from Edward Yeh (Addgene plasmid #17360). Antibodies used are shown in Table 1, and the specificity of each antibody was verified as indicated in the table.

3.3.4 Site Directed Mutagenesis

PCR was used to create two site-directed mutations in the GFP-HCN2 fusion plasmid described above: K534R and K669R. The two sets of primers are listed in Table 2. PrimeStar GXL polymerase (Takara) was used along with the buffer, nucleotides, and instructions supplied by the manufacturer. Typically, 10ng of plasmid DNA served as the template in a 50µl reaction. The cycling conditions were: 1x 98°C,1min; 30x 98°C,30sec, 68°C, 7min; 1x 68°C, 5min. Upon completion, 20 units of DpnI (Clontech) were added to the reaction, which was incubated at 37°C for 1-2hr to digest the template DNA. Afterward, 1-2µl of the reaction was added to a 50µl aliquot of subcloning grade competent XL1blue cells (Agilent) and incubated on ice for 30min. The cells were then heat-shocked at 42°C for 45sec. NZY broth (100µl) was added, and the cells

were incubated at 37°C for 20min to allow for expression of kanamycin resistance. Cells were then plated on NZY plates containing 30μg/ml kanamycin and incubated at 37°C overnight. Plasmid DNA from resultant colonies was isolated (Qiagen), the insert was sequenced in its entirety, and analyzed with Lasergene software (DNAstar) to ensure that only the intended mutation was generated. All sequencing was done by the Georgia State University Cell Protein and DNA Core Facilities. To create multiple mutations, a previously mutated GFP-HCN2 fusion plasmid was used as the template for a PCR with a different primer.

3.3.5 Cell culture, Stable and Transient Transfections

Hek-293 cells and all cell culture reagents were obtained from American Type Culture Collection (ATCC; Manassas, VA). Hek-293 cells were cultured at 37°C, and 5% CO_2 in EMEM media supplemented with 10% fetal bovine serum and 1% Penicillin-Streptomycin.

Transfections to produce stable lines: A cell line stably expressing a GFP-HCN2 fusion protein (Hek-HCN2) was generated by transfecting a 60mm plate of Hek-293 cells with the GFP-HCN2 plasmid using Lipofectamine 2000 (Invitrogen) according to instructions provided by the manufacturer. After two days, transfected cells were trypsinized, resuspended and replated to 60mm plates (5-20μl of a 1ml cell resuspension per 60mm plate) and the selection agent, G418 (Geneticin, Gibco, 500μg/ml), was added to the media. After 3-5 weeks, individual colonies were selected using cloning rings. Stable expression was checked by fluorescence and whole cell patch clamping for I_h. In all cases, a colony was selected only if GFP and I_h was observed in every cell; however, the intensity of GFP expression and I_h maximal conductance could vary between colonies from the same transfection by a factor of 10, presumably due to differences in the number of copies of plasmid integrated into the host cell genome. Stable cell lines expressing mutant versions of GFP-HCN2 were generated in a similar fashion. *Transient transfections:* In

our hands, Lipofectamine transfection efficiencies ranged from 5-25%. This was not adequate for transient transfection experiments, which required 80-100% transfection efficiency. Therefore, a high efficiency calcium phosphate transfection was employed for immunoprecipitation, biotinylation and patch clamping experiments using transient transfection to increase or decrease SUMOylation. Briefly, cells were plated at ~60% confluence on 100mm or 60mm cell culture dishes 24hr before transfection. The media was changed at least 1hr before transfection. For a single 100mm or 60mm dish, 25µg or 10µg of total plasmid DNA, respectively, was diluted in TE buffer (10mM Tris-HCl pH8, 1mM EDTA), 2M $CaCl_2$ was added dropwise to the DNA followed by the addition of 2x HBS (275mM NaCl, 10mM KCl, 12mM Dextrose, 1.4mM Na_2HPO_4, 40mM HEPES, pH 7.1). Calcium Phosphate/DNA precipitate was then immediately dropped onto cells. Cells were returned to 37°C and 5% CO_2 for 4hr followed by either a media change or passaging to 20mm Poly-L-Lysine coated coverslips and allowed to grow another 24-48hr. Cells were transfected with plasmid DNA expressing either mCherry or a mixture of mCherry+SUMO+Ubc9 or mCherry+SENP1. For co-transfection of multiple plasmids, the total amount of plasmid DNA remained the same (25µg or 10µg) but comprised equal amounts of each of the different plasmids (1:1:1 or 1:1). Transfection efficiency was determined to be the percentage of cells expressing mCherry as judged by fluorescence microscopy. The transfection efficiency of every plate was checked for each experiment, and a plate was only used if the transfection efficiency exceeded 80%.

3.3.6 Immunoprecipitations

GFP-HCN2 IP from Hek cells: 100mm plates containing Hek cells were washed twice with ice-cold PBS (137mM NaCl, 2.7 mM KCl, 10 mM Na_2HPO_4, 1.8 mM KH_2PO_4, pH 7.4) followed by the addition of RIPA buffer (1% NP40, 50mM Tris pH 7.4, 150mM NaCl, 0.1%

SDS, 0.5% DOC, 20mM EDTA, protease inhibitor cocktail at 1:100 and 20mM NEM) to the plate. Cells were lysed on the plate for 30min on ice, rocking occasionally. A disposable cell scraper was used to scrape any remaining cell debris from the bottom of the plate, and the lysate was collected and transferred to a sterile tube. Cell debris was pelleted at 12,000rpm for 10min at 4°C, and the supernatant was retained. Protein concentration was determined with a BCA assay. Immunoprecipitations (IP) were performed using the Classic Magnetic Co-IP Kit (Pierce), following the manufacturer's instructions. Typically 1mg of protein was added to the beads and the protein was eluted from the beads in a volume of 100µl. *HCN2 IP from mouse forebrain:* 1.5mg of the mouse membrane preparation with 5ug of anti-HCN2 antibody (Table 1) or IgG (Santa Cruz Biotechnology; sc-2028) were used in combination with the Classic Magnetic Co-IP Kit (Pierce), following the manufacturer's instructions. Protein was eluted from the beads in a volume of 100µl and 20µl was used for one lane of an SDS-PAGE gel.

3.3.7 Western Blotting

Protein samples were run on an SDS-PAGE gel and transferred to a PDVF membrane using a semidry electroblotting system. A membrane was blocked for 1hr in a solution of 5% non-fat powdered milk in TBS (10mM Tris-HCl pH7.5, 150mM NaCl), washed for 10min in TTBS (1x TBS, 0.1% Tween 20), and then incubated overnight at 4°C with the primary antibody, diluted as described in Table 1, in 1% non-fat powdered milk in TTBS. The membrane was then washed 3x 5min each in TTBS and then incubated with the appropriate alkaline phosphatase conjugated secondary antibody, diluted in 1% non-fat powdered milk in TTBS for 2hr at room temperature. Following incubation with the secondary antibody, the membrane was washed 3x 10min each and Immunstar AP substrate (BioRad) was added to the surface of the membrane, incubated 5min and then exposed to X-ray film to detect chemiluminescent signals.

In some cases, membranes were stripped and reprobed. Stripping involved washing the blot 2x 5min each in mild stripping buffer (200 mM Glycine, 0.1% SDS, 1% (v/v) Tween 20, pH 2.2). The blot was then washed 2x 10min each in PBS and 2x 5min each in TTBS. The blot was then exposed to film to ensure the signal was removed.

3.3.8 Patch Clamping Electrophysiology

Coverslips (20mm) were dipped in ethanol, allowed to air dry, and incubated with Poly-L- Lysine (50µg/ml in dH_2O) at 37°C for 1hr. Coverslips were then washed once with sterile dH_2O, air dried, and stored at 4°C. For an experiment, coverslips were seeded with $8x10^4$ cells, and the next day coverslips containing transiently transfected cells were placed into a chamber and constantly perfused with extracellular saline solution (138mM NaCl, 5.6mM KCl, 2.6mM $CaCl_2$, 1.2mM $MgCl_2$, 10mM HEPES, 10mM Glucose, pH 7.4). Cells were visualized on an Olympus IX70 microscope and transiently transfected cells were identified by fluorescence and only those expressing mCherry were used for whole cell patch clamping experiments. A fire-polished micropipette (Sutter Instruments, 6-8 MΩ) was filled with intracellular solution (10mM NaCl, 145mM KCl, 1mM $MgCl_2$, 5mM HEPES, pH 7.2) and connected to an Axopatch 200B amplifier (Molecular Devices, Foster City, CA). To obtain a whole cell patch, a gentle negative pressure was used to form a ≥1GΩ seal between the cell membrane and the opening of the micropipette. Suction was used to rupture the cell membrane and recordings were taken from cells that maintained a seal ≥700 MΩ following rupture. Cells were held at -50mV using pClamp 10 software and I_h was elicited using 5 sec hyperpolarizing voltage steps from -50mV to -120mV in 10mV increments with 4 seconds between each step. Steady-state peak current was measured by subtracting the initial fast leak current from the slowly activating I_h for each hyperpolarizing

voltage step. Conductance was calculated using the peak current at each voltage step ($G= I_{peak}/(V_m-V_{rev})$; V_{rev} I_h= -35mV) and fitted to a first order Boltzmann equation.

3.3.9 Cell Surface Biotinylation

Hek-HCN2 cells plated on 60mm culture dishes were transiently transfected with either mCherry alone (control) or mCherry+SUMO+Ubc9. Cells were washed twice with ice-cold PBS, supplemented with 0.2mM $CaCl_2$ and 1.5mM $MgCl_2$ (PBS-CM) and incubated for 30min at 4℃ with 0.5-1mg/ml of EZ-link Sulfo-NHS-SS-Biotin (Thermo Fisher, cat#21331). Cells were washed twice with ice cold PBS-CM, and residual biotin was quenched with PBS-CM plus 100mM glycine for 15min at 4°C. Cells were washed once more with PBS-CM followed by lysis with ice cold RIPA buffer (1% NP40, 50mM Tris pH 7.4, 150mM NaCl, 0.1% SDS, 0.5% DOC, 2mM EDTA, protease inhibitor cocktail at 1:100) for 30min on ice. A disposable cell scraper was used to remove any residual cell debris from the bottom of the plate, and the contents were transferred to a microcentrifuge tube. Cell debris was pelleted by centrifugation at 12,000 rpm for 10min. The supernatant was removed and immediately incubated for 2hr at 4℃ with Neutravidin agarose resin (Pierce, cat #29201) with agitation. The lysate/resin mixture was centrifuged in a spin column (Thermo Fisher, cat #69725) at 1000xg for 2min. The flow through containing unbiotinylated intracellular proteins was retained for western blot analysis. The resin was washed three times in PBS supplemented with 1% NP40, and 0.1% SDS and three times in PBS supplemented with 0.1% NP40 and 0.5M NaCl, centrifuging at 500xg for 1min between each wash. Columns were capped, and biotinylated proteins were eluted from the beads by incubating for 1hr at room temperature with SDS loading buffer (50mM Tris-HCL pH 6.8, 100mM DTT, 2% SDS, 0.1% Bromophenol blue, 10% glycerol). Columns were uncapped and centrifuged at 1000xg for 2min to collect the eluted extracellular proteins. Intracellular and

extracellular fractions were run on an SDS-PAGE gel and transferred to a PVDF membrane. The membrane was cut at ~50 kDa. The lower portion of the blot was probed with an anti-actin antibody (Santa Cruz Biotechnology) to confirm that there was no intracellular contamination in the extracellular samples. The top portion of the blot was dually probed with an anti-GFP antibody to detect the GFP-HCN2 channel, and an anti-Na^+/K^+-ATPase antibody to use for normalization (Table1). To confirm that expression of the Na^+/K^+-ATPase was not varying across treatment groups, samples from control and SUMO+Ubc9 transfected cells were run on a western blot. The blot was stained for total protein (SYPRO Ruby blot stain, Bio-Rad) and then probed for the Na^+/K^+-ATPase. The Na^+/K^+-ATPase signal was normalized by the total protein in the lane. A comparison of the normalized Na^+/K^+-ATPase signal across treatment groups indicated that there were no significant differences between control and SUMO+Ubc9 transfected groups (Student's t-test, $p > 0.05$, $n=5$).

3.3.10 Image analysis and Quantification

ImageJ was used to quantify signals from western blots. Optical density (OD) was measured using the Gel Analysis feature of the ImageJ software. Briefly, a rectangular box was drawn around the signal, and ImageJ software was then used to generate a profile plot of the relative intensity. A line was drawn to isolate the area under the curve and set the baseline, thereby subtracting the background, and the area under the curve was measured. In order to ensure images were not saturated, a series of exposures ranging from underexposed to overexposed was always obtained, and only intermediate exposures were quantified. Quantifying the fraction of SUMOylated GFP-HCN2 channels in Hek cells involved measuring a SUMO signal (entire GFP-HCN2 doublet) followed by stripping and reprobing the membrane to obtain a GFP signal (entire GFP-HCN2 doublet). In order to ensure that differences between treatment

groups were not due to differences created by stripping or variability in the length of SUMO relative to GFP film exposure, a complete set of treatment groups was present on each blot, and measures for each treatment group were obtained from the same exposure/film. However, variability within a treatment group could be due to stripping and/or relative lengths of exposures. At best, these experiments are semi-quantitative and the fraction of SUMOylated channels in these cell lines may be over/under-reported with this method. Nevertheless, they suffice for detecting significant differences between treatment groups.

3.3.11 Statistical analysis

All data were analyzed using Prism 7 (Graphpad Software Inc.). Each data set was checked for normality and homogeneity of variance. Data were then analyzed using parametric statistical tests, including Student's t-test and One-way ANOVA's. In all cases, the significance threshold was set at $p<0.05$. Values that were greater than two standard deviations from the mean were considered statistical outliers and were excluded from the data set. ANOVA's were followed by post hoc tests that either compared all groups to each other (Tukey's) or to the control (Dunnett's). Unless otherwise stated all values are presented as the mean ± SEM.

3.4 Results

3.4.1 Mouse HCN2 is SUMOylated In vivo

To determine if the mouse HCN2 channel was SUMOylated *in vivo,* an antibody against HCN2 (Table 3.1) or IgG (negative control) was used to IP the channel from mouse forebrain membrane preparations that were or were not denatured, followed by western blot analyses using antibodies against HCN2, SUMO1 and SUMO2/3. Note that our anti-SUMO2/3 antibody does not discriminate between SUMO2 vs. SUMO3; therefore, the post-translational modification is referred to as SUMO2/3. Fig 3.1 illustrates that HCN2 channels were post-translationally

modified by both SUMO1 and SUMO2/3 in the mouse forebrain. Two bands at ~120 and 75 kDa were observed in the experimental preparations but not in the negative controls. The band at ~120 kDa was previously identified as the HCN2 channel in mouse membrane preparations (Much, Wahl-Schott et al. 2003). It was observed in blots probed with anti-HCN2, anti-SUMO1 and anti-SUMO2/3 in both non-denaturing and denaturing IP experiments, which suggests both SUMO1 and SUMO2/3 are covalently attached to HCN2 channels in the mouse forebrain. The ~75kDa band was detected by the anti-SUMO antibodies, but not by the anti-HCN2 antibody, on the western blots containing IP experiments using nondenatured membrane preparations. Since this ~75 kDa band was not observed for the denaturing IP experiments, it most likely represents an unknown SUMOylated protein that noncovalently associates with HCN2 channels in the mouse forebrain.

3.4.2 GFP-HCN2 Channels are SUMOylated in a Heterologous Expression System

Previous work suggested that SUMOylation could be manipulated in tissue culture systems. We therefore generated a Hek-293 cell line stably expressing a GFP-HCN2 fusion protein (Hek-HCN2) as described in Materials and Methods. Note that GFP is at the N-terminus of the HCN channel. IP experiments were performed on parental Hek and Hek-HCN2 cell lysates using an anti-GFP antibody followed by western blot analyses with anti-GFP or anti-HCN2 antibodies (Fig 3.2). Both the anti-GFP and the anti-HCN2 antibodies detected the same two bands between 150 and 250 kDa (Fig 3.2A). This doublet was not observed in the parental Hek cell line (Fig 3.2B). Together these data suggested that the doublet represented the GFP-HCN2 channel. Previous studies on HCN2 channels expressed in Hek cells showed that the doublet represented two forms of the HCN2 channel (Much, Wahl-Schott et al. 2003, Akhavan, Atanasiu et al. 2005, Nazzari, Angoli et al. 2008). The slower migrating band contained a

complex N-glycosylation. The faster migrating band instead possessed a simple or no glycosylation. Complex N-glycosylation increased the efficiency of surface expression, but channels possessing only a subset of complex N-glycosylated subunits (Akhavan, Atanasiu et al. 2005) or no complex N-glycosylated subunits (Nazzari, Angoli et al. 2008) could still be detected at the plasma membrane. Relative to past studies, the doublet detected in our experiments is larger, presumably due to the GFP tag.

To determine if GFP-HCN2 channels were SUMOylated in our culture system, we performed the same anti-GFP IP with Hek-HCN2 cell lysates, followed by western blot analyses using anti-GFP (Fig 3.3, panel 1) and anti-SUMO2/3 (Fig 3.3, panel 2) antibodies. The data indicated that both antibodies recognized the same doublet between 150-250 kDa, suggesting that GFP-HCN2 channels were SUMOylated in Hek-HCN2 cells (here termed baseline SUMOylation). The SUMO signal was not due to similarly sized endogenous Hek proteins associating with GFP-HCN2 channels because the anti-SUMO2/3 antibody did not detect the doublet on western blots containing parental Hek cell lysates (Fig 3.3, panel 3).

3.4.3 Transient Transfection of SUMO2 and Ubc9 Increases HCN2 Channel SUMOylation in a Hek Cell Line Stably Expressing Mouse HCN2

We next wished to manipulate GFP-HCN2 channel SUMOylation in order to study its function. The conjugating enzyme, Ubc9, adds SUMO to a target protein. In some cases, Ubc9 is directed to a SUMOylation site by an external factor, such as a SIM domain or an E3 protein (Flotho and Melchior 2013). In other cases, Ubc9 directly recognizes a consensus sequence and adds SUMO to the K in the consensus sequence. Oftentimes the latter mechanism requires additional stabilizing interactions provided by other proteins or post-translational modifications; however, simply increasing the concentration of the Ubc9 enzyme can obviate their need at some

(but not all) consensus sequences, and previous work has demonstrated that SUMOylation of some target proteins can be increased in cell culture by overexpressing SUMO and Ubc9 (Dai, Kolic et al. 2009). Moreover, SENP has been shown to decrease SUMOylation of some proteins in a heterologous expression system (Dai, Kolic et al. 2009, Dustrude, Wilson et al. 2013) despite the fact that SENP has opposing functions: endopeptidase activity removes C-terminal amino acids to activate SUMO and promote target protein SUMOylation; isopeptidase activity removes SUMO conjugated to target proteins to promote deSUMOylation (Yeh 2009).

In order to investigate whether or not we could manipulate SUMOylation of GFP-HCN2, the Hek-HCN2 cell line was transiently transfected with plasmids expressing mCherry, SUMO2, and Ubc9 or mCherry and SENP1. Control preparations were transfected with mCherry alone. To determine the fraction of HCN2 channels that were SUMOylated in each treatment group, GFP-HCN2 channels were immunoprecipitated from lysates using an anti-GFP antibody. Western blots containing the IP products were first probed with an anti-SUMO2/3 antibody. Chemiluminescence was used to detect the SUMO signal, and the optical density (OD) for the entire GFP-HCN2 doublet was measured with ImageJ (see Materials and Methods). After recording the SUMO signal, the antibody was stripped, and the same blot was reprobed with an anti-GFP antibody. Again, chemiluminescence was used to detect the GFP signal, and the optical density (OD) of the entire GFP-HCN2 doublet was measured. The fraction of SUMOylated channels was defined as the OD of the SUMO signal divided by the OD of the GFP signal (Fig 3.4A). This non-linear, semi-quantitative method indicated that GFP-HCN2 SUMOylation was significantly increased in the SUMO+Ubc9 group, by an average of 50.7±16.01% relative to the control (Fig 3.4B). There was no significant difference in the amount of SUMOylated channels in cells transfected with SENP1 relative to control. This might suggest a low level of baseline

HCN2 SUMOylation in the Hek-HCN2 cell line. On the other hand, since SENP has two opposing functions it is also possible that the balance of these two functions doesn't change upon SENP1 overexpression, leaving baseline SUMOylation unaltered. In sum, transient transfection of SUMO and Ubc9 increases HCN2 SUMOylation in Hek-HCN2 cells.

3.4.4 HCN2 Channel SUMOylation Increases I_h G_{max}

Hyperpolarization of Hek-HCN2 cells to -120mV consistently elicited an average peak I_h of 710pA. This current was never detected in the parental Hek cell line (n>10); thus, it is mediated by GFP-HCN2 channels. We examined if/how SUMOylation affected I_h using whole cell patch clamp recordings on Hek-HCN2 cell lines that were transiently transfected with mCherry, mCherry+SUMO+Ubc9 or mCherry+SENP1. Transfected cells were identified by mCherry fluorescence. I_h was elicited by stepping the voltage from -50mV to -120 mV in 10 mV increments (Fig 3.5A). The data showed the treatment that produced a ~50% increase in HCN2 SUMOylation (SUMO+Ubc9, Fig 3.4B) also produced a mean 77±18.8% increase in I_h G_{max} relative to control (Fig 3.5B). Overexpression of SENP1 produced a detectable but not significant mean 31.7±14% decrease relative to control (Fig 3.5B), which was consistent with the finding that SENP1 did not significantly alter baseline SUMOylation of HCN2 channels. The change in I_h G_{max} was not accompanied by any change in the voltage-dependence of activation (Fig 3.5C). Neither the mean V_{50}, nor the mean slope of the activation curve were significantly different between control, SUMO+Ubc9, or SENP1 treatment groups (Fig 3.5C). Similarly, the time constant for activation was not significantly different between treatment groups (Fig 3.5A). In sum, increased SUMOylation of GFP-HCN2 produced a corresponding increase in I_h G_{max} with no change in voltage dependence or kinetics of activation.

3.4.5 SUMOylation Increases HCN2 Channel Surface Expression

We next tested whether or not the SUMOylation-dependent increase in I_h G_{max} was accompanied by an increase in GFP-HCN2 channel surface expression. A biotinylation assay was used on Hek-HCN2 cells that were transiently transfected with mCherry or mCherry+SUMO+Ubc9. After 2 days, transfected cells were incubated with biotin, which binds to cell surface proteins. The cells were then lysed, and the biotinylated proteins were pulled out using Neutravidin. The unbiotinylated (intracellular) and biotinylated (extracellular surface) proteins were run on a western blot, and the blot was subsequently divided at ~50kDa. The portion of the blot containing proteins <50 kDa was probed with an antibody against actin. The ~37kDa band corresponding to actin was only seen in the intracellular fractions, indicating there were no intracellular proteins contaminating the extracellular surface samples (Fig 3.6A). The section of the blot corresponding to proteins >50 kDa was dually probed with an anti-GFP antibody and an antibody against the Na^+/K^+-ATPase (Fig 3.6A). The doublet was detected with the anti-GFP antibody. The band at ~120 kDa represents the Na^+/K^+-ATPase. The OD of the GFP signal (entire GFP-HCN2 doublet) was normalized by that for the Na^+/K^+-ATPase signal. We observed a significant mean 70.6±18.2% increase in HCN2 surface expression in cells transfected with SUMO+Ubc9 relative to control (Fig 3.6B). Based on these findings, we concluded that the ~77% increase in I_h G_{max} observed upon enhanced GFP-HCN2 channel SUMOylation was due, at least in part, to a ~70% increase in the surface expression of the GFP-HCN2 channel.

3.4.6 Only One of Six Putative SUMOylation Sites is Necessary for the Increase in GFP-HCN2 Surface Expression and I_h G_{max} Elicited by Overexpression of SUMO and Ubc9

GFP-HCN2 channels can be SUMOylated in our culture system, and increased SUMOylation leads to an augmentation of I_h G_{max} due, at least in part, to enhanced GFP-HCN2 channel surface expression. Approximately 63% of all SUMOylation occurs within a SUMOylation consensus sequence (Hendriks, D'Souza et al. 2015), e.g. ΨKXD/E, with Ψ being a hydrophobic residue and X being any amino acid (Rodriguez, Dargemont et al. 2001, Sampson, Wang et al. 2001, Flotho and Melchior 2013). We next investigated if HCN channels possessed SUMOylation consensus sequences. SUMOplot freeware (www.abgent.com/sumoplot) was used to identify potential HCN SUMOylation sites for all mouse HCN channel isoforms and for the spiny lobster HCN channel. The amino acid sequences for all five channels were aligned, SUMOylation consensus sequences were highlighted for all isoforms and the probability of SUMOylation, as calculated by SUMOplot, was indicated (Fig 3.7). There were 6 putative HCN2 SUMOylation sites with probabilities ranging from 32% to 93%. One site was extracellular (K210) and was not considered further. Two of the five intracellular HCN2 consensus sequences (K464 and K484) were observed in all mammalian HCN channel isoforms and in the lobster HCN channel. The other three consensus sequences were isoform/species specific. The consensus sequence containing K669 was exclusive to mouse HCN1 and HCN2 channels. The consensus sequence that included K534 was found only in mouse HCN2 and lobster HCN channels. The consensus sequence containing K75 was unique to the mouse HCN2 channel. Additional putative SUMOylation sites not observed in mouse HCN2 channels existed in other mouse and lobster HCN channel isoforms.

We next investigated if HCN2 consensus sequences were substrates for SUMOylation in our culture system. Because K534 and K669 showed a greater than 90% probability of SUMOylation (Fig 3.7), we chose to examine these first. These two sites were mutated individually and together by changing the positively charged K residue to a positively charged arginine (R), which should prevent SUMO conjugation without disrupting charge interactions (Feliciangeli, Bendahhou et al. 2007). Three Hek cell lines stably expressing the mutated channels were generated: Hek-HCN2 K534R+K669R, Hek-HCN2 K534R, and Hek-HCN2 K669R. Each stable mutant cell line was transiently transfected with mCherry or mCherry+SUMO+Ubc9. After ~48hr the fraction of SUMOylated GFP-HCN2 channels was measured as previously described for Fig 3.4. Based on our semi-quantitative measures, the mutations did not appear to alter baseline HCN2-GFP SUMOylation in the mCherry treatment group (mean±SEM; wild-type = 0.31±0.025, K534R+K669R = 0.41±0.04, K534R = 0.31±0.02 and K669R = 0.37±0.015; One-way ANOVA $F(3,19) = 2.644$, $p = 0.0788$). On the other hand, the mutations did disrupt the increase in HCN2-GFP SUMOylation normally elicited by SUMO+Ubc9 overexpression (Fig 3.8). Increased SUMOylation was no longer observed in the Hek-HCN2 K534R+K669R cell line (Fig 3.8A) or the Hek-HCN2 K669R cell line (Fig 3.8C); however, the Hek-HCN2 K534R cell line still displayed increased SUMOylation upon SUMO+Ubc9 overexpression (Fig 3.8B). In sum, the data suggest that overexpression of SUMO+Ubc9 increases SUMOylation at K669; furthermore, because SUMOylation is still observed when this site is mutated, at least one additional site on the GFP-HCN2 channel must be SUMOylated.

We next examined I_h G_{max} in the mutant cell lines. Consistent with the previous finding, we observed that mutating K669 but not K534 prevented the increase in I_h G_{max} upon

SUMO+Ubc9 overexpression. I_h G_{max} was not significantly different between the SUMO+Ubc9 vs. control treatment groups in Hek-HCN2 K534R+K669R (Fig 3.9A) or Hek-HCN2 K669R cell lines (Fig 3.9C). However, in Hek-HCN2 K534R cells, a 58.2±16.1% increase in I_h G_{max} was still observed in the SUMO+Ubc9 treatment group relative to control (Fig 3.9B). Together these data suggest that SUMOylation of K669 is responsible for the increase in I_h G_{max} observed upon overexpression of SUMO+Ubc9.

Lastly, we tested if mutating K669 prevented the increase in GFP-HCN2 surface expression normally elicited by overexpression of SUMO and Ubc9. Hek-HCN2 K669R cells were transiently transfected with mCherry or mCherry+SUMO+Ubc9 and the biotinylation assay was performed as described for Fig 3.6. The data indicated then when K669 was mutated, overexpression of SUMO and Ubc9 could no longer elicit an increase in GFP-HCN2 surface expression (Fig 3.10). In sum, the K669R mutation blocked the increase in SUMOylation, I_h G_{max} and surface expression normally elicited by overexpression of SUMO+Ubc9. This suggests that enhanced SUMOylation at K669 augments GFP-HCN2 surface expression which in turn amplifies I_h G_{max}.

3.5 Discussion

Ion channels are emerging as targets of SUMOylation. The extent to which different classes of ion channels are SUMOylated and the function and regulation of ion channel SUMOylation are only beginning to be investigated. Here we report, for the first time, that HCN channels are SUMOylated *in vivo* and in a heterologous expression system. IP experiments with mouse forebrain membrane preparations followed by western blotting showed that mouse HCN2 channels were post-translationally modified by SUMO1, as well as SUMO2 and/or SUMO3 *in vivo*. HCN2 channels were also SUMOylated under baseline conditions in a Hek cell line stably

expressing a GFP-HCN2 construct, and transient transfection with SUMO and the SUMO-conjugating enzyme, Ubc9, increased GFP-HCN2 channel SUMOylation above baseline. This, in turn, augmented GFP-HCN2 channel surface expression and produced a corresponding increase in I_h G_{max} without altering the voltage dependence or kinetics of activation. Using site-directed mutagenesis of HCN2 and Hek cell lines stably expressing mutant GFP-HCN2 channels, we showed that SUMOylation at amino acid K669 was increased upon overexpression of SUMO+Ubc9, and this alone was responsible for enhanced GFP-HCN2 channel surface expression and augmentation of I_h G_{max}. However, the K669R mutation, which prevented SUMOylation at this site, did not alter baseline SUMOylation of HCN2 channels, suggesting an additional site(s) on the GFP-HCN2 channel may be SUMOylated under baseline conditions.

3.5.1 Ion Channels are SUMOylated In vivo

The effect of SUMO modification on ion channels has become an area of increasing interest. Previous studies have identified additional ion channel targets of SUMOylation, and the effect of SUMOylation on these channels is quite diverse. For example, SUMO modification of Kv2.1 inhibits the current by speeding time-dependent inactivation and slowing recovery from inactivation in pancreatic cells (Dai, Kolic et al. 2009). However, SUMOylation of the same channel in hippocampal neurons results in a depolarized shift in the voltage dependence of activation, making the neurons more excitable (Plant, Dowdell et al. 2011). Studies looking at SUMOylation of the Kv1.5 channel found that it produced a shift in the voltage dependence of inactivation (Benson, Li et al. 2007). A recent study showed that in SENP2 null mice hyperSUMOylation of Kv7 channels diminished the M-current and resulted in neuronal hyperexcitability, leading to seizures and sudden death (Qi, Wang et al. 2014). In addition to altering the biophysical properties of ion channels, SUMOylation can alter their surface

expression. For example, kainite receptor SUMOylation leads to internalization of the receptor, and this effect can be enhanced by agonist binding and PKC phosphorylation (Martin, Nishimune et al. 2007, Konopacki, Jaafari et al. 2011, Chamberlain, Gonzalez-Gonzalez et al. 2012). Here we have shown that HCN2 channel SUMOylation at K669 increases surface expression and I_h G_{max}. It is important to note that the change in surface expression may not be the sole explanation for the change in I_h G_{max}; though it was not examined here, changes in biophysical properties, such as an increase in the open probability (Po) of the channel, could also contribute to the observed increase in I_h G_{max}. In addition, silent channels in the membrane could be activated by enhancing protein-protein interactions.

3.5.2 HCN channels contain multiple SUMOylation Consensus Sequences

The conjugating enzyme, Ubc9, adds SUMO to target proteins. In some cases, Ubc9 is directed to a SUMOylation site by an external factor, such as a SIM domain or an E3 ligase. In these instances, SUMOylation does not necessarily occur at a known consensus sequence (Flotho and Melchior 2013). In other cases, Ubc9 itself recognizes a consensus sequence and adds SUMO to the K in the consensus sequence. One study indicates that SUMOylation at known consensus sequences accounts for ~63% of all SUMOylation, although this may vary with the condition, e.g. normal growth conditions vs. heatshock (Hendriks, D'Souza et al. 2015). There are five predicted intracellular SUMOylation consensus sequences in HCN2 (Fig 3.7). Using Hek cell lines stably expressing wild type and mutant GFP-HCN2 channels, we clearly demonstrated that overexpression of SUMO and Ubc9 increased SUMOylation at only one of the five sites, K669. However, when K669 was mutated, GFP-HCN2 channel SUMOylation was still observed, suggesting additional sites were SUMOylated under baseline conditions. Since additional consensus sequences exist on both the GFP tag and the HCN2 channel, either or both

could contribute to the observed baseline SUMOylation. It is not clear why SUMOylation did not increase at these site(s) upon overexpression of SUMO and Ubc9. They may be maximally SUMOylated and/or additional proteins or regulatory mechanisms may be necessary for SUMOylation to occur. Alternatively, baseline SUMOylation may not occur at consensus sequences, in which case increasing SUMO and Ubc9 should have no effect.

The five putative HCN2 consensus sequences ranged from being unique to HCN2 channels to being conserved across all mouse HCN and lobster channel isoforms. The consensus sequence that is known to be SUMOylated and which contains K669 is present exclusively in mouse HCN1 and HCN2 channels. Our data indicated that SUMOylation at K669 was not necessary to produce a functional current: I_h was not observed in whole cell patch clamp recording from parental Hek cells, but it was recorded in Hek cells stably expressing GFP-HCN2 channels with a K669R mutation that prevented SUMOylation at this site. Although K669 SUMOylation was not necessary, increased SUMOylation at K669 augmented GFP-HCN2 channel surface expression and I_h G_{max}. These data suggest that SUMOylation at K669 may alter the rates of channel trafficking to and/or from the plasma membrane and/or alter channel retention in the plasma membrane. The surface expression of HCN1 channels can be rapidly adjusted in response to changes in activity, including seizures (Shah, Anderson et al. 2004, Noam, Zha et al. 2010, Jung, Warner et al. 2011). Activity can also regulate the SUMOylation of target proteins and the expression and localization of SUMO and the SUMOylation machinery in neurons (Jaafari, Konopacki et al. 2013, Loriol, Khayachi et al. 2013, Sun, Lu et al. 2014). Thus, it is possible that changes in activity might alter HCN channel surface expression by altering SUMOylation at this conserved site.

The putative HCN2 channel SUMOylation sites at K464 and K484 were observed in all mouse HCN channel isoforms and even in the lobster HCN channel (Fig 3.7), suggesting that they may play important functional roles. Both K464 and K484 are in the C-linker that connects the CNBD to the transmembrane region. The C-linker is necessary for channel trafficking and cAMP gating (Ulens and Siegelbaum 2003, Zagotta, Olivier et al. 2003, Zhou, Olivier et al. 2004). The C-linker contains seven α-helices, A-F (Zagotta, Olivier et al. 2003); K464 lies between α-helices A and B while K484 lies between α-helices B and C. Since SUMOylation is thought to occur only in regions lacking secondary structure, it is noteworthy that both putative SUMOylation sites lie just outside of the α-helices. The A and B α-helices in one subunit are thought to interact with the C and D α-helices in a neighboring subunit (Zagotta, Olivier et al. 2003). We have not yet tested whether these two SUMOylation sites are involved in channel folding, assembly and/or trafficking, but it may be that SUMOylation plays a fundamental role in these processes for all HCN channels.

The K534 SUMOylation consensus site lies within the CNBD, which is also necessary for trafficking and cAMP gating (Akhavan, Atanasiu et al. 2005). According to a previous crystallography study of the solubilized C-terminus (Zagotta, Olivier et al. 2003), this site lies within α-helix A of the CNBD. The K534R mutation did not appear to alter baseline SUMOylation in our studies, nor did it prevent the increase in HCN2 SUMOylation observed upon overexpression of SUMO+Ubc9. Together these data suggest that K534 may not be SUMOylated in the mature channel. However, this site was assigned a high score by SUMOplot, and it is conserved across species, which often suggests functionality. Since SUMOylation is a dynamic and highly regulated process (Watts 2013), it may be that this site is transiently SUMOylated in response to a specific signal not mimicked in our experiments.

3.5.3 Potential SUMO-dependent HCN2 Channel Interactions

SUMOylation can produce several distinct physiological consequences, but its primary function is to facilitate protein-protein interactions through the binding of a SUMO post-translational modification on the target protein to a SUMO interaction motif (SIM) on the interacting partner protein (Hickey, Wilson et al. 2012). Other interaction motifs also exist (Flotho and Melchior 2013). We have demonstrated that HCN2 channel SUMOylation can regulate surface expression, and that (putative) HCN2 SUMOylation sites are located in domains that are important for channel trafficking and surface expression (Proenza, Tran et al. 2002, Tran, Proenza et al. 2002, Akhavan, Atanasiu et al. 2005, Nazzari, Angoli et al. 2008). Thus, while SIM containing interaction partners for HCN2 channels have not yet been identified, it seems likely that they may include trafficking and scaffold proteins. HCN2 synthesis and assembly begin in the ER where heavily glycosylated subunits associate through N- and C-terminal domains (Proenza, Tran et al. 2002, Tran, Proenza et al. 2002). Channels transit from the ER, through the Golgi and to the plasma membrane via their interactions with a host of proteins that mediate vesicular trafficking. Plasma membrane HCN2 channels can be recycled. Recycled HCN channels are stored in the endosome recycling compartments below the plasma membrane until a signal, such as Phospholipase D activation, triggers insertion back into the plasma membrane (Hardel, Harmel et al. 2008). SUMOylation could be involved at any of these trafficking stages. Scaffold and trafficking proteins are known to interact with three distinct domains in the C-terminus of the HCN2 channel: the C-linker, the CNBD, and the ~230 amino acids distal to the CNBD (Kimura, Kitano et al. 2004, Santoro, Wainger et al. 2004, Lewis, Schwartz et al. 2009, Han, Noam et al. 2011). S-SCAM, mint, and talamin are scaffold and trafficking proteins that form an assemblage with HCN2 channels through unknown interactions

involving the distal ~230 amino acids. SUMOylation site K669 is located in this distal fragment, suggesting that SUMOylation at this site may enhance surface expression by promoting these assemblages (Han, Noam et al. 2011). SUMOylation in the C-linker and/or the distal fragment could also potentially promote or prevent the binding of trafficking/scaffolding proteins like TRIP8b (Santoro, Wainger et al. 2004, Lewis, Schwartz et al. 2009, Han, Noam et al. 2011) and S-SCAM (Kimura, Kitano et al. 2004) to the CNBD.

3.5.4 HCN Channel SUMOylation and Neurological Disorders

Multiple neurological disease states may be linked to aberrant SUMOylation. Normally SUMOylation of α-synuclein promotes a functional, soluble conformation of the protein, but deSUMOylation leads to α-synuclein aggregation and cytotoxicity, which are hallmarks of Parkinson's Disease (Eckermann 2013). Also, the parkin gene is frequently mutated in autosomal recessive Parkinson's patients (Guerra de Souza, Prediger et al. 2016). Parkin is a ubiquitin ligase that mediates the degradation of misfolded mitochondrial proteins. SUMOylation regulates parkin shuttling from the cytosol to the nucleus, thereby controlling its availability at the mitochondria (Um and Chung 2006). Alzheimer's disease is characterized by the formation of neurofibrillary tangles and amyloid-beta (Aβ)-containing plaques. Two proteins closely associated with these features, amyloid precursor protein (APP) and tau, have recently been identified as targets of SUMOylation (Hoppe, Salbego et al. 2015). Their improper SUMOylation could contribute to misfolding and aggregation (Flotho and Melchior 2013). Altering the expression of enzymes in the SUMOylation pathway can lead to seizures due, at least in part, to hyperSUMOylation of Kv7 channels (Qi, Wang et al. 2014). If SUMOylation is globally disrupted in a given disease, then multiple targets could be affected, including HCN2 channels. Indeed, HCN2 channel activity is progressively reduced in a mouse model of

Parkinson's disease leading to altered pacemaking in globus pallidus neurons (Chan, Glajch et al. 2011), and altered HCN2 channel expression has been associated with seizures in a variety of instances (Ludwig, Budde et al. 2003, DiFrancesco, Barbuti et al. 2011, Nakamura, Shi et al. 2013, DiFrancesco and DiFrancesco 2015). Future studies on the function and regulation of HCN channel SUMOylation could provide important insights into HCN2 channel dysfunction in these disease states.

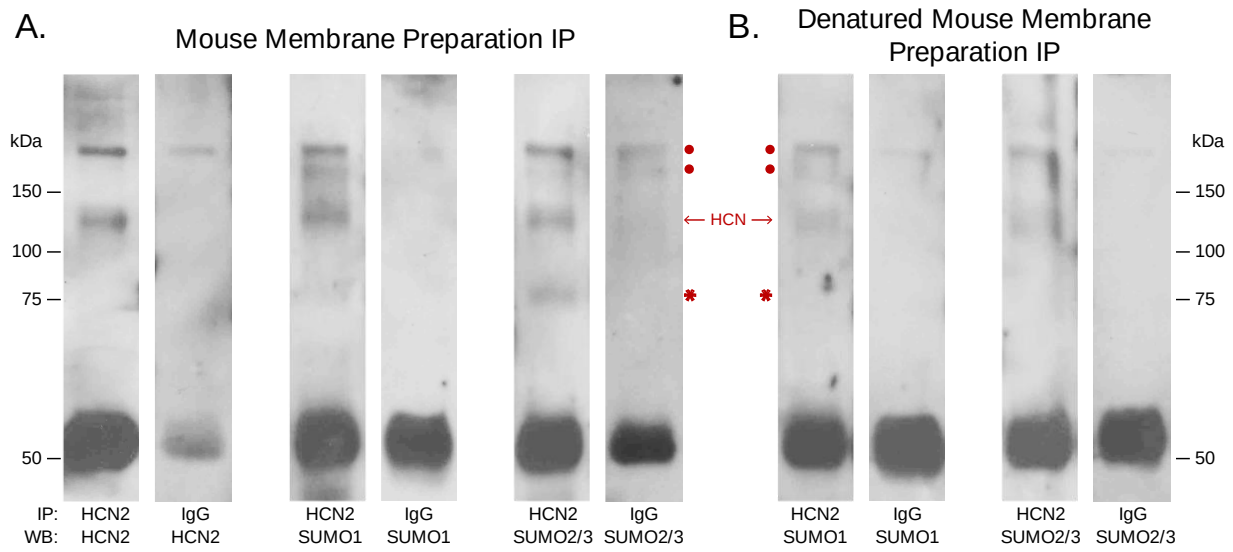

Figure 3.1 Mouse HCN2 is SUMOylated in vivo

Mouse forebrain non-denatured **(A)** and denatured **(B)** membrane fractions were used in immunoprecipitation experiments (IP) with an antibody against HCN2 or IgG (negative control). Western blots containing the IP products were probed for HCN2, SUMO1, and SUMO2/3. The experiment was repeated three times using the brains from three different mice. Representative western blots are shown from a single experiment. The red dots indicate non-specific products pulled down in the IP. The single band at ~120kDa represents HCN2 channels. The asterisk indicates a non-covalently bound, SUMOylated protein

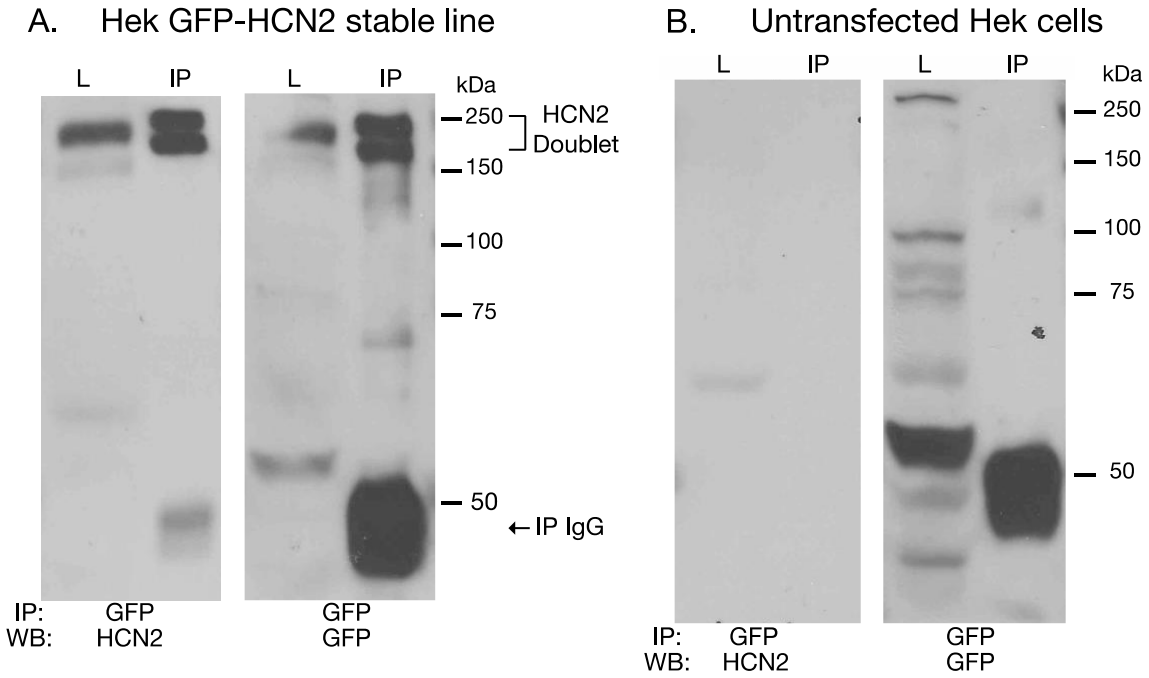

Figure 3.2 Establishing a culture system to investigate HCN2 channel SUMOylation
Cell lysates from a Hek cell line stably expressing GFP-HCN2 channels **(A)** and the parental Hek cell line **(B)** were used in IP experiments with an antibody against GFP. Western blots (WB) containing the lysate (L) and IP products (IP) were then probed with anti-HCN2 and anti-GFP antibodies. A doublet was recognized by both antibodies in the stably transfected but not parental Hek cell line, suggesting that the doublet represents GFP-HCN2 channels. The band present at 50kDa in the IP lanes corresponds to the heavy chain of the anti-rabbit antibody used in the IP experiment. The anti-rabbit secondary antibody used in the GFP western blot produced a strong signal. The anti-mouse secondary antibody used in the HCN2 western blot produced a much weaker signal

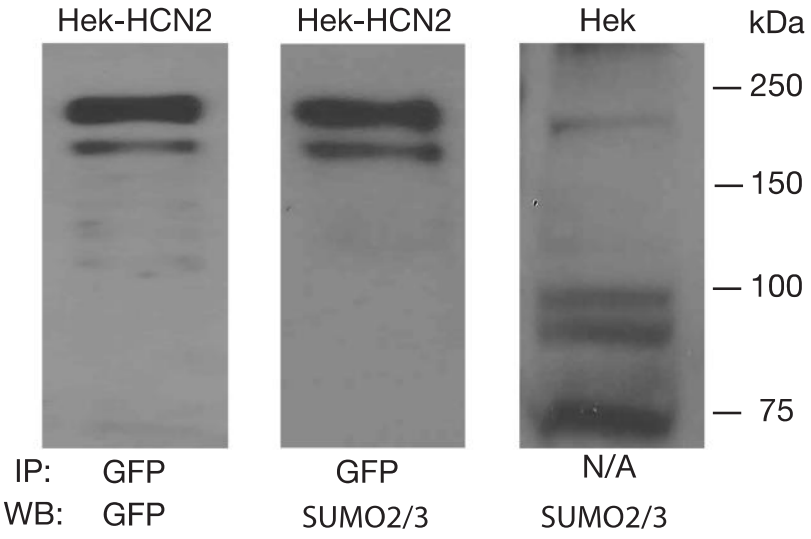

Figure 3.3 GFP-HCN2 channels are SUMOylated in Hek-HCN2 cells
Cell lysates from the Hek-HCN2 cell line were used in IP experiments with an antibody against GFP. Western blots containing the IP products were then probed with an anti-GFP antibody or an anti-SUMO2/3 antibody. Parental Hek cell lysates were also probed with the anti-SUMO2/3 antibody. The anti-SUMO2/3 antibody recognized the GFP-HCN2 doublet in the Hek-HCN2 cell line, but not in the parental cell line, suggesting that GFP-HCN2 channels are SUMOylated

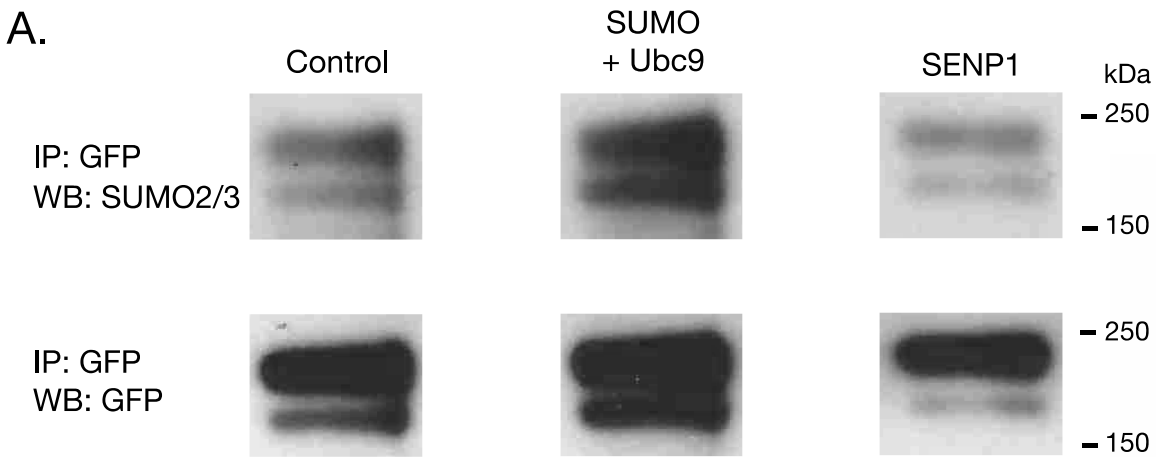
A.
Control
SUMO
+ Ubc9
SENP1
kDa
IP: GFP
WB: SUMO2/3
250
150
IP: GFP
WB: GFP
250
150

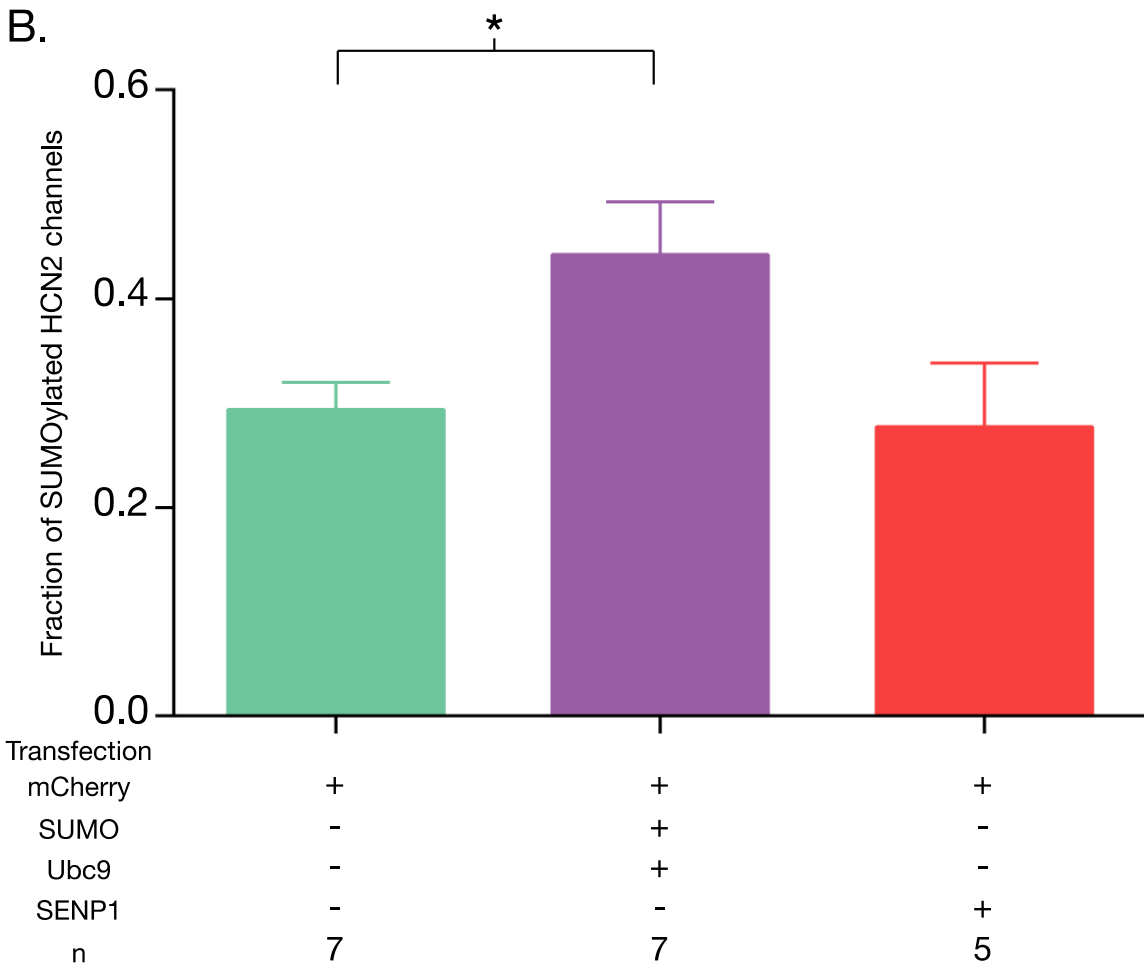
B.
*
0.6
0.4
0.2
0.0
Fraction of SUMOylated HCN2 channels
Transfection
mCherry + + +
SUMO - + -
Ubc9 - + -
SENP1 - - +
n 7 7 5

Figure 3.4 Transient transfection with SUMO and Ubc9 leads to an increase in GFP-HCN2 channel SUMOylation

The stable Hek-HCN2 cell line was transiently transfected with mCherry (control), or mCherry+SUMO+Ubc9, or mCherry+SENP1. Two days after transfection, cell lysates were used in IP experiments with an anti-GFP antibody. IP products were resolved with SDS-PAGE and transferred to western blots (WB). Blots were probed with an anti-SUMO2/3 antibody. After recording the result, blots were stripped and reprobed with an anti-GFP antibody. **(A)** Representative blots showing typical chemiluminescent signals for the GFP-HCN2 channel doublet after probing with the anti-SUMO2/3 antibody (upper panel) followed by stripping and re-probing with the anti-GFP antibody (bottom panel). Note that the amount of IP product varied between experiments but not across treatment groups as determined by measures of the GFP OD's (One-way ANOVA, $F(2,16)= 0.1285$; $p=0.8804$). **(B)** The fraction of SUMOylated HCN2 channels in each treatment group (SUMO doublet OD÷GFP doublet OD, see text) is plotted as the mean+SEM. The treatment and the n are shown below each plot. Each n represents a single plate that was transfected and carried through the experiment to produce a single lane on a western blot. Asterisk represents a statistically significant difference from control (One-way ANOVA with a Dunnett's post-hoc, $F(2,16)= 4.121$; $p=0.0360$)

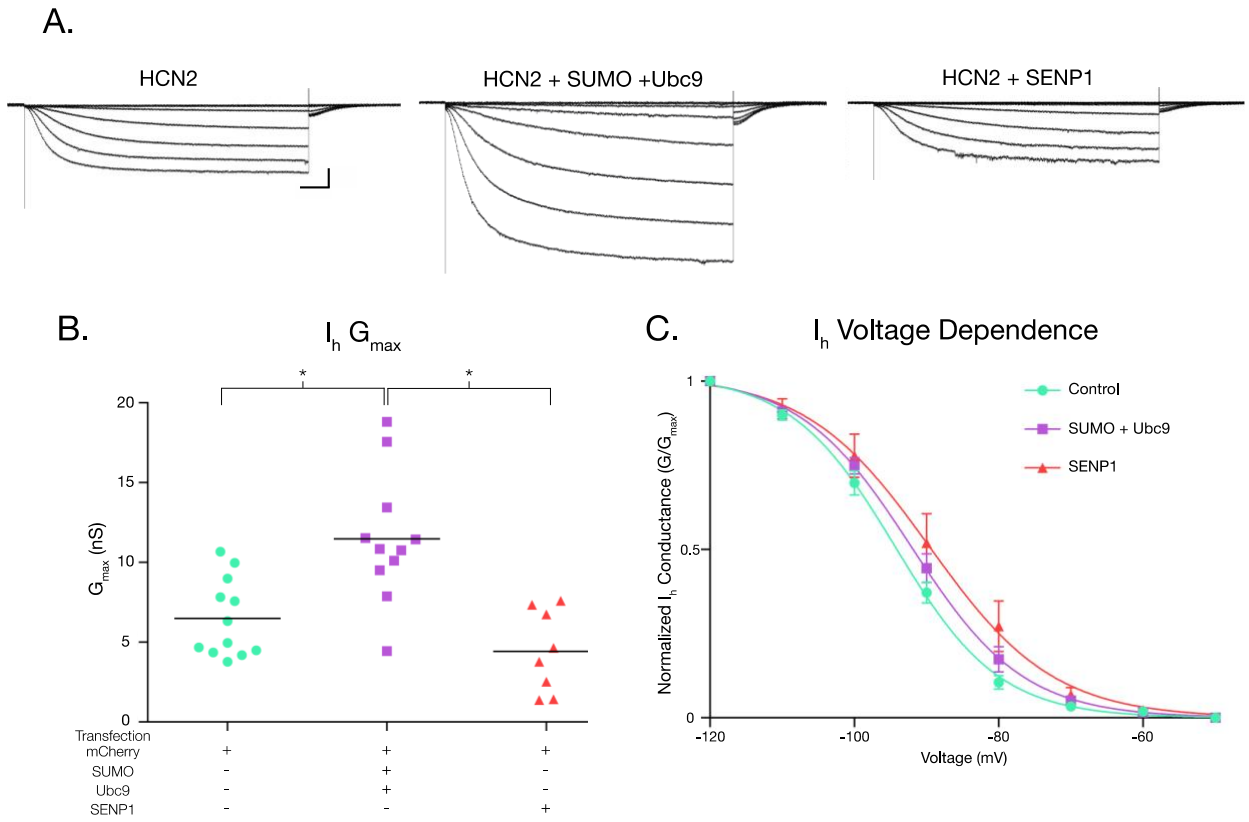

Figure 3.5 Increased HCN2 channel SUMOylation augments I_h G_{max}

I_h was measured in Hek-HCN2 cells transiently transfected with either mCherry (control), mCherry+SUMO+Ubc9, or mCherry+SENP1. For each treatment group, data were pooled from ≥ 3 transfections. **(A)** Representative traces for each treatment group, elicited by stepping the voltage from -50mV to -120mV in 10mV increments. Scale bars, 500ms and 200pA. The kinetics of activation at -120mV were not altered across treatment groups. Mean activation time constants: control, 400.9 ± 23.01; SUMO+Ubc9, 407.3 ± 33.67; SENP1, 497.4 ± 50.79; One-way ANOVA, $F(2,32)= 2.224$; $p=0.1246$. **(B)** Plots of I_h G_{max} for each treatment group. Each data point represents a single cell. Bar represents the mean. Transfection with SUMO+Ubc9 significantly increased I_h G_{max} relative to SENP1 and control treatment groups (asterisks, $p<0.05$; One-way ANOVA with Tukey's post-hoc, $F(2,28)= 13.23$; $p< 0.0001$). **(C)** Plots of voltage dependence of activation. Each data point represents the mean ± SEM. There were no significant differences between treatment groups for mean V_{50} (control, -93.88 ± 1.12; SUMO+Ubc9, -91.6 ± 1.29; SENP1, -87.8 ± 3.03; One-way ANOVA, $F(2,32)= 3.006$; $p=0.0636$) or mean slope (control, -6.61 ± 0.29; SUMO+Ubc9, -7.42 ± 0.41; SENP1, -6.84 ± 0.4; One-way ANOVA, $F(2,32)= 1.439$; $p= 0.252$)

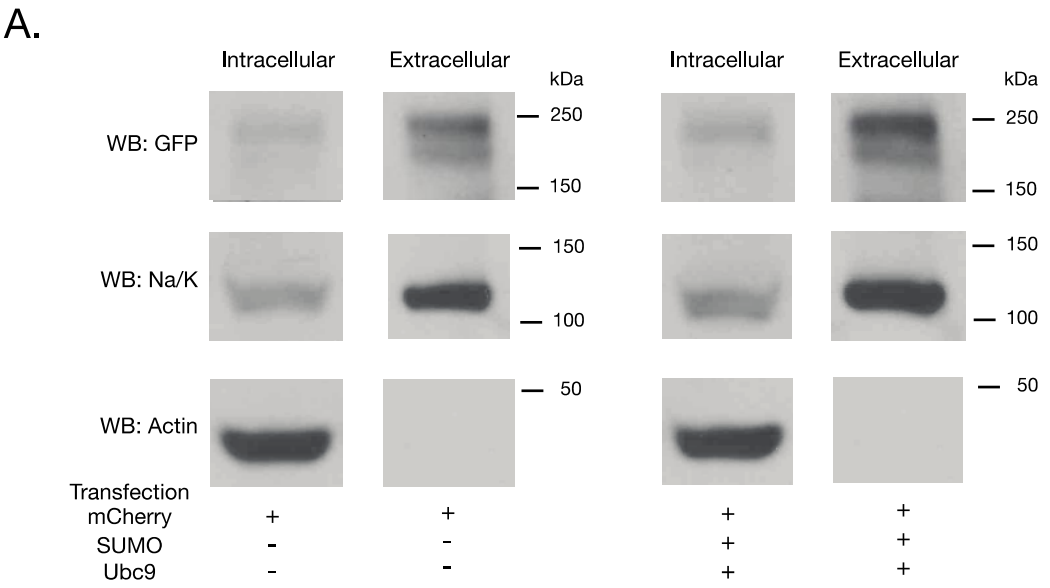
A.
Intracellular
Extracellular
kDa
Intracellular
Extracellular
kDa
WB: GFP
250
150
250
150
WB: Na/K
150
100
150
100
WB: Actin
50
50
Transfection
mCherry + + + +
SUMO - - + +
Ubc9 - - + +

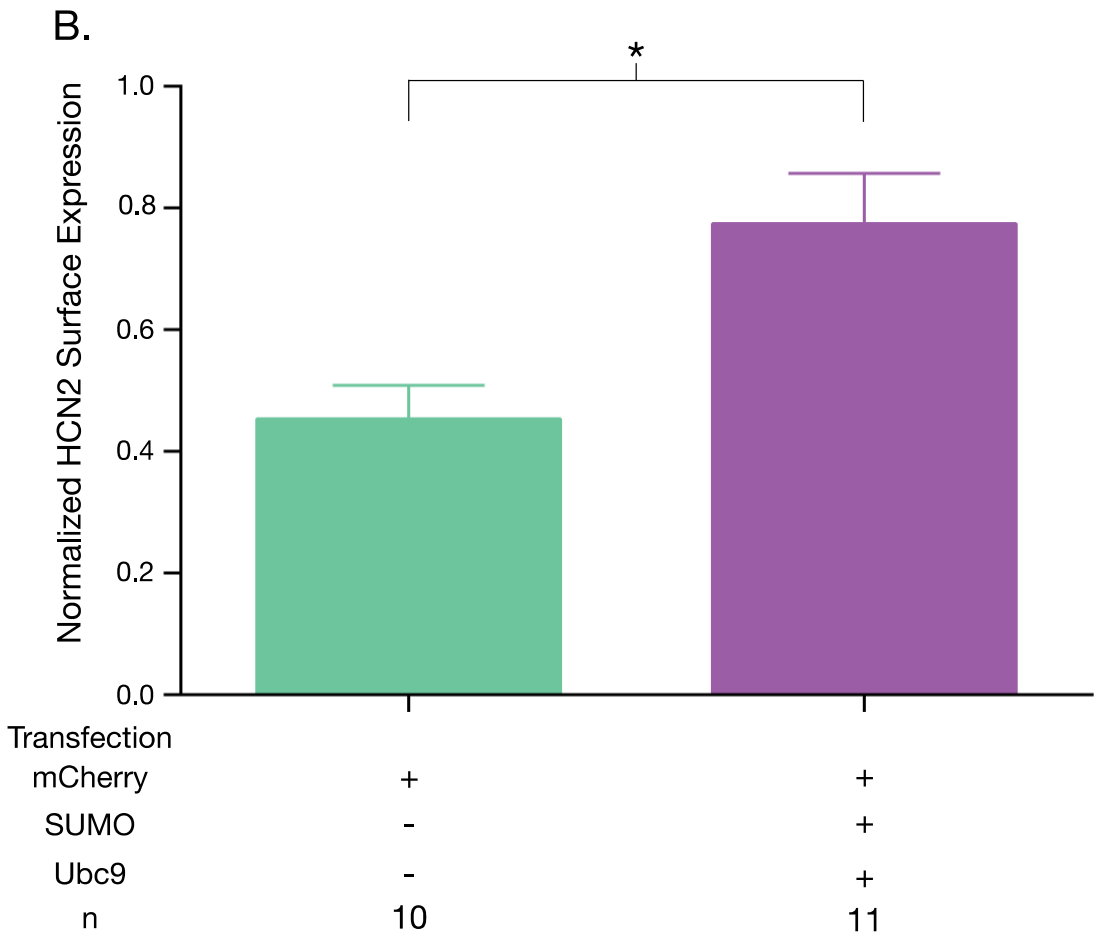
B.
*
Normalized HCN2 Surface Expression
1.0
0.8
0.6
0.4
0.2
0.0
Transfection
mCherry + +
SUMO - +
Ubc9 - +
n 10 11

Figure 3.6 Increased SUMOylation augments HCN2 channel surface expression

GFP-HCN2 channel cell surface expression was monitored using a biotinylation assay. Hek-HCN2 cells were transiently transfected with mCherry alone or mCherry+SUMO+Ubc9. Two days after transfection cultures were biotinylated and cell surface proteins were isolated from cell lysates using Neutravidin. Both the intracellular and cell surface fractions were run on a western blot and probed with antibodies recognizing GFP, Na^+/K^+-ATPase, and Actin. **(A)** Representative western blots. **(B)** Plots depicting average normalized GFP-HCN2 channel surface expression (GFP doublet OD÷Na^+/K^+-ATPase OD). The treatment and the n are shown below the graph. Each n represents a single plate that was transfected, biotinylated and carried through the experiment to produce a single lane on a western blot. Asterisk indicates significant difference between treatment groups (Student's t-test, $p<0.05$)

Figure 3.7 Identification of HCN2 channel SUMOylation sites

Amino acid sequences for the vertebrate and invertebrate HCN channel were aligned: mouse HCN1 (NP_034538), mouse HCN2 (NP_032252), mouse HCN3 (NP_032253), mouse HCN4 (NP_001074661), spiny lobster HCN (ABI94038). Putative SUMOylation sites predicted by SUMOplot freeware are indicated in blue (not mutated this study) or red (mutated in this study). The six transmembrane domains (yellow) and CNBD (blue) have been highlighted

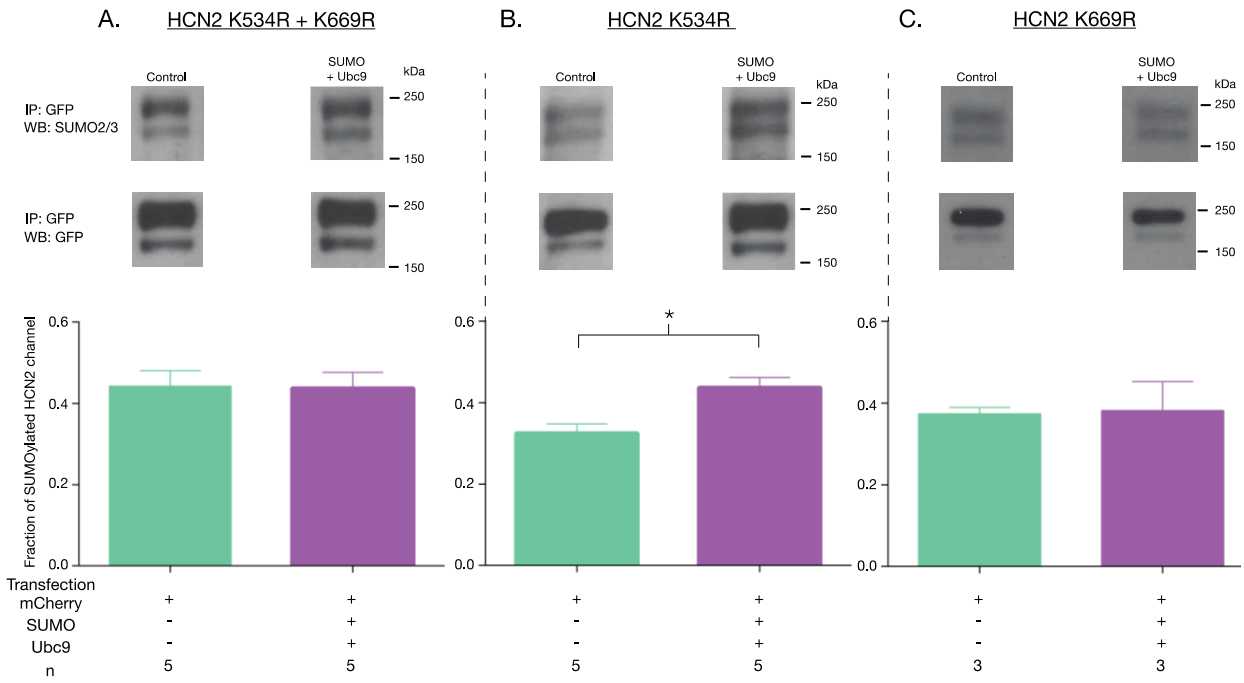

Figure 3.8 Overexpression of SUMO and Ubc9 enhances SUMOylation at K669
The three mutant cell lines **(A-C)** were transiently transfected with mCherry or mCherry+SUMO+Ubc9. Cell lysates were used in IP experiments with anti-GFP antibodies. Western blots containing IP products were probed with the anti-SUMO2/3 antibody, stripped and reprobed with the anti-GFP antibody. *Top Panel*: Representative blots showing the GFP-HCN2 doublet that was measured. *Bottom Panel:* Plots of the fraction of SUMOylated GFP-HCN2 channels in each mutant cell line, mean+SEM. The treatment and the n are shown below the graph. Each n represents one plate that was transfected and carried through the experiment to produce a single lane on a western blot. Asterisk, significantly different (Student's t-test, $p<0.05$)

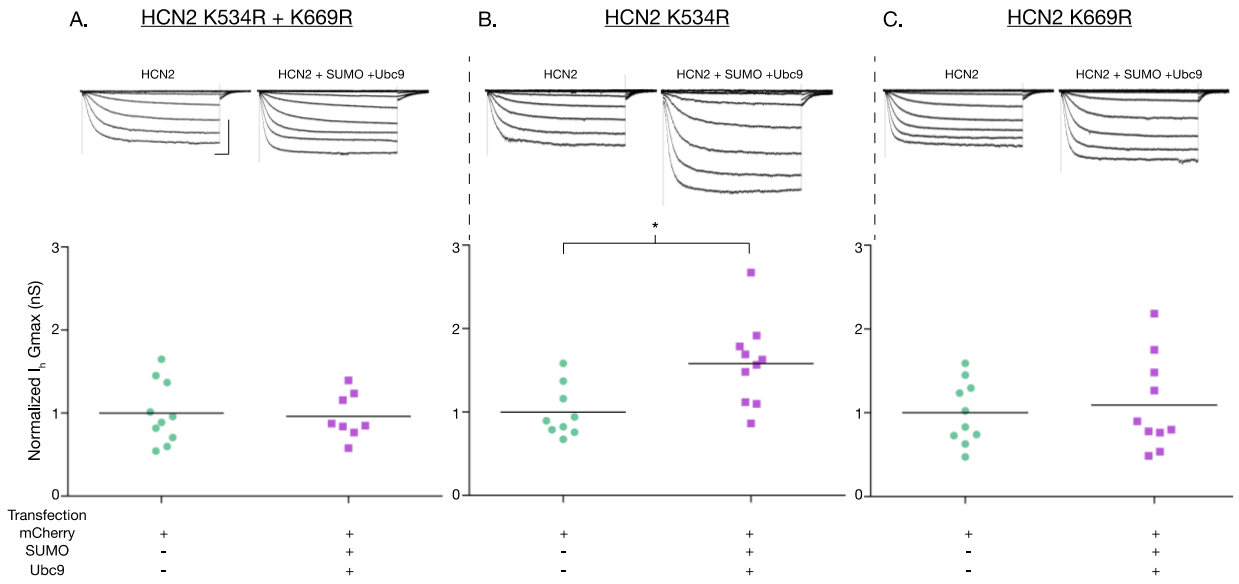

Figure 3.9 Enhanced SUMOylation at K669 augments I_h G_{max}

I_h G_{max} was measured following transient transfection with mCherry or mCherry+SUMO+Ubc9 in the three mutant cell lines **(A-C)**. *Top panel*: Representative traces for each treatment group for each mutant cell line. Scale bars, 500 ms, and 500 pA, *Bottom Panel*: Plots of normalized I_h G_{max} (G_{max} ÷ mean mCherry G_{max}) for each mutant cell line. I_h G_{max} was normalized to account for differences in overall expression of the HCN2 channels between the different mutant cell lines, most likely due to difference in the copy number of the plasmid integrated into the genome. Each data point represents a single cell. Asterisk, significantly different (Student's t-test $p<0.05$, recordings were pooled from ≥ 3 separate transfections)

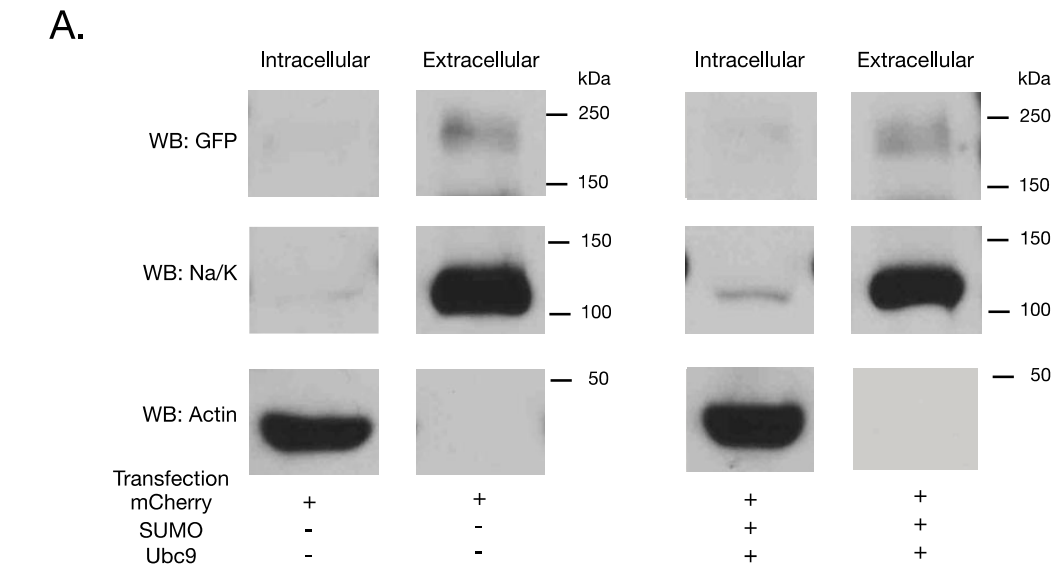
A.
Intracellular
Extracellular
kDa
Intracellular
Extracellular
kDa
WB: GFP
250
150
250
150
WB: Na/K
150
100
150
100
WB: Actin
50
50
Transfection
mCherry + - + +
SUMO - - + +
Ubc9 - - + +

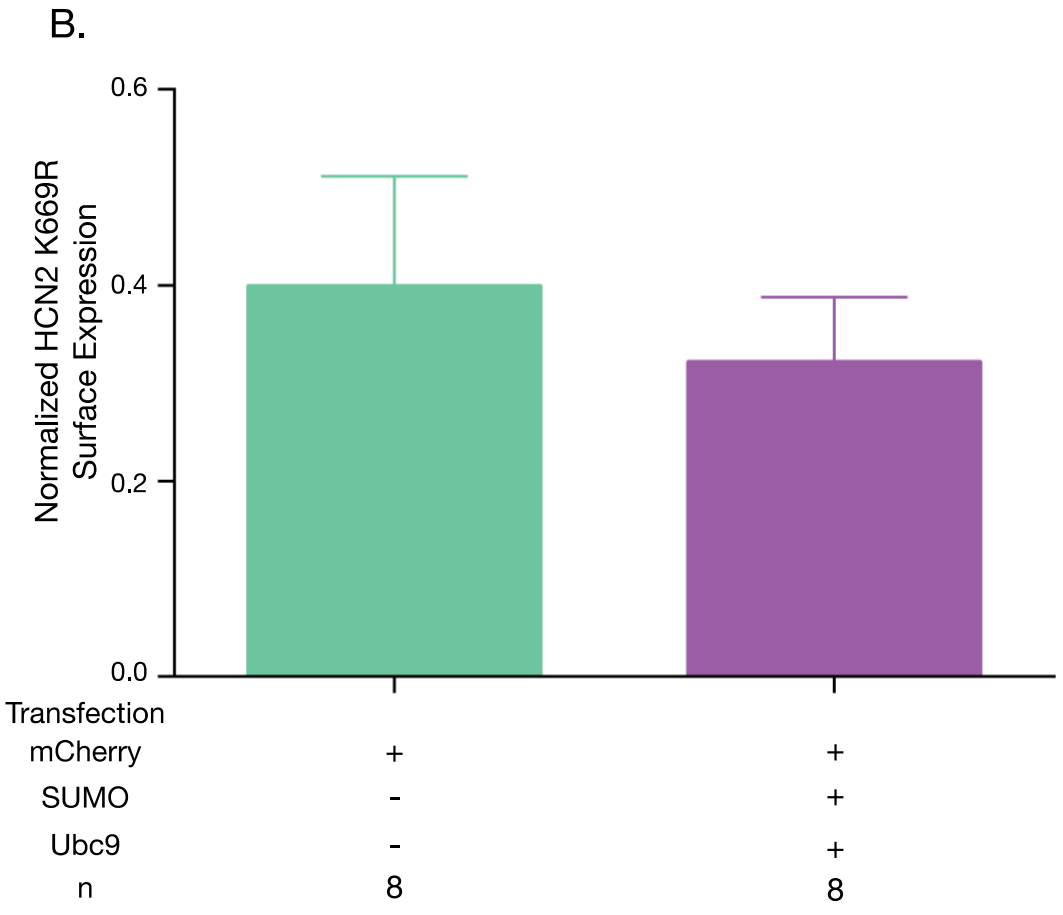
B.
Normalized HCN2 K669R Surface Expression
0.6
0.4
0.2
0.0
Transfection
mCherry + +
SUMO - +
Ubc9 - +
n 8 8

Figure 3.10 Enhanced SUMOylation at K669 increases GFP-HCN2 channel surface expression

The K669R mutant cell line was transiently transfected with mCherry or mCherry+SUMO+Ubc9, followed by the biotinylation assay to measure GFP-HCN2 surface expression. **(A)** Representative blots probed with anti-GFP and anti-Na/K ATPase antibodies **(B)** Plots of normalized GFP-HCN2 channels in each treatment group. The treatment and the n are shown below the graph. Each n represents a single plate that was transfected, biotinylated and carried through the experiment to produce a single lane on a western blot. There was no significant difference between treatment groups (Student's t-test, p=0.5606)

Table 3.1 Primary Antibodies

Antigen	Verification of specificity	Manufacturer, Species, cat no.	Concentration used
SUMO2/3	Specificity verified by company through WB analysis of Hek-293 cells transfected with SUMO2	Santa Cruz Biotechnology, rabbit polyclonal, cat. no. sc-32873	WB: 1:3000
SUMO1	Specificity verified by company through WB analysis of Hek-293 with and without SUMO1 expressed	Santa Cruz Biotechnology, rabbit polyclonal, sc-9060	WB: 1:3000
GFP (for WB)	Specificity verified by company through WB analysis of cells with and without GFP expressed	Santa Cruz Biotechnology, rabbit polyclonal, cat. no. sc-8334	WB: 1:4000
GFP (for IP)	We verified specificity through WB analysis (Fig 3.2)	Abcam, rabbit polyclonal, cat. no. ab290	1µl per 500µg of lysate
HCN2	Specificity verified by company through WB analysis of cells with and without HCN2 expressed	Santa Cruz Biotechnology, goat polyclonal, sc-19708	WB: 1:3000 (Hek cells)
HCN2	Specificity verified by company through WB analysis of mouse and rat membrane proteins	UC Davis/NIH NeuroMab, mouse monoclonal, N71/37	WB 1:200 (Mouse brain)
Actin	Specificity verified by company through WB analysis of non-transfected and β-Actin transfected Hek-293 cells	Santa Cruz Biotechnology, rabbit polyclonal, sc-1616-R	WB: 1:2000
Na^+/K^+-ATPase	Specificity verified by company through WB analysis of Human, Mouse and Rat tissues expressing the Na^+/K^+-ATPase	Abcam, mouse monoclonal, cat. no. ab7671	WB: 1:3000

Table 3.2 Site directed mutagenesis primers

Primer Name	Primer Sequence
mHCN2K534RFor	5’-CACAGCCATGCTGACAAAGCTCAgATTTGAGGTCTTCCAGCCTGG-3’
mHCN2K534RRev	5’ –CCAGGCTGGAAGACCTCAAATcTGAGCTTTGTCAGCATGGCTGTG-3’
mHCN2K669RFor	5’ –GCCATCATCCAGGAGATTGTCAgATATGACCGTGAGATGGTGCAGC-3’
mHCN2K669RRev	5’ –GCTGCACCATCTCACGGTCATATcTGACAATCTCCTGGATGATGGC-3’

4 CHAPTER 2: TONIC NM DOPAMINE CAN PERMIT OR PREVENT SUMOYLATION-MEDIATED ACTIVITY-DEPENDENT REGULATION OF IONIC CURRENTS

In Preparation: **Parker, A. R.**, L. A. Forster and D. J. Baro (2017). " Tonic nM dopamine can permit or prevent SUMOylation-mediated activity-dependent regulation of ionic currents "

Contribution Disclosure: Authors A. Parker and D. Baro were responsible for the conception and design of the research presented here. Authors A. Parker and L. Forster provided substantial contribution to the acquisition and analysis of the data presented here. All authors also provided input during the drafting and revision of the manuscript.

4.1 Abstract

Homeostatic mechanisms can co-regulate ionic conductances to stabilize neuronal activity features. In the Lateral Pyloric neuron (LP) of the crustacean stomatogastric ganglion, a positive correlation between the transient potassium current (I_A) and the hyperpolarization-activated current (I_h) stabilizes activity phase. Previous studies indicated a slow mechanism produced a positive correlation between the transcripts encoding the channels mediating LP I_A and I_h. Here we show a second mechanism exists whereby activity can rapidly co-regulate the currents by controlling the level of post-translational modification by Small Ubiquitin-like Modifier (SUMO). Changes in activity produced opposing changes in the SUMOylation associated with LP I_A and I_h. SUMOylation had opposing effects on LP I_A and I_h amplitudes. Thus activity-dependent SUMOylation specified a positive correlation between LP I_A and I_h. Tonic nM DA reconfigured the targets of the SUMOylation machinery, suggesting that the composition of modulatory tone will permit or prevent the correlations specified by activity-dependent SUMOylation.

4.2 Introduction

Homeostatic processes stabilize neuronal output by producing compensatory changes in synaptic strengths and ionic current densities in response to altered activity (O'Leary and Wyllie 2011, Davis 2013). One of the earliest demonstrations that neuronal output could be stabilized by adjusting ionic current densities in an activity-dependent manner was a computational model based on the lateral pyloric neuron (LP) that produces rhythmic bursts of action potentials (Fig 4.1A). The computational neuron attained a robust output by modulating the maximal conductances (G_{max}) of its seven ionic currents in response to activity perturbations that altered Ca^{2+} concentration (LeMasson, Marder et al. 1993). Subsequent experimentation demonstrated that compensatory changes in current densities may be evoked by a variety of activity perturbations produced by physically isolating network neurons (Turrigiano, Abbott et al. 1994), chronic pharmacological applications (Desai, Rutherford et al. 1999, Ishikawa, Mu et al. 2009, O'Leary, van Rossum et al. 2010, Driscoll, Muraro et al. 2013) and genetic knock-out/over-expression of a specific conductance(s) (Linsdell and Moody 1994, Swensen and Bean 2005, Peng and Wu 2007). These experimental approaches inevitably highlighted slow mechanisms that operated at the level of transcription and/or translation (Driscoll, Muraro et al. 2013, Kirchheim, Tinnes et al. 2013, Pozzi, Lignani et al. 2013), which led to computational models of activity homeostasis that used slow feedback control mechanisms to regulate ionic current densities (Golowasch, Casey et al. 1999, Olypher and Prinz 2010, O'Leary, Williams et al. 2014). The term Homeostatic Intrinsic Plasticity (HIP) is used to describe slow, activity-dependent, compensatory adjustments in ionic current densities that persist beyond the initiating stimuli (Mitchell and Johnson 2003). While HIP appears to stabilize neuronal output over the long-term, it cannot offset the fast positive feedback associated with Hebbian learning (Zenke, Gerstner et

al. 2017). There are examples of rapid compensatory changes in ionic current densities that stabilize neuronal activity over shorter timescales (van Welie, van Hooft et al. 2004, Fan, Fricker et al. 2005, Steinert, Robinson et al. 2011). These mechanisms are thought to act post-translationally and produce transitory alterations in current densities, as such, they do not fall under the heading of plasticity. Transient changes that do not significantly outlast their stimuli are classified as modulation (Mitchell and Johnson 2003), and here we use the term Homeostatic Intrinsic Modulation (HIM) to mean rapid and transitory, activity-dependent modifications in ionic current densities that compensate for changes in activity.

We have been studying HIM in LP, a component of the pyloric pattern generating circuit which produces a constant rhythmic output (Marder and Bucher 2007). Although the frequency of the cyclic pyloric output can vary, the phase relationships of the neurons within each rhythmic cycle are invariant (Bucher, Prinz et al. 2005, Goaillard, Taylor et al. 2009), suggesting that a homeostatic mechanism(s) maintains LP activity phase. Covariation of ionic conductances can maintain specific neuronal activity features (Hudson and Prinz 2010, Soofi, Archila et al. 2012, Zhao and Golowasch 2012). LP phase depends, in part, on the balance between the transient potassium (I_A) and hyperpolarization activate (I_h) currents (Harris-Warrick, Coniglio et al. 1995, Zhao and Golowasch 2012). These two conductances are positively correlated in LP neurons (Temporal, Desai et al. 2012). We previously demonstrated that reducing LP I_A with bath-applied 5µM DA (Rodgers, Fu et al. 2011, Krenz, Hooper et al. 2013) or 4mM 4-AP (Krenz, Rodgers et al. 2015) altered LP phasing, but then, phase recovered over minutes. Further investigation showed that when the preparation was superfused with 5nM DA, incremental bi-directional changes in activity produced corresponding changes in LP I_h with a time constant of ~10min (Krenz, Rodgers et al. 2015). The phase recovery observed in our experiments could be

explained as follows: the reduction in I_A produced an incremental change in activity, which in turn led to a similar reduction in I_h through a DA-enabled, Ca^{2+}-dependent mechanism, and this restored the correlation. These findings are somewhat perplexing. Presumably, manipulation of non-I_A currents could produce a comparable change in activity, leading to an incremental reduction in LP I_h that would then disrupt the correlation between I_A and I_h. One possibility is that I_A and I_h are similarly regulated by activity. But if this were true, then a given change in either of the two conductances must alter activity in the same manner to maintain the correlation. This seems unlikely given that I_A and I_h are opposing conductances. It is reasonable to think that HIP and HIM are guided by similar principles. Studies on HIP show that multiple currents are simultaneously correlated (Zhao and Golowasch 2012) and that current compensation is non-reciprocal (Kim, Vienne et al. 2017). A recent computational model of HIP that required a neuron to preserve a set Ca^{2+} concentration was able to successfully maintain conductance correlations and activity features by regulating ion channel transcription in an activity-dependent fashion (O'Leary, Williams et al. 2014). A major limitation of this model was that it assumed functional protein levels were determined solely by mRNA abundance. This model could be improved by incorporating compensatory, activity-dependent post-translational mechanisms, but the molecular pathways involved in HIM are currently unknown.

In this study, we delve into the molecular mechanism responsible for the correlation between LP I_A and I_h and how it is regulated by modulatory tone. We reasoned that the Small Ubiquitin-like Modifier (SUMO) could be involved in HIM because it has been shown to regulate the surface expression of the Hyperpolarization-activated, Cyclic Nucleotide-gated (HCN) channels that mediate I_h (Parker, Welch et al. 2016). SUMO is a peptide that is post-translationally conjugated to target proteins in order to alter their protein-protein interaction

(Flotho and Melchior 2013). Target protein SUMOylation states are dynamically regulated by the opposing actions of conjugating and deconjugating enzymes (Flotho and Melchior 2013). The SUMO system is thought to coordinately regulate groups of proteins that are functionally related (Hay 2005, Jentsch and Psakhye 2013, Seifert, Schofield et al. 2015), and it has the potential to coordinate fast and slow negative feedback loops by simultaneously decorating proteins mediating HIM, e.g., ion channels, and HIP, e.g., transcription factors. Neuronal activity and activation of G-protein coupled receptors can alter the location and activity of the SUMOylation machinery (Jaafari, Konopacki et al. 2013, Loriol, Khayachi et al. 2013, Loriol, Casse et al. 2014), and target proteins can be SUMOylated in an activity-dependent manner (Chamberlain, Gonzalez-Gonzalez et al. 2012, Sun, Lu et al. 2014). SUMO is emerging as an important regulator of synaptic plasticity and in some cases, it is necessary for long-term potentiation (LTP) (Jaafari, Konopacki et al. 2013), long-term depression (LTD) (Chamberlain, Gonzalez-Gonzalez et al. 2012), and synaptic scaling (Craig, Jaafari et al. 2012); thus, the SUMO system also has the potential to coordinate positive and negative feedback loops. Here we explore the function of SUMOylation in specifying the correlation between LP I_A and I_h, and the permissive role of tonic 5nM DA in this process.

4.3 Methods

4.3.1 Animals

California spiny lobsters, *Panulirus interruptus*, were purchased from Marinus Scientific (Long Beach, CA) and Catalina Offshore Products (San Diego, CA). Lobsters were maintained at 16°C in aerated and filtered seawater. Animals were anesthetized on ice before dissection.

4.3.2 Chemicals

Tetrodotoxin (TTX) was purchased from Tocris Bioscience (Bristol, UK), Tween20 was purchased from Fisher Scientific and all other chemicals were purchased from Sigma-Aldrich (St. Louis, MI, USA). DA was made fresh every 30min to minimize oxidation.

4.3.3 Antibodies

An antibody against the lobster HCN channel (anti-HCN) was synthesized. DNA corresponding to amino acids 362-390 (Genbank Accession# DQ865250) was cloned into a PGex vector (Amersham) and the peptide was isolated according to the manufacturer's instructions. The peptide served as an immunogen and was injected into a rabbit. Serum obtained from an immunized rabbit was affinity purified on a column containing the antigenic peptide. Antibody specificity was demonstrated in IP and western blot experiments using Hek cells that stably overexpressed the lobster HCN channel (Supp Fig 4.2).

Bethyl Laboratories (Montgomery, TX) was contracted to produce a custom affinity purified goat polyclonal antibody against a peptide corresponding to ORF-J (5'-CVGGPPLHPSAITTTNTNTAT-3') of the shal (Kv4) protein (Baro, Quinones et al. 2001). Anti-ORF-J and a previously validated antibody against a different region of the lobster Kv4 protein (Baro, Ayali et al. 2000) recognized the same ~75kD band on western blots containing lobster nervous system protein lysates (Supp Fig 4.2).

All other antibodies were commercially obtained as indicated in the text and validated as indicated in Supp Fig 4.1 and Supp Fig 4.2. All secondary antibodies were obtained from Jackson ImmunoResearch Laboratories (West Grove, PA).

4.3.4 STNS Dissection and LP Identification

The stomatogastric nervous system (STNS) was dissected and pinned into a Sylgard dish. The stomatogastric ganglion (STG) was desheathed and isolated with a Vasoline well. The STG was constantly superfused with aerated *Panulirus* saline (479mM NaCl, 12.8mM KCl, 13.7mM $CaCl_2$, 39mM Na_2SO_4, 10mM $MgSO_4$, 2mM glucose, 4.99mM HEPES, 5mM TES at pH 7.4). Extracellular recordings were obtained by placing stainless-steel pin electrodes, connected to a differential AC amplifier (A-M Systems, Everett, WA, USA), directly against the pyloric dilator nerve (*pdn*) and lateral ventricular nerve (*lvn*) and insulating them with Vasoline. Intracellular somatic recordings were obtained using a high resistance electrode filled with 3M KCl (20–30 MΩ) and an Axoclamp 900A amplifier (Axon Instruments, Foster City, CA, USA). Neurons were identified by correlating action potentials from somatic intracellular recordings with extracellularly recorded action potentials on identified motor nerves, and by their characteristic shape and timing of oscillations. The process of dissection and cell identification took ~2–4h.

4.3.5 Somatic Two-Electrode Voltage Clamp (TEVC)

All experiments were performed at 19–22°C as measured with a temperature probe in the bath. Temperature changed by less than 1°C during an experiment. For TEVC experiments LP was impaled with two low resistance glass microelectrodes filled with 3M KCl (7-10MΩ) connected to an Axoclamp 900A amplifier. The STG was superfused with *Panulirus* saline containing TTX (100nM) to block voltage-dependent Na^+ channels. No other ion channel blockers were included.

LP I_h was elicited from a holding potential of -50mV using a series of 4sec voltage steps from the holding potential of -50mV to -120mV in 10 mV increments with 6sec between each step. LP I_h steady state peak current was measured by subtracting the initial fast leak current

from the slowly developing I_h at the end of each voltage step. Current was converted to conductance using E_{rev}=-35mV (Kiehn and Harris-Warrick 1992) and fitted to a first order Boltzmann equation.

LP I_A was measured as the peak difference current between a 50ms depolarizing step to +40mV that was preceded by a 200msec prepulse to -90mV vs. -40mV (Baro, Levini et al. 1997). I_A is largely blocked by 4mM 4-AP (Tierney and Harris-Warrick 1992). In our experiments, 5mM 4-AP blocked approximately 85-90% of the peak current. The current that remained in 4-AP appeared to be a mix of inward and outward currents. An inward current observed from ~ -10 to +20mV could be blocked by 200□M Cd^{2+} and was most likely the previously described small (~6nA), transient P/Q type calcium current that has a steady-state inactivation profile highly similar to I_A in crustacean motor neurons (Ransdell, Temporal et al. 2013). Ca^{2+} currents could not be blocked since we were studying activity-dependent changes in I_A and I_h. The outward currents observed in 4-AP were presumably residual I_A, I_{KCa} and I_{KD}. The small mixed current that remained in 4-AP was not obviously modulated by activity in the presence or absence of 5nM DA (Kruskal Wallis test, *no DA*: p=0.9286, n=3; *5nM DA*: p=0.5107, n=3), suggesting that the activity- and DA-dependent changes we observed represented alterations in peak I_A.

4.3.6 SUMO cloning

A complete *Panulirus interruptus* SUMO cDNA was isolated using a combination of degenerate PCR and RACE. Total RNA was isolated from lobster nervous system tissue with Trizol and used as the template in a reverse transcription with Superscript according to manufacturer's instruction. The resulting cDNA served as a template in a degenerate PCR and RACE reactions (Baro, Cole et al. 1994). Degenerate primers (Table 4.1) were designed based

on an alignment of *Drosophila melanogaster* Smt3 (Genbank accession:NM_058063), *Mus musculus* SUMO 2 (Genbank accession:NM_133354), and *Mus musculus* SUMO 3 (Genbank accession:BC115488). The predicted ~180bp PCR product was gel isolated and cloned into a pDrive vector (Qiagen) and sequenced. Lobster specific RACE primers (Table 4.1) were designed. The 3' end of the SUMO transcript was obtained using lobster specific forward primers (Table 4.1; Specific For1 and For2) and a SMARTer RACE kit (Clontech), following the manufacturer's instructions. The 5' end of the SUMO transcript was obtained using lobster specific reverse primers (Table 4.1; Specific Rev1 and Rev2) and a FirstChoice RLM RACE Kit (Ambion). All sequencing was performed by the GSU DNA core facility, and sequences were analyzed and manipulated with the Lasergene 10 suite of DNASTAR software.

4.3.7 Tat-SUMO Peptide Synthesis

cDNA representing the activated form of lobster SUMO, i.e. ending in diglycine (Supp Fig 4.1), was obtained in a PCR using lobster specific primers (Table 4.1; Tat-SUMO For and Rev). Standard recombinant DNA techniques were used to clone the predicted 274bp gel isolated PCR product into the EcoRI site of the pcDNA3 Tat HA vector (a gift from Matija Peterlin (Cujec, Okamoto et al. 1997); Addgene plasmid #14654), thereby creating an N-terminal Tat-HA-His tagged SUMO construct. In order to synthesize the Tat-SUMO peptide, the plasmid was transformed in BL21-CodonPlus (DE3)-RIPL E. coli (Agilent). A single isolated colony was grown overnight in 200ml of broth containing ampicillin (100µg/ml) at 37°C with agitation. The 200ml overnight culture was then added to 1L of broth containing 500µM IPTG to induce expression of the peptide, and further incubated for 5hr. Cells were pelleted at 8,000rmp for 10min at 4°C, and the pellet was washed with ice cold PBS (137mM NaCl, 2.7mM KCl, 10mM Na_2HPO_4, 1.8mM KH_2PO_4, pH7.4). Pelleted cells were resuspended in 20ml of Buffer Z (8M

Urea, 100mM NaCl, 20mM HEPES, pH8) and sonicated on ice using a 10sec "on" 30sec "off" protocol at 15% amplitude for a total of 10min. Sonicate was cleared by centrifuging at 12,000rpm for 10mins at 4°C. Cleared sonicate was equilibrated with 10mM imidazole and incubated with 10ml of Ni-NTA agarose resin (Qiagen) at 4°C for 1hr. Resin was washed with 100ml of Buffer Z equilibrated with 10mM imidazole. Peptide was eluted with incrementally increasing concentrations of imidazole (100, 250, 500mM, and 1M; 10ml each) and the buffer was exchanged for PBS with 10% glycerol using PD-10 desalting columns (GE Healthcare). Peptide concentration was determined by BCA assay (Pierce).

4.3.8 Immunoprecipitation and Western Blots

Lobster nervous system lysates were prepared by homogenizing lobster nervous system tissue in NP-40 lysis buffer (50mM Tris HCl pH7.4, 150mM NaCl, 1% NP-40, 20mM NEM, protease inhibitor cocktail at 1:100). Homogenate was incubated at 4°C with agitation and then centrifuged at 12,000rpm for 20min to pellet cell debris. Protein concentration was determined by BCA assay (Pierce). Immunoprecipitation (IP) was performed using Dynabeads Protein G (Invitrogen). Briefly, 10µg of antibody was incubated with the beads in 0.1M Na acetate pH 5.3 for 1hr at room temperature with agitation. Beads were washed three times with 0.1M Na acetate pH 5.3 plus 0.01% Tween-20, 2mg of cell lysate was added to the beads and the mixture was incubated for 90min at room temperature with agitation. Finally, the beads were washed three times with PBS plus 0.01% Tween-20 and eluted in 20µl of 50mM Glycine pH 2.8 by heating to 70°C for 10min. Western blot experiments were as previously described (Parker, Welch et al. 2016). Primary antibody concentrations used for western blots were as follows: anti-HCN, 1:5000, anti-ORF-J, 1:4000, anti-SUMO, 1:4000.

4.3.9 Statistical Analysis

All data were analyzed using Prism 7 (Graphpad Software Inc.). No statistical methods were used to compute sample size. Each data set was checked for normality and homogeneity of variance and unless otherwise stated data were analyzed using parametric statistical tests. In all cases, the significance threshold was set at $p < 0.05$. Values that were greater than two standard deviations from the mean were considered statistical outliers and were excluded from the data set. ANOVA's were followed by post hoc tests as indicated. All values are presented as the mean±SEM.

4.4 Results

4.4.1 DA reconfigures the activity-dependence of LP I_h and I_A

LP phase depends, in part, upon a positive correlation between LP I_A and I_h (Zhao and Golowasch 2012). When LP phase is disrupted by reducing LP I_A, phase can recover over minutes, but only in the presence of tonic nM DA; and, tonic nM DA permits activity to regulate LP I_h (Rodgers, Fu et al. 2011, Krenz, Hooper et al. 2013, Krenz, Rodgers et al. 2015). We hypothesize that LP I_A is regulated by activity in the presence and/or absence of DA, and that DA allows activity-dependent co-regulation of I_A and I_h to maintain LP phase. We tested this hypothesis by examining if/how activity regulated LP I_A in the presence and absence of tonic nM DA.

LP shows spontaneous ~1Hz, ~20mV oscillations in membrane potential that traverse the ~ -60 to -40mV range. There is a plateau of variable duration at the depolarized potential (Fig 4.1A). This slow wave activity is generated in the somatodendritic compartment. Spiking activity is generated at the spike initiation zone on the axon/primary process. Spikes do not actively propagate into the somatodendritic compartment; rather, they passively spread and can be seen

riding on the depolarized plateau in somatic intracellular recordings (Fig 4.1A). Duty cycle, defined as plateau duration divided by cycle period, represents the fraction of the cycle during which LP is maximally depolarized. We previously demonstrated that changes in duty cycle can regulate LP I_h in the presence of tonic nM DA (Fig 4.1B). We used the same standard paradigm to investigate whether changes in slow wave activity affected LP I_A in the presence and absence of tonic 5nM DA. LP spontaneous slow wave and spike activities were blocked with 10-7M TTX, and TEVC was used to implement a repetitive voltage step that mimicked slow waves (Fig 4.1A).

The experiment is diagrammed in Fig 4.1A. The preparation was dissected and continuously superfused with saline. The LP neuron was identified with electrophysiological recordings. At t=-10min LP plateau duration, cycle period, peak and nadir voltages were measured, and three voltage protocols were constructed for that particular neuron using Clampex. A 0%ΔDC protocol exactly mimicked LP plateau duration, cycle period, peak and nadir voltages. A +50%ΔDC protocol increased the duration of the depolarized step by 50% and decreased the time between steps to maintain a constant cycle period. A -100%ΔDC protocol abolished slow waves by holding LP at its resting potential in TTX (-59mV on average) with no voltage step applied. TTX was applied at t=-5min, and the voltage protocols were implemented as depicted. The percent change in the peak I_A resulting from the +50%ΔDC and -100%ΔDC relative to 0%ΔDC voltage protocols was plotted (Fig 4.1C). The results demonstrated that in the absence of tonic 5nM DA, peak LP I_A was regulated by slow wave activity in a manner very similar to that observed for LP I_h G_{max} in the presence of DA. The -100%ΔDC protocol significantly increased the mean peak LP I_A by 13 ± 2.2% while the +50%ΔDC protocol produced a significant 14 ± 3.3% decrease in the mean peak LP I_A.

In order to test the effect of tonic 5nM DA, a separate series of experiments was performed exactly as described except that 5nM DA was added to the superfusate immediately after the first measure of LP I_A (t=0). Previous work showed tonic 5nM DA did not obviously alter LP I_A G_{max} over the short term (Zhang, Rodgers et al. 2010, Rodgers, Krenz et al. 2011, Rodgers, Krenz et al. 2013). The addition of 5nM DA to the superfusate abolished slow wave activity-dependent changes in LP I_A (Fig 4.1C). These data disproved our hypothesis. Even though changes in slow wave activity similarly regulated LP I_A and I_h, tonic nM DA simultaneously disabled and enabled their respective activity-dependence. Thus, the two conductances would not be correlated in the presence of tonic nM DA alone (i.e. all modulatory input blocked with TTX and 5nM DA added to a constant superfusate). However, we have shown that addition of DA to an unblocked preparation (no TTX to block modulatory input) permitted phase recovery (Rodgers, Fu et al. 2011, Krenz, Rodgers et al. 2015). This suggests that slow wave activity may correlate LP I_A and I_h under the appropriate modulatory conditions.

4.4.2 Logic supporting link between SUMOylation and activity-dependent regulation of LP I_A and I_h

We previously demonstrated that tonic 5nM DA permitted bi-directional LP I_h activity-dependence by eliciting two simultaneous PKA-dependent events that could be pharmacologically uncoupled (Krenz, Rodgers et al. 2015): *event 1*- a ~12% activity-independent increase in LP I_h G_{max}, and *event 2*- a calcineurin-mediated decrease in LP I_h G_{max}. Calcineurin is a Ca^{2+}-calmodulin (CaM)-dependent phosphatase, and event 2 relied on Ca^{2+} entry through voltage-gated Ca^{2+} channels and Ca^{2+} release from stores, suggesting a Ca^{2+} induced Ca^{2+} release process. Bi-directional activity-dependence was achieved through the additive effects of events 1 and 2. Since event 1 was activity-independent, it was constant in all three voltage protocols

(~12% increase in I_h G_{max}). On the other hand, event 2 (Ca^{2+}-dependent decrease in I_h G_{max}) was minimal, maximal and intermediate during the -100%ΔDC, +50%ΔDC, and 0%ΔDC protocols, respectively. The addition of events 1 and 2 produced an increase and a decrease in LP I_h G_{max}, respectively, during the -100%ΔDC and +50%ΔDC protocols relative to the 0%ΔDC protocol (Fig 4.1B). SUMOylation of mouse HCN channels, which mediate I_h, increased their surface expression and augmented I_h G_{max} in human embryonic kidney (Hek) cells (Parker, Welch et al. 2016). We therefore surmised that events 1 and 2 could correspond to an increase and decrease in HCN channel SUMOylation, respectively. Here we begin to test this hypothesis.

4.4.3 HCN and Kv4 channels are SUMOylated in vivo

To determine if lobster HCN and Kv4 channels, which respectively mediate I_h and I_A, were SUMOylated *in vivo*, we performed immunoprecipitation (IP) experiments with lobster CNS protein lysates followed by western blotting. IP experiments were carried out using custom affinity-purified antibodies against the lobster HCN channel (anti-HCN), the lobster Kv4 channel (anti-ORF-J) and IgG (negative control). Western blots containing the resulting IP products were probed with a commercially available affinity-purified antibody against SUMO (anti-SUMO), and either anti-HCN (Fig 4.2A) or anti-ORF-J (Fig 4.2B). Both HCN and Kv4 channels appeared to be SUMOylated *in vivo*. The anti-HCN and anti-SUMO antibodies recognized multiple matching bands in the anti-HCN but not the IgG IP product. The bands were in the correct size range for post-translationally modified HCN channel alternately-spliced isoforms (Ouyang, Goeritz et al. 2007). The anti-ORF-J and anti-SUMO antibodies recognized a single, appropriately sized, matching band in the anti-ORF-J but not the IgG IP product. The anti-SUMO antibody recognized additional bands not recognized by the channel antibodies in both

the anti-HCN and anti-ORF-J but not the IgG IP products. These may represent SUMOylated proteins that non-covalently interact with the channels.

4.4.4 SUMOylation is necessary for activity-dependent changes in LP I_h and I_A

We next determined if I_h and I_A were affected by anacardic acid, a cell permeable SUMOylation blocker (Fukuda, Ito et al. 2009). Either I_h or I_A was measured, then 100μM anacardic acid was or was not added to the superfusate and a 1hr 0%ΔDC voltage protocol was applied followed by TEVC to re-measure the current. No significant changes were observed in the absence of anacardic acid (Wilcoxon test, $p>0.1$, $n=3$ each for I_h and I_A). In the presence of anacardic acid, the mean LP I_h G_{max} significantly decreased by 14±4.5% and the mean peak I_A significantly increased by 9.7±2.8% (Fig 4.3A). These data suggest that dynamic SUMOylation contributes to the maintenance of LP I_h and I_A. We asked if anacardic acid could also block activity-dependence. Experiments similar to those diagrammed in Fig 4.1A were repeated except that anacardic acid was added to the superfusate for 1hr prior to the addition of TTX. The data indicated that blocking SUMOylation with anacardic acid abolished the DA-enabled activity-dependence of LP I_h (Fig 4.3B) and the activity-dependence of LP I_A in the absence of DA (Fig 4.3C). These data indicated that SUMOylation was necessary for activity-dependent changes in LP I_h and I_A.

4.4.5 Enhanced SUMO availability converts bi-directional into one-way DA-enabled LP I_h activity-dependence

If dynamic SUMOylation regulates LP I_h G_{max}, then enhancing SUMOylation should have the opposite effect of blocking SUMOylation. Furthermore, if DA enables activity-dependent SUMOylation, then enhancing SUMOylation should disrupt the permissive effect of tonic 5nM DA. We tested these hypotheses. The enzyme Ubc9 covalently links SUMO to a

lysine on a target protein (Desterro, Thomson et al. 1997). Ubc9 can either recognize a SUMO consensus sequence on a target protein and conjugate SUMO to the consensus sequence, or Ubc9 can be directed to a target by an E3 ligase or a SUMO Interaction Motif (SIM), in which case SUMOylation does not occur at a consensus sequence (Flotho and Melchior 2013). Approximately 63% of all SUMOylation occurs at consensus sequences, though this can change in a state-dependent manner (Hendriks and Vertegaal 2016). Simply increasing the concentration of SUMO and/or Ubc9 can enhance SUMOylation at consensus sequences (Dai, Kolic et al. 2009). We used this method to increase mouse HCN2 channel SUMOylation at an identified consensus sequence in a heterologous expression system, which resulted in augmentation of channel surface expression and I_h G_{max} (Parker, Welch et al. 2016). Here we used the same logic to increase SUMOylation at consensus sequences in the LP neuron to test if/how this affected I_h G_{max} and activity-dependent regulation of I_h.

We cloned lobster SUMO cDNA (GenBank accession: MF770707) and used standard techniques to generate an N-terminal Tat-tagged SUMO peptide (Supp Fig 4.1). The activated form of the peptide that ends in a C-terminal di-glycine was created; it required no further proteolytic processing before addition to a target (See Supp Fig 4.1)(Mukhopadhyay and Dasso 2007). Peptides tagged with an HIV-Tat sequence are rapidly taken up by cells (Fawell, Seery et al. 1994). After confirming that the activated Tat-SUMO peptide was successfully taken up by crustacean neurons (Supp Fig 4.1), we tested its effect on LP I_h G_{max}.

The three standard voltage protocols were used in experiments as diagramed in Fig 4.4A. A 30min wash-in of activated Tat-SUMO had the opposite effect of blocking SUMOylation; it produced a stable and significant 11±1.5% increase in the mean LP I_h G_{max} in the absence of DA (Fig 4.4B) as opposed to the ~14% decrease produced by anacardic acid blockade (Fig 4.3A).

The mean τ for the increase was 7.1min. The same result was obtained when the Tat-SUMO peptide was applied during a 30min -100%ΔDC or 0%ΔDC voltage protocol (Fig 4.4B), indicating that an activity-independent process transduced enhanced SUMO availability into an increase in LP I_h G_{max}. Note that DA-enabled event 1 produced an activity-independent, ~12% increase in LP I_h with a time constant of 9.9min (Krenz, Rodgers et al. 2015). Thus, enhancing SUMO availability in LP mimicked DA-enabled event 1. Enhanced SUMO availability also occluded DA-enabled event 1. A 30min activated Tat-SUMO wash-in was followed by application of the -100%ΔDC protocol in the presence or absence of 5nM DA. The data showed that application of the -100%ΔDC protocol in the presence of DA produced no further change in LP I_h (Fig 4.4C).

Enhanced activated SUMO availability mimics and occludes DA-enabled event 1. An increase in activated SUMO ultimately translates into enhanced target protein SUMOylation. Lobster HCN channels are targets of SUMOylation (Fig 4.2A). HCN channel SUMOylation can augment HCN channel surface expression (Parker, Welch et al. 2016). Together, these data suggest that DA-enabled event 1 may represent enhanced HCN channel SUMOylation.

Using the same experimental protocol (Fig 4.4A), we also examined whether or not enhanced SUMO availability blocked the DA-enabled, calcineurin-mediated, activity-dependent decrease in LP I_h (event 2). Enhanced SUMO availability did not obviously alter event 2 (Fig 4.4C). In the presence of tonic 5nM DA and limitless activated SUMO, the +50%ΔDC protocol still produced a significant average 9.5±1.8% decrease in LP I_h G_{max}. This decrease was not observed in the absence of tonic DA. Thus, enhanced SUMO availability did not block the calcineurin-mediated decrease in LP I_h, and event 2 still required DA's permissive effect.

4.4.6 *DA blocks the effect of enhanced SUMO availability on LP I_A*

We previously demonstrated that increasing Kv4.2 channel SUMOylation at an identified consensus sequence significantly decreased I_A G_{max} in Hek cells (Welch, Forster et al.). Note that in Hek cells, increased channel SUMOylation drove G_{max} in opposite directions for I_A and I_h. In order to determine the effect of increased activated SUMO availability on LP I_A, experiments using the three standard voltage protocols were performed as diagramed in Figure 4.5A. In the absence of Tat-SUMO wash-in, LP peak I_A was stable during a 30min 0%ΔDC voltage protocol (Fig 4.5B). Enhancing the availability of activated SUMO, while keeping duty cycle constant, mimicked and occluded the decrease in peak I_A normally elicited by an increasing LP duty cycle. A 30min wash-in of activated Tat-SUMO during a 0%ΔDC voltage protocol produced a significant 10.1±1.4% reduction in the mean peak I_A that was stable by 30min (Fig 4.5B). This was opposite to the ~10% increase produced by blocking SUMOylation with anacardic acid (Fig 4.3A). Additionally, there was no further change in LP peak I_A when the +50%ΔDC protocol was implemented after the 30min wash-in of activated Tat-SUMO (Fig 4.5C). On the other hand, decreasing duty cycle by implementing the -100%ΔDC protocol after a 30min activated Tat-SUMO wash-in produced a slightly lower, but still significant, mean 7.6±2.3% increase in peak I_A (Fig 4.5C). Together these data suggest that bi-directional activity-dependent regulation of LP I_A may be similar to I_h in that it involves two events: *event 1*- An activity-independent process that increases SUMOylation and *event 2*- An activity-dependent process that may reduce SUMOylation.

If enhanced SUMOylation mediates the decrease in LP I_A elicited by an increased duty cycle, and tonic 5nM DA can block the activity-dependent decrease in LP I_A (Fig 4.1C), then DA should block the effect of enhanced activated SUMO availability. In a separate series of

experiments, 5nM DA was added to the superfusate 10min prior to the start of the 30min Tat-SUMO wash-in; otherwise, the experimental protocol was identical. Tonic 5nM DA completely blocked the decrease in LP I_A due to enhanced activated SUMO availability (Fig 4.5B). This result is consistent with our hypothesis that DA reconfigures the targets of the SUMOylation machinery to remove activity-dependence from one conductance and bestow it on another.

4.5 Discussion

Neurons exhibit several types of activity-dependent plasticity that act on synaptic strength and dynamics (Blitz, Foster et al. 2004, Turrigiano 2011, Daur, Bryan et al. 2012), intrinsic properties (Rodgers, Fu et al. 2011, Krenz, Hooper et al. 2013, Krenz, Rodgers et al. 2015) and even electrical coupling (Lane, Samarth et al. 2016); but, it is unclear how the plurality of mechanisms is organized to simultaneously effect both change and stability, and how this organization is restructured with changes in state. We investigated one mechanism of HIM that promotes stability by maintaining a positive correlation between LP I_A and I_h to preserve neuronal activity phase. Our study showed that activity-dependent SUMOylation specified a positive correlation between LP I_A and I_h, but that modulatory tone played a permissive role in implementing that correlation. Fig 4.6 summarizes SUMOylation-mediated, activity-dependent regulation of the two conductances. Alterations in LP duty cycle drove changes in SUMOylation that modified current amplitudes (Fig 4.6). The activity-dependent changes in SUMOylation were opposite for the two conductances, but the effect of SUMOylation on current amplitudes was also opposite; thus, a positive correlation was specified. We initially hypothesized that DA alone permitted the positive correlation between LP I_A and I_h; however, our data proved the hypothesis wrong. Tonic 5nM DA disabled activity-dependent regulation of LP I_A, and thereby prevented the correlation. The data suggest that the correlation will only be observed when LP is

bathed by the appropriate modulatory mélange that allows the simultaneous activity-dependent regulation of both conductances.

We previously demonstrated that DA permitted activity-dependent regulation of LP I_h by enabling two distinguishable events (Krenz, Rodgers et al. 2015). Event 1 produced an activity-independent increase in I_h G_{max}. Here we showed that event 1 was mimicked and occluded by increasing the availability of activated SUMO in the LP neuron. Furthermore, event 1 could be blocked by globally inhibiting LP SUMOylation with anacardic acid. Previous experimentation on Hek cells overexpressing mouse HCN2 channels showed that increasing SUMO availability enhanced SUMOylation of the HCN channel at a specific consensus sequence, and this resulted in increased surface expression and augmentation of I_h G_{max} (Parker, Welch et al. 2016). Western blot experiments indicated that lobster HCN channels were SUMOylated *in vivo*. The most parsimonious interpretation of these data is that DA-enabled event 1 produces an increase in LP I_h G_{max} by enhancing HCN channel SUMOylation and surface expression. We previously demonstrated that event 2 produced an activity-dependent, CaM-calcineurin-mediated decrease in I_h G_{max} (Krenz, Rodgers et al. 2015). Here we demonstrated that globally blocking LP SUMOylation, mimicked and occluded the decrease associated with event 2. One of the most straight forward interpretations is that event 2 represents a DA-enabled, Ca^{2+}-dependent reduction in HCN channel SUMOylation and surface expression. In the simplest case, the combination of DA-enabled events 1 and 2 help to bi-directionally regulate the SUMOylation profile and surface expression of HCN channels in an activity-dependent fashion.

Activity-dependent regulation of LP I_A also appeared to depend on two separable events that may regulate Kv4 channel SUMOylation. Western blot experiments showed that lobster Kv4 channels, which mediate LP I_A (Baro, Levini et al. 1997, Baro, Ayali et al. 2000), were

SUMOylated *in vivo*. Blocking SUMOylation mimicked and occluded the activity-dependent increase in LP peak I_A that was observed during the -100%ΔDC protocol. Enhanced activated SUMO availability produced an activity-independent decrease in LP I_A that mimicked and occluded the reduction observed during the +50%ΔDC voltage protocol. Blocking SUMOylation prevented the activity-dependent decrease observed during the +50%ΔDC voltage protocol. In another study on Hek cells, we showed that increased SUMOylation reduced I_A mediated by mouse Kv4.2 channels, and that the decrease was blocked by mutating a specific SUMO consensus sequence on Kv4.2 (Welch, Forster et al.). It is not yet clear whether the surface expression and/or biophysical properties of mouse Kv4.2 channels were altered, as SUMOylation can affect both characteristics (Henley, Craig et al. 2014). In the simplest case, the data suggest that an activity-independent process (event 1) increases LP Kv4 channel SUMOyaltion to reduce I_A, while an activity-dependent process (event 2) decreases LP Kv4 channel SUMOylation to augment I_A. Tonic 5nM DA blocked events 1 and 2.

DA could permit (I_h) and prevent (I_A) activity-independent event 1 by reconfiguring the targets of the SUMOylation machinery. The literature suggests that this could be accomplished by alterations in target protein phosphorylation states (Hietakangas, Anckar et al. 2006, Konopacki, Jaafari et al. 2011, Loriol, Casse et al. 2014, Dustrude, Moutal et al. 2016). Target phosphorylation can either promote or prevent target SUMOylation. For example, one target protein, cytosolic axonal collapsin response mediator protein 2 (CRMP2), which enhances the surface expression of NaV1.7 channels, has phosphorylation sites with opposing effects (Dustrude, Wilson et al. 2013, Dustrude, Moutal et al. 2016). Phosphorylation at S522 by Cdk5 promoted CRMP2 SUMOylation. Conversely, phosphorylation at Y32 by Fyn inhibited CRMP2 SUMOylation. Ultimately, the phosphorylation state of CRMP2 helped determine its

SUMOylation state and thereby NaV1.7 surface expression. These findings provide a simple potential mechanism for how modulatory tone could (re)configure the targets of the SUMOylation machinery.

It is not clear how DA permits/prevents activity-dependent event 2. Activity can regulate SUMOylation in a cell specific manner. SUMOylation was globally increased by either KCl depolarization in SHSY5Y cells and hippocampal neurons (Lu, Liu et al. 2009, Lee, Dale et al. 2014) or TTX activity blockade in cortical neurons (Craig, Jaafari et al. 2012). Activity-dependent changes in SUMOylation profiles are often mediated by altering the abundance, location and/or activity of the SUMOylation machinery. The SUMO conjugating enzyme, Ubc9, is increased both pre- and post-synaptically in response to LTP (Feligioni, Nishimune et al. 2009, Jaafari, Konopacki et al. 2013). In hippocampal neurons, KCl depolarization localizes Ubc9 to presynaptic but not postsynaptic densities (Loriol, Khayachi et al. 2013). Increased neuronal activity and activation of mGluR5 leads to diffusional trapping of Ubc9 in hippocampal dendritic spines (Loriol, Casse et al. 2014). The N-terminus of the SENP family of SUMO deconjugating enzymes controls their abundance, localization and activity (Hickey, Wilson et al. 2012, Nayak and Muller 2014, Mendes, Grou et al. 2016). SENP was decreased by TTX activity blockade in cortical neurons (Craig, Jaafari et al. 2012). In hippocampal neurons, KCl depolarization led to a transient presynaptic redistribution of SENP (Loriol, Khayachi et al. 2013). Phosphorylation is known to regulate both SUMO conjugating and deconjugating enzymes (Baldwin, Julius et al. 2009, Hickey, Wilson et al. 2012, Su, Yang et al. 2012, Lin, Liu et al. 2016), and it is reasonable to assume that Ca^{2+}-dependent kinases and phosphatases could alter Ubc9 and/or SENP activity, abundance and localization in the LP neuron to produce activity-dependent deSUMOylation. DA could influence this pathway through any number of mechanisms.

Dynamic SUMOylation appears to contribute to baseline LP I_A and I_h. Blocking SUMOylation over the course of 1hr, in the absence of DA while keeping activity constant, produced a significant decrease in LP I_h G_{max} and a significant increase in LP peak I_A. This suggests that ongoing processes of SUMOylation and deSUMOylation dynamically tune LP ionic conductances and that SUMOylation states may reflect the continuous integration of chemical signals and electrical activity. Identifying ion channel SUMOylation profiles, their effects and their regulation could provide insight into how activity correlates multiple conductances and how modulatory tone permits or prevents those correlations.

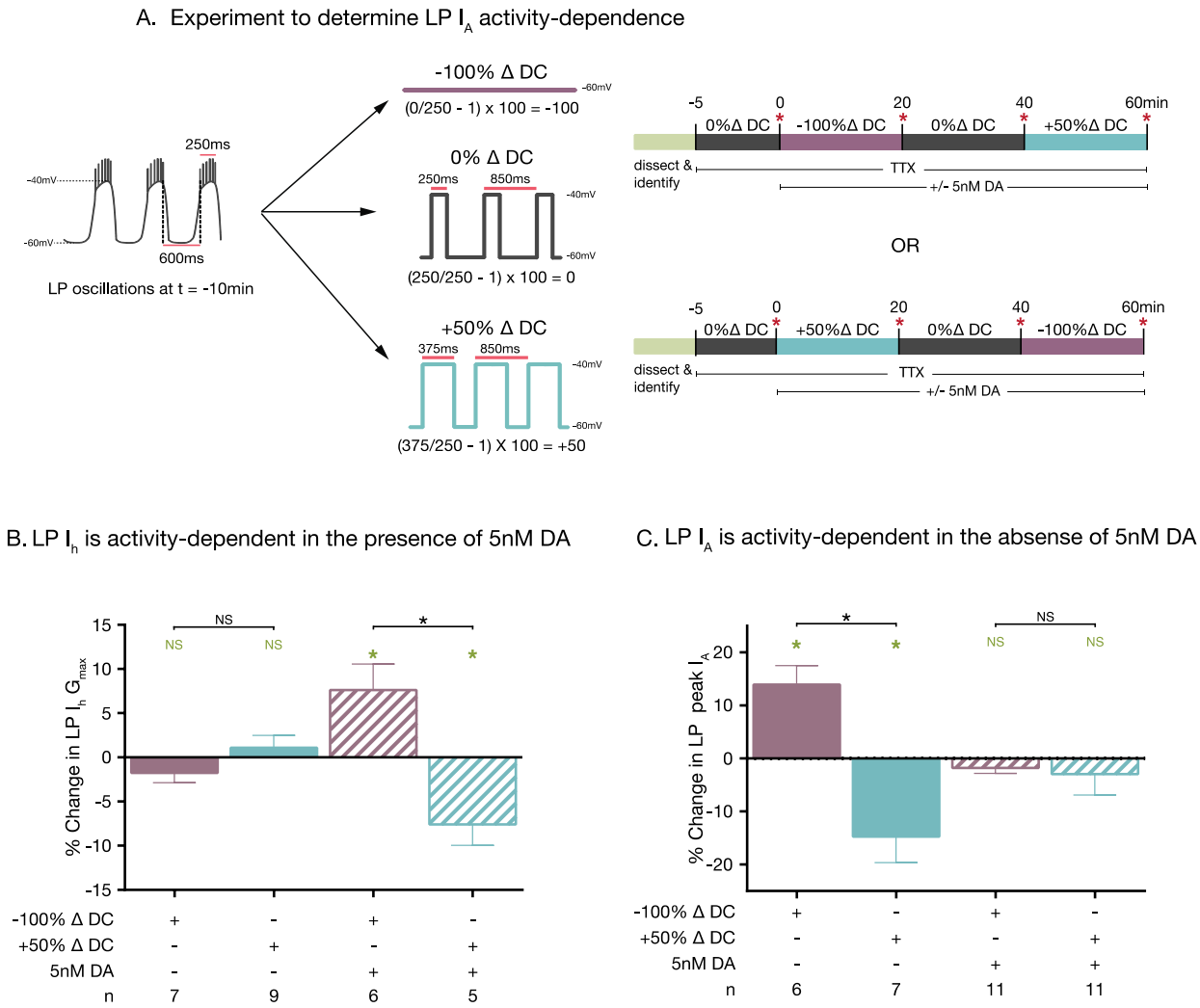

Figure 4.1 Tonic 5nM DA reconfigures the activity-dependence of LP I_A and I_h

(A) Experimental Protocol for examining activity-dependence of LP I_A. The diagram depicts LP slow wave activity at t=-10min. Plateau duration (250ms), peak (-40mV) and nadir (-60mV) voltages, and cycle period (850ms) were measured and used to create the three diagrammed voltage protocols. Note voltage protocols were always specifically designed for each cell based on measurements from that cell. The protocols were used in standard experiments as diagramed. At t=-5min, TTX was bath applied and the 0%ΔDC protocol was initiated. At t_0 the current was measured (red asterisk) and one of the two indicated series of voltage protocols was implemented in the presence or absence of 5nM DA. The current was measured at the end of each protocol as indicated by the red asterisks. The order of the voltage protocols was varied between experiments as shown in the two timelines. **(B)** LP I_h activity-dependence. Data were taken from (Krenz, Rodgers et al. 2015). The plot represents the percent change in LP I_h G_{max} resulting from a 10min change in duty cycle in the presence or absence of 5nM DA, as indicated. Green asterisks represent a significant difference within a treatment group using paired t-tests, $p<0.05$. Black asterisks indicate significant differences using a One-way ANOVA with Bonferroni's

multiple comparisons *post hoc* tests to compare selected pairs, as indicated, $F(3,23)= 9.146$; $p=0.0004$. **(C)** LP I_A activity-dependence. The plot represents the percent change in LP peak I_A following a 20min change in duty cycle [($t_{60}\div t_{40}$ or $t_{20}\div t_0$)-1x100] using the indicated voltage protocol in the presence or absence of 5nM DA. Green asterisks, significant difference within a treatment group using paired t-tests (t_0 vs t_{20}, or t_{40} vs t_{60}), $p\leq 0.05$. Black asterisks, significant differences using a One-way ANOVA with Bonferroni's multiple comparisons *post hoc* tests to compare selected pairs, as indicated, $F(3,31)= 8.512$; $p<0.0003$

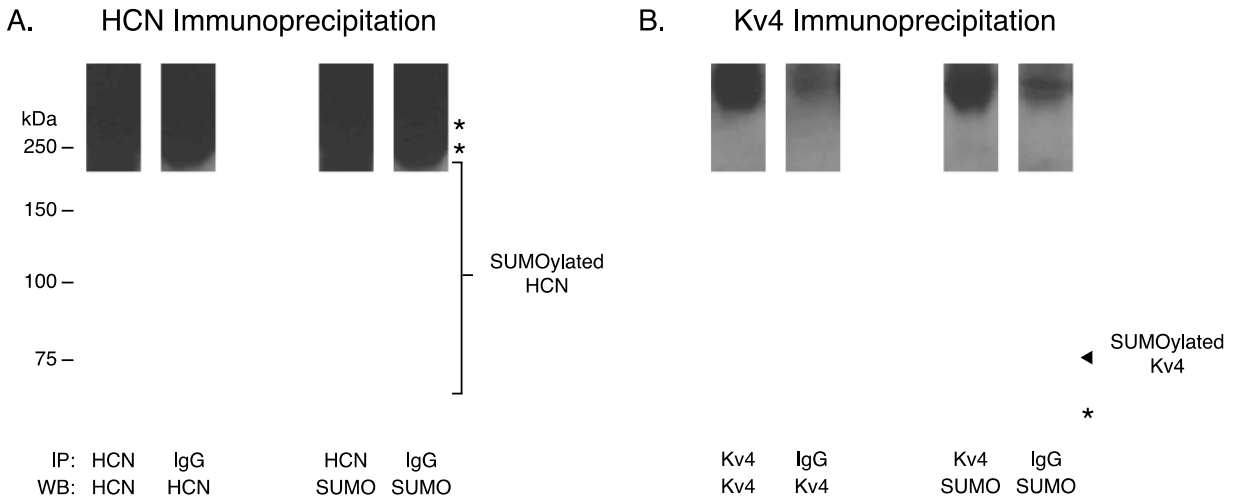

Figure 4.2 Panulirus interruptus HCN and Kv4 channels are SUMOylated in vivo
Lysates prepared from lobster nervous system tissue were used in immunoprecipitation (IP) experiments with antibodies against the lobster HCN channel (anti-HCN) **(A)**, the lobster Kv4 channel (anti-ORF-J) **(B)** or IgG **(A** and **B**, negative control**)**. Western blots (WB) containing the IP products were probed with anti-HCN, anti-ORF-J, or mouse anti-SUMO as indicated. Immunoprecipitation experiments were repeated with at least three animals for each channel and representative results are shown. The SUMO modified HCN and Kv4 channels have been indicated. Asterisks indicate SUMOylated proteins that potentially interact with the immunoprecipitated channel. Unmarked bands present in the IgG IP represent noise

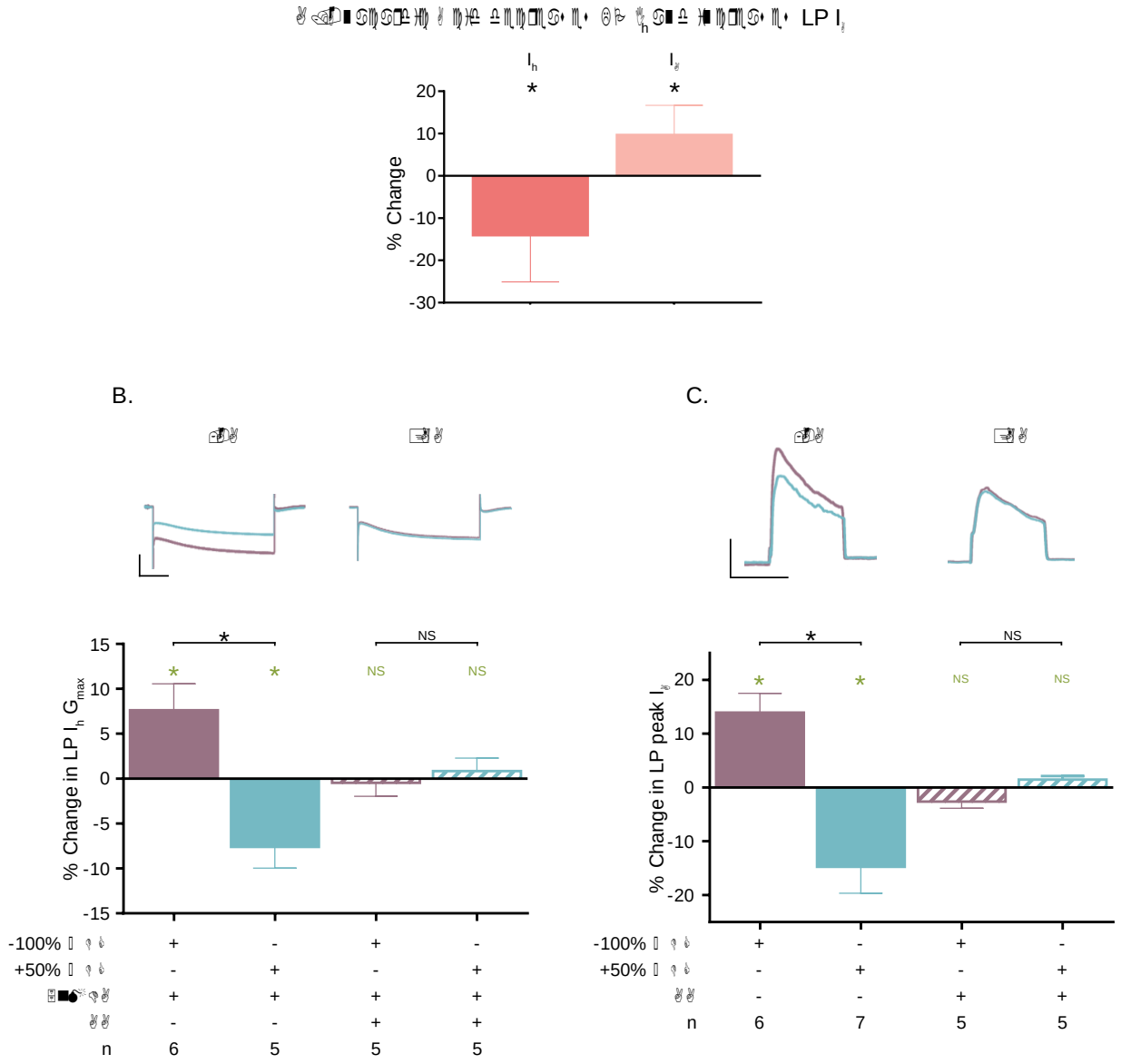

Figure 4.3 SUMOylation is necessary for the maintenance and activity-dependence of LP I_h and I_A

(A) SUMOylation contributes to the maintenance of LP I_h and I_A. Either I_h or I_A was measured at t=0, anacardic acid (AA) was added to the superfusate and the 0%ΔDC protocol was implemented for 1hr after which the current was re-measured. The mean percent change in each current is plotted [(t_{60}÷t_0)-1x100]. Asterisk, paired t-test $p<0.05$, n=6 each. **(B)** The effect of AA on activity-dependent changes in LP I_h. The experiment was similar to that depicted in Fig 4.1A, except that AA was added to the superfusate 1hr prior to TTX. Upper panel: Current traces from two representative experiments are shown. Two current traces elicited by a hyperpolarizing testpulse to -120mV during a single experiment were overlaid. The two traces from the same cell represent LP I_h immediately after a 20min -100%ΔDC protocol (purple) or a +50%ΔDC protocol

(cyan); scale bars, 10nA and 1s. Lower panel: Plot of the mean percent change in LP I_h G_{max} following a 20min change in duty cycle in the presence of AA. Experiments lacking AA are shown for comparison. Green asterisks significant difference within a treatment group using a paired t-test, $p<0.05$. Black asterisk significant difference between the four treatment groups using a One-way ANOVA with Bonferroni's multiple comparisons *post hoc* tests to compare selected pairs, as indicated, $F(3,17)= 7.814$; $p=0.0017$. NS, no significant difference **(C)** The effect of AA on activity-dependent changes in LP I_A. The experiment was similar to that depicted in Fig 4.1A, except that AA was added to the superfusate 1hr prior to TTX. Upper panel: Current traces from two representative experiments are shown. Two current traces elicited by a depolarizing testpulse to +40mV during a single experiment were overlaid. The two traces from the same cell represent LP I_A immediately after a 20min -100%ΔDC protocol (purple) or a +50%ΔDC protocol (cyan); scale bars, 100nA and 40ms. Lower panel: Plot of the mean percent change in peak LP I_A following a 20min change in duty cycle in the presence of AA. Experiments lacking AA were shown for comparison. Green asterisks, significant difference within a treatment group using a paired t-test, $p<0.05$. Black asterisks, significant differences using a One-way ANOVA with Bonferroni's multiple comparisons *post hoc* tests to compare selected pairs, as indicated, $F(3,19)= 11.87$; $p=0.0001$. NS, no significant difference

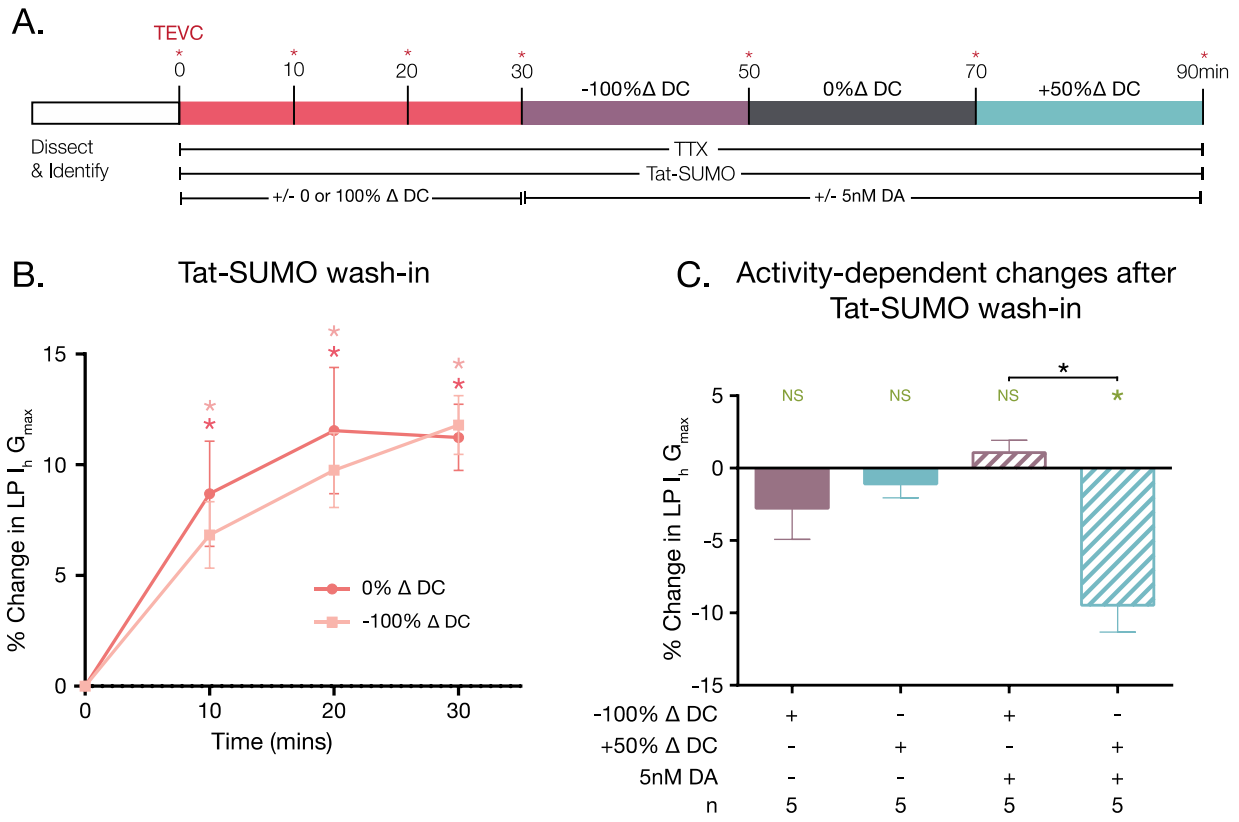

Figure 4.4 Enhancing SUMO availability converts DA-enabled, LP I_h activity-dependence from bi-directional to uni-directional

(A) Experimental Protocol. The diagram generally depicts the experiments; red asterisks indicate points where LP I_h was measured; the order of the -100%ΔDC and +50%ΔDC voltage protocols was varied between experiments; some experiments ended at t_{30} or t_{50}. **(B)** Tat-SUMO wash-in increases LP I_h G_{max}. Activated Tat-SUMO was added to the superfusate and LP I_h was measured every 10min for 30min. The percent change in LP I_h G_{max} at t_{10}, t_{20}, and t_{30} relative to t_0 is plotted. Asterisks, significantly different using Repeated Measures ANOVAs with Dunnett's post-hoc tests that compared each data point to t_0. *0%ΔDC*: $F(4,12)= 21.03$; $p=0.0026$, n=5; *-100%ΔDC*: $F(5,15)=23.01$; $p=0.0002$, n=6. **(C)** Enhancing SUMO availability occludes the DA-enabled, activity-dependent increase in LP I_h G_{max} but does not alter the DA-enabled activity-dependent decrease. After a 30min activated Tat-SUMO wash-in, DA was or was not added to the superfusate containing activated Tat-SUMO, and the indicated voltage protocols were applied. The percent change in LP I_h G_{max} [(t_{50}÷t_{30} or t_{90}÷t_{30})-1x100] in the presence and absence of DA was plotted. Green Asterisks, significant change within a treatment group (t_{50} vs t_{30} or t_{90} vs t_{30}), paired t-test $p<0.01$. Black asterisk, significant difference using a One-way ANOVA with Bonferroni's multiple comparisons *post hoc* tests to compare selected pairs, as indicated, $F(3,16)= 7.101$; $p<0.003$

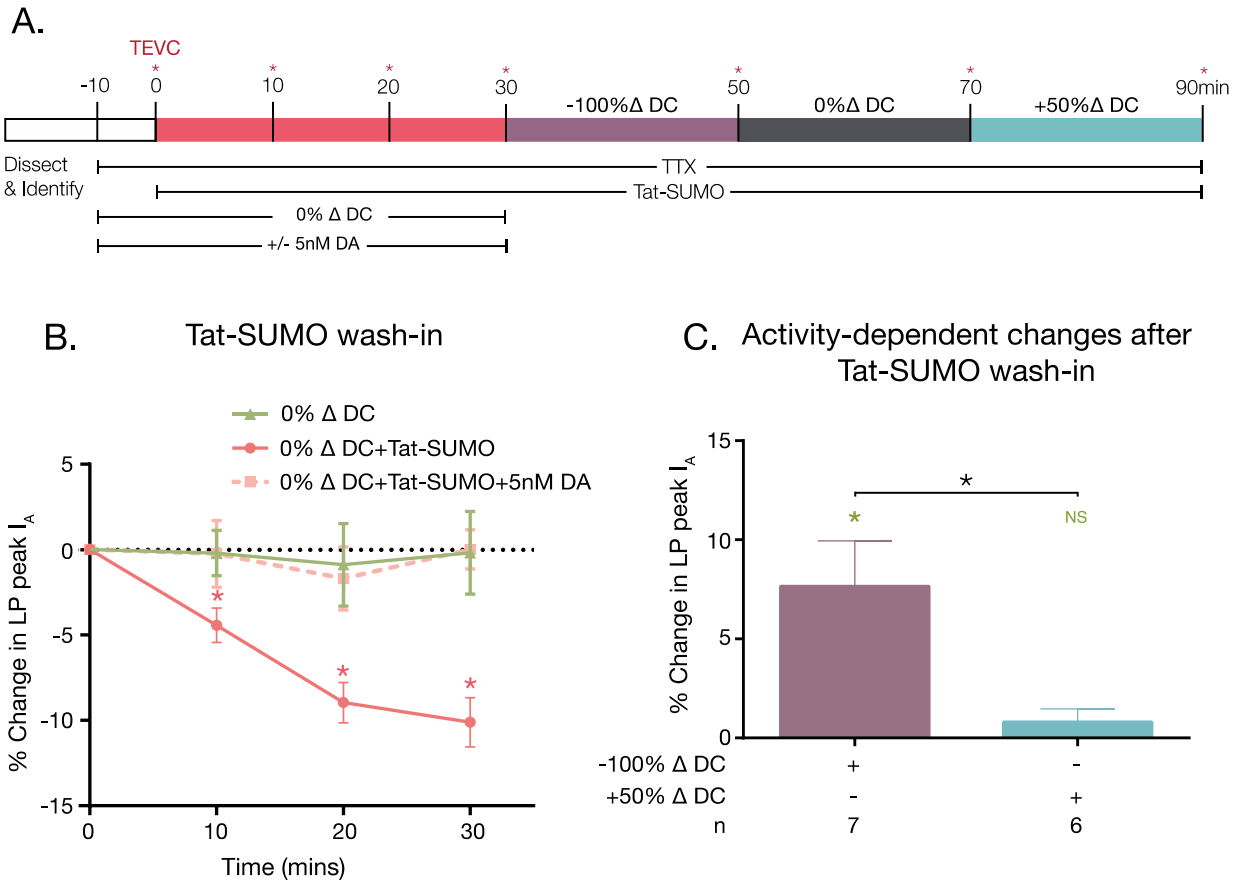

Figure 4.5 Enhancing SUMO availability converts LP I_A activity-dependence from bi-directional to uni-directional

(A) Experimental Protocol. The diagram generally depicts the experiments; red asterisks indicate points where LP I_A was measured; the order of the -100%ΔDC and +50%ΔDC voltage protocols was varied between experiments; some experiments ended at t_{30} or t_{50}. **(B)** Tat-SUMO wash-in decreases LP peak I_A. Percent change in LP peak I_A at t_{10}, t_{20}, and t_{30} relative to t_0. Asterisks, significantly different using Repeated Measures ANOVA with Dunnett's post-hoc that compared each data point to t_0; *0%ΔDC*: $F(4,12)=0.1682$; $p=0.7381$, n=5; *0%ΔDC + Tat-SUMO*: $F(10,30)= 13.65$; $p=0.0011$, n=11; *0%ΔDC + Tat-SUMO + DA*: $F(5,15)= 0.3438$; $p=0.7086$, n=6. **(C)** Enhancing SUMO availability occludes the activity-dependent decrease in LP peak I_A. Plot of the percent change in LP peak I_A [(t_{50}÷t_{30} or t_{90}÷t_{30})-1x100] after the indicated change in duty cycle. Green Asterisks, significant change within a treatment group (t_{50} vs t_{30} or t_{90} vs t_{30}), paired t-test $p<0.05$. Black Asterisks, significant change between groups, student t-test $p<0.05$

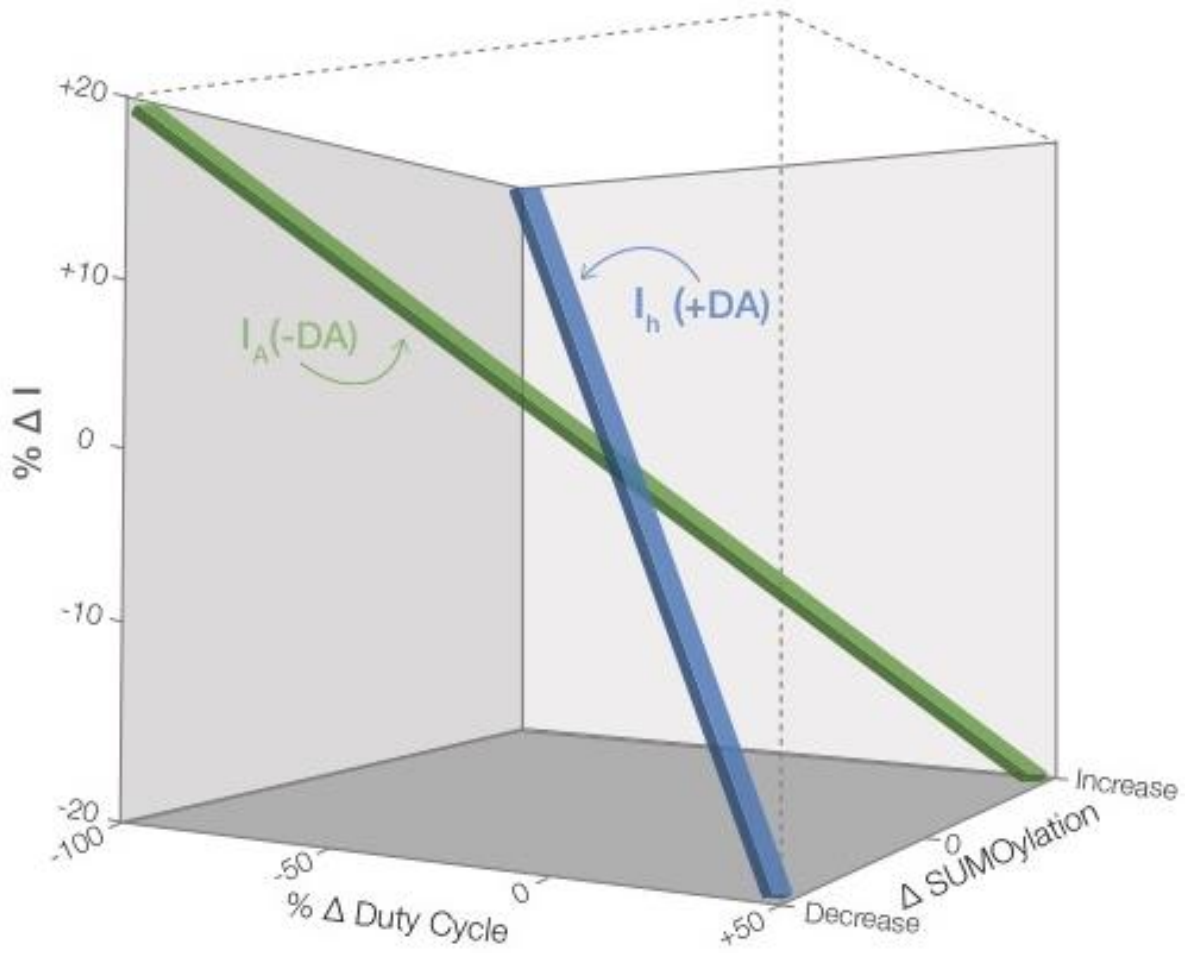

Figure 4.6 Summary of SUMO-mediated, activity-dependent regulation of LP I_h and I_A
The diagram represents a data-driven 3-dimensional sketch of how current amplitude (y-axis) and ion channel SUMOylation (z-axis) change according to LP duty cycle (x-axis). The blue bar represents LP I_h in the presence of 5nM DA and the green bar represents LP I_A in the absence of 5nM DA. Activity-dependent changes in current amplitude were similar for both currents: Increasing duty cycle reduced the current. Activity-dependent changes in SUMOylation were opposite for target proteins associated with I_A and I_h: Increasing duty cycle increased vs. decreased SUMOylation associated with LP I_A vs. I_h, respectively. SUMOylation of the target proteins produced opposite effects on current amplitude: increasing SUMOylation decreased LP I_A and increased LP I_h. We hypothesize that the ion channels mediating LP I_A (Kv4) and I_h (HCN) were the targets of activity-dependent SUMOylation, but this was not shown directly, and we cannot rule out the idea that the changes in SUMOylation evoked in this study may occur on unknown targets

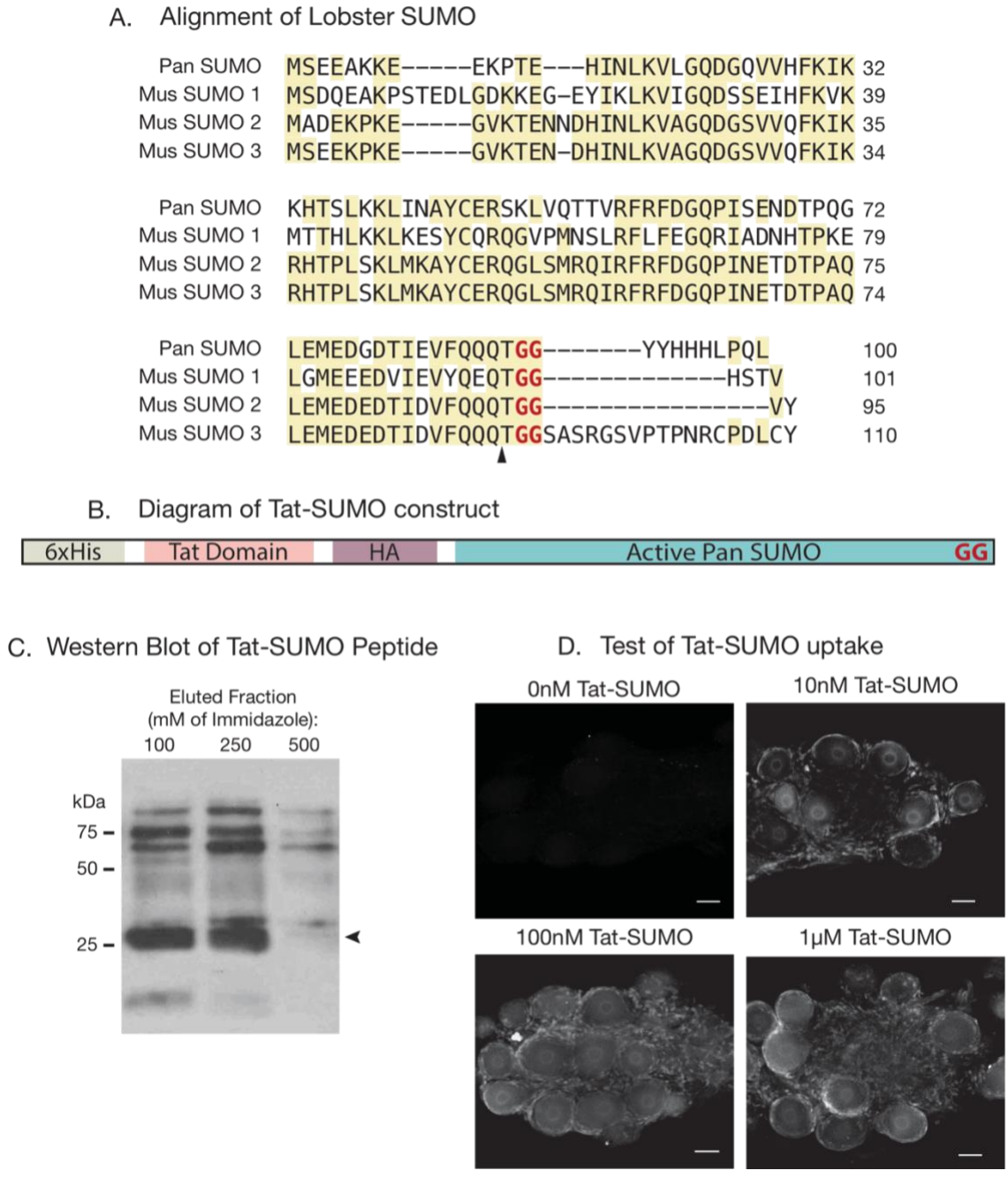

Figure 4.7 Supplemental 1 - Validation for Tat-SUMO experiments

(A) Comparison of lobster SUMO with each of the mouse SUMOs. SUMO was cloned from spiny lobster nervous system tissue (GenBank accession: MF770707). Aligning the amino acid sequence showed that *Panulirus* SUMO shares ~47% identity with mouse SUMO1(Genbank accession: P63166) and ~67% identity with mouse SUMO2 and 3 (Genbank accession: P61957 and Q9Z172 respectively). Highlighted areas represent regions of conservation. Arrowhead indicates the site where SUMO is cleaved to generate the mature peptide ending in di-glycine. **(B)** Tat-HA-His-SUMO Construct. Active *Panulirus* SUMO (C-terminal di-glycine) was

subcloned into a Tat-HA-His vector, which was then used to synthesize a Tat-tagged *Panulirus* SUMO peptide. **(C)** Western blot of recovered Tat-SUMO peptide. Tat-SUMO peptide was purified using Ni-NTA agarose resin and was eluted from the resin with incrementally increasing concentrations of imidazole (100mM, 250mM, 500mM, 1M). Purity of Tat-SUMO peptide was confirmed by western blotting. Eluted fractions were probed with a rabbit polyclonal anti-mouse SUMO1 antibody (Santa Cruz Biotechnology, sc-9060; used at 1:4000). Strong band at ~25kDa in 100mM and 250mM fractions represents Tat-SUMO peptide. Note that this experiment also validates that the mouse anti-SUMO 1 antibody can recognize the lobster peptide. **(D)** Tat-SUMO is efficiently taken up by live cells in the STG. Tat-SUMO uptake into STG cells was tested by bath applying varied concentrations of the peptide to the STG (0nM, 10nM, 100nM, and 1µM). The preparations were then fixed and immunostained with a validated, commercially available anti-Tat antibody (Abcam, ab63957, used at 1:200) as previously described (Baro, Ayali et al. 2000). Tat-SUMO immunostaining was not visible in the absence of bath applied Tat-SUMO (0nM). When Tat-SUMO was bath applied, immunostaining was clearly visible in the nucleus and cytoplasm of the neurons as well as in the surrounding glial cells. Tat-SUMO uptake appeared to increase in a concentration-dependent manner; 100nM appeared to be optimal with no detectable improvement at a higher concentration. scale bar, 50µm

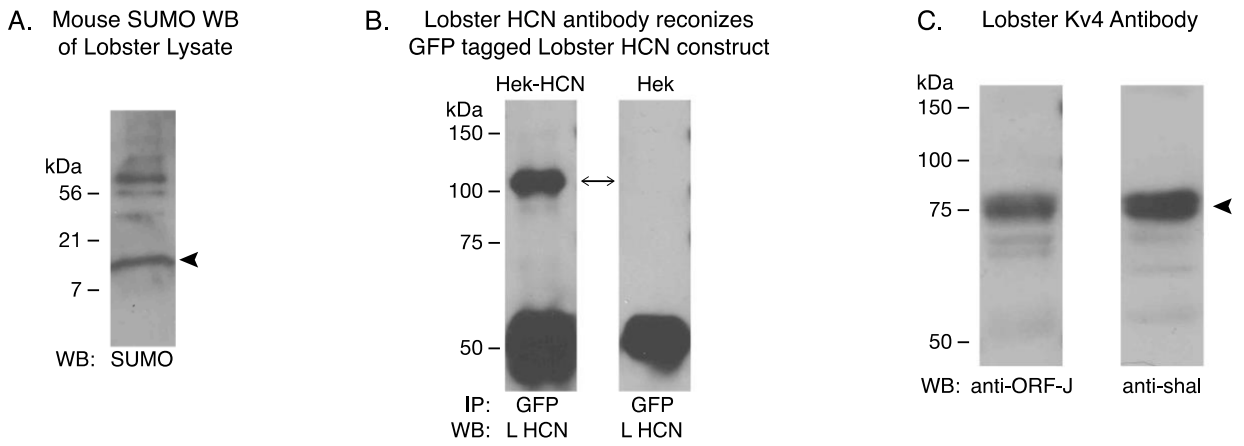

Figure 4.8 Supplemental 2 - Validation of antibodies used for immunoprecipitation and western blotting

(A) An antibody against mouse SUMO 1 recognized lobster SUMO. The lobster and mouse SUMO proteins are highly conserved and a mouse anti-SUMO 1 antibody is capable of recognizing a purified recombinant lobster SUMO peptide (Supp Fig 4.1). A western blot containing lobster nervous system lysate was probed with the same rabbit polyclonal anti-SUMO1 antibody. The antibody successfully recognized the ~10kDa free SUMO (arrow) in addition to other higher molecular weight bands representing other SUMOylated proteins. **(B)** The anti-HCN antibody recognized lobster HCN channels expressed in Hek cells. The lobster HCN channel was subcloned into a GFP expression vector and a GFP-HCN fusion protein was stably expressed in Hek cells using previously described methods (Parker, Welch et al. 2016). The GFP-HCN channel was isolated from Hek cell lysates in IP experiments using an antibody against GFP. Western blots containing the IP product were probed with anti-HCN (see materials and methods). The strong signal visible at ~110kDa represents the channel (arrow). As a negative control, the IP-western blot experiment was repeated with parental Hek cells that did not express the GFP-HCN construct. **(C)** The anti-ORF-J antibody recognized the lobster Kv4 channel in lobster nervous system lysates. Western blots containing lobster nervous system protein lysates were probed with anti-ORF-J or anti-shal, a previously validated antibody against the lobster Kv4 channel (Baro, Ayali et al. 2000). Both antibodies recognized the same ~75kDa band (arrow)

Table 4.1 Lobster SUMO Primers

Primer description	**Sequence 5' to 3'**
Degenerate For1	CAYATHAAYYCIAARGCISYIGG
Degenerate For2	GTIGTICARTTYAARATHAARMRICAYAC
Degenerate Rev1	GTRTCIKTYTCRTTDATNGGYTG
Degenerate Rev2	TTDATNGGYTGICCRTCRAAICKRAA
Specific For1	CTCAAAAAGCTCATCAATGCCTACTG
Specific For2	ATCAAAACTTGTCCAGACTACAGTGAG
Specific Rev1	CTCACTGTAGTCTGGACAAGTTTTGAT
Specific Rev2	CAGTAGGCATTGATGAGCTTTTTGAG
Tat-SUMO For	TTTTGAATTCGATGTCCGAGGAAGCCAAGAA
Tat-SUMO Rev	GGGGGAATTCTCACCCACCAGTTTGCTGCTGGAACAC

5 GENERAL DISCUSSION

5.1 SUMO regulation of neuronal homeostasis

The work presented here demonstrates that within a single neuron, SUMO can orchestrate the activity-dependent regulation of multiple ionic conductances. This speaks to a much larger potential role for SUMOylation in coregulating activity-dependent mechanisms involved in the maintenance of neuronal homeostasis. Recent studies have found linked changes in neuronal SUMOylation with changes in neuronal excitability. In hippocampal neurons for example, including SUMO in a patch pipette increases neuronal excitability, with the inverse being true when the deSUMOylating enzyme, SENP, was included in the pipette (Plant, Dowdell et al. 2011). Altering neuronal excitability can also impact the SUMOylation machinery and consequently, SUMOylation of target proteins. Suppression of activity with TTX results in a global decrease in SENP and therefore an increase in SUMOylated proteins (Craig, Jaafari et al. 2012). Depolarizing hippocampal neurons with KCl reorganizes the SUMOylation machinery and SUMOylated proteins at pre- and postsynaptic sites (Loriol, Khayachi et al. 2013). With global changes in SUMOylation affecting neuronal excitably, and SUMOylation being under the influence of changes in neuronal excitability it is not a stretch to infer that SUMO may be important for some types of activity-dependent regulation. Our work further supports this idea by showing that SUMOylation mediates the correlated activity-dependent regulation of two ionic conductances whose coregulation is known to be important for homeostasis of network activity.

This study has shown that under the appropriate modulatory tone, SUMO can mediate activity-dependent regulation of two ionic conductances within a single neuron. There have been many studies examining what SUMO is doing in hippocampal neurons, and when assembled they illustrate a complex system of regulation. For example, SUMO regulates multiple glutamate

receptors in distinct ways in hippocampal neurons. SUMOylation of the metabotropic glutamate receptor subunit, mGluR7, stabilizes the receptor in the cell membrane (Choi, Park et al. 2016). The ionotropic glutamate receptor subunit, GluK2, is SUMOylated following phosphorylation of the receptor and results in increased internalization of GluK2 containing receptors (Chamberlain, Gonzalez-Gonzalez et al. 2012). Kainate binding promotes SUMOylation of GluR6 containing receptors and their subsequent internalization (Martin, Nishimune et al. 2007). Specific K^+ channels were also identified as SUMO substrates in hippocampal neurons. For example, SUMOylation of the Kv2.1 channel positively shifts its voltage of half activation (Plant, Dowdell et al. 2011), and SUMOylation of the Kv7 channel diminishes the M current leading to hyperexcitability (Qi, Wang et al. 2014). Direct SUMOylation of each of these channels and receptor subunits and all of the diverse outcomes are occurring in a single neuronal cell type. Is SUMO simultaneously regulating all of these processes? The evidence presented here and the work of other investigators suggest that there may be mechanisms, like tonic DA modulation and phosphorylation, which can promote or prevent SUMO regulation of specific targets within a single cell (Dustrude, Wilson et al. 2013, Dustrude, Moutal et al. 2016).

5.2 The function of tonic DA

DA can be present in two functionally distinct concentrations (tonic and phasic). Phasic DA corresponds to a transient increase in DA concentrations (μM-mM) resulting from burst firing of dopaminergic neurons. Phasic DA functions to encode reward signals and can promote the later phase of plasticity in the prefrontal cortex, hippocampus, and striatum (Frey, Matthies et al. 1991, Grace 1991, Gurden, Tassin et al. 1999, Gurden, Takita et al. 2000, Reynolds, Hyland et al. 2001, Floresco, West et al. 2003, Huang, Simpson et al. 2004). Tonic DA refers to low steady-state concentrations of DA (nM) produced by the slow single spike activity of DA

neurons (Grace 1991, Keefe, Zigmond et al. 1993, Goto, Otani et al. 2007). Although less is known about the function of tonic DA, the consensus is that dopaminergic tone stabilizes neural network activity or maintains a specific neuronal activity state (Durstewitz, Seamans et al. 2000, Durstewitz, Seamans et al. 2000, Durstewitz and Seamans 2002, Bilder, Volavka et al. 2004, Matsuda, Marzo et al. 2006, Sikstrom and Soderlund 2007, Kroener, Chandler et al. 2009). Our work has begun to characterize the mechanisms through which tonic DA can act to stabilize neuronal activity states.

5.2.1 Tonic spiking of DA neurons

One important question to address first is, why do DA neurons fire tonically? Is it solely to maintain a specific level of extracellular dopaminergic tone, or is there more to the story? DA neurons fire tonically due to the presence of pacemaker channels (Grace and Bunney 1983), and this firing can be up and down-regulated based on afferent glutamatergic or GABAergic input (Grace and Bunney 1984, van Zessen, Phillips et al. 2012, Chang and Grace 2014). Within a given population of DA neurons, only a fraction is tonically active. Tonic spiking of DA neurons doesn't just establish the nM levels of extracellular DA, but it provides a pool of neurons that can respond to phasic stimulation (Floresco, West et al. 2003, Lodge and Grace 2006, Belujon and Grace 2015, Grace 2016). Only DA neurons that are tonically active can respond to a stimulus with phasic bursting activity. Therefore, increasing or decreasing the number of tonically firing DA neurons will up or downregulate, the magnitude of the phasic response. This means that the tonic activity of DA neurons themselves functions to modulate the extent of the system's phasic response. Therefore, neurons providing afferent inputs on DA neurons (ventral pallidum, pedunculopontine tegmental nucleus) can contextualize phasic stimulation by modulating the

number of tonically active neurons (Blaha, Yang et al. 1997, Lokwan, Overton et al. 1999, Floresco, Todd et al. 2001, Lodge and Grace 2006).

5.2.2 Dopaminergic tone stabilizes neuronal activity states

The stabilizing effect of tonic DA is thought to be mediated by the nM levels of DA present in the extracellular space rather than the tonic spiking activity of the DA neurons themselves. There are two different schools of thought on how tonic nM levels of DA can stabilize neuronal activity states, and it is likely that both mechanisms exist *in vivo*, either simultaneously or under contextually different circumstances. The first model suggests that tonic DA acts through either autoreceptors or desensitization of DA receptors to "set the gain" for the phasic response, thus maintaining stable neuronal activity (Belujon and Grace 2015, Grace 2016). There are multiple theories about how this function is accomplished. Some investigators have said that tonic DA can set the threshold needed for phasic activity to alter an activity state. This would permit the maintenance of an activity state while still allowing a degree of flexibility if the phasic response can exceed that threshold (Durstewitz, Seamans et al. 2000, Durstewitz, Seamans et al. 2000, Durstewitz and Seamans 2002, Bilder, Volavka et al. 2004). Other investigators have demonstrated that tonic DA acting on autoreceptors can determine the magnitude of the phasic response. When tonic DA levels are enhanced the magnitude of phasic release is reduced, and conversely, a decrease in dopaminergic tone will enhance phasic release (Grace 2000, Floresco, West et al. 2003, Bilder, Volavka et al. 2004, Sikstrom and Soderlund 2007). Tonic DA levels have also been shown to have a desensitizing effect on DA receptors, with agonist binding leading to internalization of DA receptors (Grace 1991, Grace 2000). However, it is worth noting that different responses have been observed in heterologous expression systems versus slice cultures. Even between heterologous expression systems, the

mechanisms mediating DA receptor internalization appear to differ in some respects (Ito, Haga et al. 1999, Kim, Valenzano et al. 2001, Celver, Sharma et al. 2013, Robinson, Bunzow et al. 2017).

The second prevailing theory proposes that tonic DA, acting at high-affinity DA receptors, stabilizes neuronal activity by regulating ionic conductances and certain types of plasticity. In the crustacean STG, many studies have shown that conductance correlations maintain specific neuronal activity features (Temporal, Desai et al. 2012, Zhao and Golowasch 2012, O'Leary, Williams et al. 2013, Temporal, Lett et al. 2014, Marder, Goeritz et al. 2015). Specifically, DA has been shown to play an important role in the maintenance of conductance correlations (Khorkova and Golowasch 2007, Krenz, Parker et al. 2015). In LP, the correlation of I_A and I_h is important to maintain LP timing within the circuit (MacLean, Zhang et al. 2003). When the ratio of I_A to I_h is disrupted, LP activity phase is altered and in the presence but not the absence of tonic nM DA, and LP activity phase is restored (Rodgers, Fu et al. 2011, Krenz, Hooper et al. 2013, Krenz, Rodgers et al. 2015). Tonic DA mediates LP phase recovery by permitting activity-dependent regulation of I_h that restored the correlation between LP I_A and I_h (Krenz, Rodgers et al. 2015). The work that was presented in this study further illuminated the mechanism through which tonic DA acts to stabilize activity. Tonic DA can select the ionic conductance target for activity-dependent regulation by SUMO.

In addition to regulating ionic conductances to maintain a stable rhythmically active network, studies using rodent models have also described a role for tonic DA in the regulation of synaptic plasticity. Recent behavioral research in mice has shown that tonic DA is important for preserving and maintaining a learned association (Ellwood, Patel et al. 2017). In this study, optogenetic stimulation was used to drive either tonic or phasic firing of DA neurons while

examining the function of each in a task that requires the mice to learn a specific association and then switch to a new association. The researchers found that phasic DA mediated the learning of new associations while tonic DA preserved the previously learned association, hindering the learning of a new one (Ellwood, Patel et al. 2017). While this behavior based study does not yet speak to a specific mechanism, it highlights the importance of tonic DA maintaining a learned plasticity state. Research in the rat prefrontal cortex has found that tonic DA is needed for the appropriate induction of LTP. In the presence of "normal" physiological levels of tonic DA, high-frequency stimulation induces LTP (Matsuda, Marzo et al. 2006). However, through the use of either DA agonist/antagonist or PFC slice cultures that are absent of dopaminergic tone, researchers have discovered phasic DA can trigger either LTD or LTP in the prefrontal cortex depending on the level of dopaminergic tone (Otani, Bai et al. 2015). Phasic DA stimulation in the presence of low/no or elevated tonic DA induces LTD (Otani, Blond et al. 1998, Otani, Auclair et al. 1999); conversely, phasic DA stimulation in the presence of physiological levels of tonic DA induces LTP (Matsuda, Marzo et al. 2006). Taken together, these studies illustrate diverse roles for tonic DA that may vary based on cell type and cellular context.

5.2.3 Dysfunctions associated with dopaminergic tone

Understanding disease states that are associated with alterations in dopaminergic tone can provide valuable insight into its behavioral and physiological functions. This is not always an easy task, however, because many dysfunctions that result from alterations in the DA system may affect both tonic and phasic DA. Yet, researchers are making efforts to distinguish between the two, because understanding whether certain symptoms result from alterations in dopaminergic tone versus phasic DA release can better inform what treatments may be most effective. For example, in Parkinson's Disease, a majority of the symptoms associated with the

disease (resting tremors, rigidity, and bradykinesia) result from the loss of dopaminergic neurons in the substantia nigra (Hammond, Bergman et al. 2007). This would mean that dopaminergic tone would be significantly depleted. Researchers have linked this decrease in tonic DA to a significant down-regulation in HCN channel expression in globus pallidus neurons, leading to the motor dysfunction associated with Parkinson's Disease (Chan, Glajch et al. 2011). These findings are particularly relevant to the work presented here because we have also shown that tonic DA plays a significant role in both short-term and long-term regulation of I_h (Rodgers, Fu et al. 2011, Krenz, Hooper et al. 2013, Krenz, Parker et al. 2014, Krenz, Rodgers et al. 2015).

Disruption in tonic DA has also been suggested to play an important role in Attention Deficit Hyperactivity Disorder (ADHD). Recent studies have shown that in human subjects diagnosed with ADHD tonic DA in the right caudate was significantly reduced, whereas phasic DA release in the right caudate was significantly increased (Sikstrom and Soderlund 2007, Badgaiyan, Sinha et al. 2015). These results are consistent with the attentional deficits associated with ADHD because the right caudate is known to control executive inhibition and selective attention, and dysfunctional regulation of this region could lead to attentional deficits. Substance addiction is also correlated to alterations in tonic DA. Specifically, it has been shown that repeated drug administration increases tonic DA, consequently decreasing the phasic response (Grace 2000). This subdued phasic response would increase drug-seeking behavior because stronger doses would be needed to elicit the desired phasic response, further increasing the dopaminergic tone in a vicious cycle. Lastly, Schizophrenia is associated with hyper-responsiveness of the dopaminergic system (Grace 1991, Durstewitz and Seamans 2008, Grace 2016). The evidence indicates that this hyperdopaminergic state results from hyperactivity of the hippocampus, which supplies excitatory afferent stimulation to VTA dopaminergic neurons

(Heckers 2001, Medoff, Holcomb et al. 2001, Grace 2016). This leads to an increase in tonically active DA neurons and thereby an enhanced phasic response. It is clear that dysregulation of the dopamine system has far reaching implication, and it has become more apparent over time that to fully understand these disease states we must examine the distinct role of both tonic and phasic DA and how the two intersect.

5.3 Limitations of Exogenous Expression and Heterologous Expression Systems

With any form of research, it is important to understand the limitations of your chosen system and experimental techniques. A significant portion of the research presented here utilizes Hek cells as a heterologous expression system to stably express the HCN channel, which can then be used to study the effects of SUMOylation on the channel. Hek cells are widely used for studies investigating protein-protein interactions because they divide quickly and are easily transfected and cultured in a laboratory setting. However, stable expression of a protein requires the gene for the new protein be integrated into the Hek cell genome, and there is no way to control the number of copies that have been integrated into the genome. This means that when comparing across separate stable cell lines, for example, cell lines expressing the wild-type protein versus a mutated form of the protein, each cell line could have a different copy number. In our study, we look at SUMO modification of HCN channels stably expressed in Hek cells. Therefore, if a particular cell line expresses the channel at a significantly higher level, the endogenous SUMOylation machinery may not be able to maintain the baseline (control) level of SUMOylated HCN channels at a level that is consistent with the other cells lines with lower HCN channel expression. These types of differences are important to consider when interpreting your findings using a heterologous expression system.

Researchers also commonly use exogenous expression of a protein or gene of interest to study its effects. For example, in our study we transfected SUMO and Ubc9 to overexpress those proteins in Hek cells. We also used Tat-SUMO to exogenously increase SUMOylation in the STG neurons. Four our research, these techniques provide valuable information about the effects SUMOylation on a specific channel or ionic current, but these findings should also be considered in a biological context. Is increasing SUMOylation to the maximum level that the endogenous enzymes can accommodate producing a change that could be observed under normal biological conditions? For this reason, it is important also to consider including experiments that examine changes that occur through endogenous mechanisms and then the effect of the response to exogenous expression can be compared to the endogenous response.

5.4 Conclusions

This dissertation has provided evidence of a novel regulatory role for SUMOylation in the coregulation of I_A and I_h. This finding is significant because, conductance correlations play an important part in neuronal homeostasis, and this study can further illuminate the mechanisms that mediate rapid homeostatic coregulation of ionic conductances because they are as of yet not well understood. This work has also demonstrated a mechanism by which tonic DA can select ionic conductance targets for activity-dependent regulation by SUMO. This is an important finding because researchers are only just beginning to investigate the specific mechanisms that underlie tonic DA regulation of neural network activity. Until now there has been no evidence that modulatory tone is involved in SUMO regulation of ionic conductances. Therefore, this study has provided a new line of investigation that can have far-reaching implication in the study of neuronal homeostasis, tonic DA regulation of neuronal activity, and SUMO regulation of ionic conductances in vertebrates as well as invertebrates.

REFERENCES

Akhavan, A., R. Atanasiu, T. Noguchi, W. Han, N. Holder and A. Shrier (2005). "Identification of the cyclic-nucleotide-binding domain as a conserved determinant of ion-channel cell-surface localization." J Cell Sci **118**(Pt 13): 2803-2812.

Ayali, A. and R. M. Harris-Warrick (1999). "Monoamine control of the pacemaker kernel and cycle frequency in the lobster pyloric network." J Neurosci **19**(15): 6712-6722.

Badgaiyan, R. D., S. Sinha, M. Sajjad and D. S. Wack (2015). "Attenuated Tonic and Enhanced Phasic Release of Dopamine in Attention Deficit Hyperactivity Disorder." PLoS One **10**(9): e0137326.

Baldwin, M. L., J. A. Julius, X. Tang, Y. Wang and J. Bachant (2009). "The yeast SUMO isopeptidase Smt4/Ulp2 and the polo kinase Cdc5 act in an opposing fashion to regulate sumoylation in mitosis and cohesion at centromeres." Cell Cycle **8**(20): 3406-3419.

Baro, D. J., A. Ayali, L. French, N. L. Scholz, J. Labenia, C. C. Lanning, K. Graubard and R. M. Harris-Warrick (2000). "Molecular underpinnings of motor pattern generation: differential targeting of shal and shaker in the pyloric motor system." J Neurosci **20**(17): 6619-6630.

Baro, D. J., C. L. Cole, A. R. Zarrin, S. Hughes and R. M. Harris-Warrick (1994). "Shab gene expression in identified neurons of the pyloric network in the lobster stomatogastric ganglion." Receptors Channels **2**(3): 193-205.

Baro, D. J., R. M. Levini, M. T. Kim, A. R. Willms, C. C. Lanning, H. E. Rodriguez and R. M. Harris-Warrick (1997). "Quantitative single-cell-reverse transcription-PCR demonstrates that A-current magnitude varies as a linear function of shal gene expression in identified stomatogastric neurons." J Neurosci **17**(17): 6597-6610.

Baro, D. J., L. Quinones, C. C. Lanning, R. M. Harris-Warrick and M. Ruiz (2001). "Alternate splicing of the shal gene and the origin of I(A) diversity among neurons in a dynamic motor network." Neuroscience **106**(2): 419-432.

Belujon, P. and A. A. Grace (2015). "Regulation of dopamine system responsivity and its adaptive and pathological response to stress." Proc Biol Sci **282**(1805).

Benson, M. D., Q. J. Li, K. Kieckhafer, D. Dudek, M. R. Whorton, R. K. Sunahara, J. A. Iniguez-Lluhi and J. R. Martens (2007). "SUMO modification regulates inactivation of the voltage-gated potassium channel Kv1.5." Proc Natl Acad Sci U S A **104**(6): 1805-1810.

Bilder, R. M., J. Volavka, H. M. Lachman and A. A. Grace (2004). "The catechol-O-methyltransferase polymorphism: relations to the tonic-phasic dopamine hypothesis and neuropsychiatric phenotypes." Neuropsychopharmacology **29**(11): 1943-1961.

Birnbaum, S. G., A. W. Varga, L. L. Yuan, A. E. Anderson, J. D. Sweatt and L. A. Schrader (2004). "Structure and function of Kv4-family transient potassium channels." Physiol Rev **84**(3): 803-833.

Blaha, C. D., C. R. Yang, S. B. Floresco, A. M. Barr and A. G. Phillips (1997). "Stimulation of the ventral subiculum of the hippocampus evokes glutamate receptor-mediated changes in dopamine efflux in the rat nucleus accumbens." Eur J Neurosci **9**(5): 902-911.

Blitz, D. M., K. A. Foster and W. G. Regehr (2004). "Short-term synaptic plasticity: a comparison of two synapses." Nat Rev Neurosci **5**(8): 630-640.

Bossis, G. and F. Melchior (2006). "SUMO: regulating the regulator." Cell Div **1**: 13.

Brennan, G. P., T. Z. Baram and N. P. Poolos (2016). "Hyperpolarization-Activated Cyclic Nucleotide-Gated (HCN) Channels in Epilepsy." Cold Spring Harb Perspect Med **6**(3): a022384.

Bromberg-Martin, E. S., M. Matsumoto and O. Hikosaka (2010). "Dopamine in motivational control: rewarding, aversive, and alerting." Neuron **68**(5): 815-834.

Bucher, D., A. A. Prinz and E. Marder (2005). "Animal-to-animal variability in motor pattern production in adults and during growth." J Neurosci **25**(7): 1611-1619.

Celver, J., M. Sharma, V. Thanawala, J. Christopher Octeau and A. Kovoor (2013). "Arrestin-dependent but G-protein coupled receptor kinase-independent uncoupling of D2-dopamine receptors." J Neurochem **127**(1): 57-65.

Chamberlain, S. E., I. M. Gonzalez-Gonzalez, K. A. Wilkinson, F. A. Konopacki, S. Kantamneni, J. M. Henley and J. R. Mellor (2012). "SUMOylation and phosphorylation of GluK2 regulate kainate receptor trafficking and synaptic plasticity." Nat Neurosci **15**(6): 845-852.

Chan, C. S., K. E. Glajch, T. S. Gertler, J. N. Guzman, J. N. Mercer, A. S. Lewis, A. B. Goldberg, T. Tkatch, R. Shigemoto, S. M. Fleming, D. M. Chetkovich, P. Osten, H. Kita and D. J. Surmeier (2011). "HCN channelopathy in external globus pallidus neurons in models of Parkinson's disease." Nat Neurosci **14**(1): 85-92.

Chang, C. H. and A. A. Grace (2014). "Amygdala-ventral pallidum pathway decreases dopamine activity after chronic mild stress in rats." Biol Psychiatry **76**(3): 223-230.

Cheng, J., X. Kang, S. Zhang and E. T. Yeh (2007). "SUMO-specific protease 1 is essential for stabilization of HIF1alpha during hypoxia." Cell **131**(3): 584-595.

Choi, J. H., J. Y. Park, S. P. Park, H. Lee, S. Han, K. H. Park and Y. H. Suh (2016). "Regulation of mGluR7 trafficking by SUMOylation in neurons." Neuropharmacology **102**: 229-235.

Clark, M. C. and D. J. Baro (2006). "Molecular cloning and characterization of crustacean type-one dopamine receptors: D1alphaPan and D1betaPan." Comp Biochem Physiol B Biochem Mol Biol **143**(3): 294-301.

Clark, M. C., R. Khan and D. J. Baro (2008). "Crustacean dopamine receptors: localization and G protein coupling in the stomatogastric ganglion." J Neurochem **104**(4): 1006-1019.

Cleland, T. A. and A. I. Selverston (1997). "Dopaminergic modulation of inhibitory glutamate receptors in the lobster stomatogastric ganglion." J Neurophysiol **78**(6): 3450-3452.

Craig, T. J., N. Jaafari, M. M. Petrovic, S. C. Jacobs, P. P. Rubin, J. R. Mellor and J. M. Henley (2012). "Homeostatic synaptic scaling is regulated by protein SUMOylation." J Biol Chem **287**(27): 22781-22788.

Cujec, T. P., H. Okamoto, K. Fujinaga, J. Meyer, H. Chamberlin, D. O. Morgan and B. M. Peterlin (1997). "The HIV transactivator TAT binds to the CDK-activating kinase and activates the phosphorylation of the carboxy-terminal domain of RNA polymerase II." Genes Dev **11**(20): 2645-2657.

Dai, X. Q., J. Kolic, P. Marchi, S. Sipione and P. E. Macdonald (2009). "SUMOylation regulates Kv2.1 and modulates pancreatic beta-cell excitability." J Cell Sci **122**(Pt 6): 775-779.

Daur, N., A. S. Bryan, V. J. Garcia and D. Bucher (2012). "Short-term synaptic plasticity compensates for variability in number of motor neurons at a neuromuscular junction." J Neurosci **32**(45): 16007-16017.

Davis, G. W. (2013). "Homeostatic signaling and the stabilization of neural function." Neuron **80**(3): 718-728.

Desai, N. S., L. C. Rutherford and G. G. Turrigiano (1999). "Plasticity in the intrinsic excitability of cortical pyramidal neurons." Nat Neurosci **2**(6): 515-520.

Desterro, J. M. P., J. Thomson and R. T. Hay (1997). "Ubch9 conjugates SUMO but not ubiquitin." FEBS Letters **417**(3): 297-300.

DiFrancesco, J. C., A. Barbuti, R. Milanesi, S. Coco, A. Bucchi, G. Bottelli, C. Ferrarese, S. Franceschetti, B. Terragni, M. Baruscotti and D. DiFrancesco (2011). "Recessive loss-of-function mutation in the pacemaker HCN2 channel causing increased neuronal excitability in a patient with idiopathic generalized epilepsy." J Neurosci **31**(48): 17327-17337.

DiFrancesco, J. C. and D. DiFrancesco (2015). "Dysfunctional HCN ion channels in neurological diseases." Front Cell Neurosci **6**: 174.

Driscoll, H. E., N. I. Muraro, M. He and R. A. Baines (2013). "Pumilio-2 regulates translation of Nav1.6 to mediate homeostasis of membrane excitability." J Neurosci **33**(23): 9644-9654.

Durstewitz, D. and J. K. Seamans (2002). "The computational role of dopamine D1 receptors in working memory." Neural Netw **15**(4-6): 561-572.

Durstewitz, D. and J. K. Seamans (2008). "The dual-state theory of prefrontal cortex dopamine function with relevance to catechol-o-methyltransferase genotypes and schizophrenia." Biol Psychiatry **64**(9): 739-749.

Durstewitz, D., J. K. Seamans and T. J. Sejnowski (2000). "Dopamine-mediated stabilization of delay-period activity in a network model of prefrontal cortex." J Neurophysiol **83**(3): 1733-1750.

Durstewitz, D., J. K. Seamans and T. J. Sejnowski (2000). "Neurocomputational models of working memory." Nat Neurosci **3 Suppl**: 1184-1191.

Dustrude, E. T., A. Moutal, X. Yang, Y. Wang, M. Khanna and R. Khanna (2016). "Hierarchical CRMP2 posttranslational modifications control NaV1.7 function." Proc Natl Acad Sci U S A **113**(52): E8443-E8452.

Dustrude, E. T., S. M. Wilson, W. Ju, Y. Xiao and R. Khanna (2013). "CRMP2 protein SUMOylation modulates NaV1.7 channel trafficking." J Biol Chem **288**(34): 24316-24331.

Eckermann, K. (2013). "SUMO and Parkinson's disease." Neuromolecular Med **15**(4): 737-759.

Ellwood, I. T., T. Patel, V. Wadia, A. T. Lee, A. T. Liptak, K. J. Bender and V. S. Sohal (2017). "Tonic or Phasic Stimulation of Dopaminergic Projections to Prefrontal Cortex Causes Mice to Maintain or Deviate from Previously Learned Behavioral Strategies." J Neurosci **37**(35): 8315-8329.

Fan, Y., D. Fricker, D. H. Brager, X. Chen, H. C. Lu, R. A. Chitwood and D. Johnston (2005). "Activity-dependent decrease of excitability in rat hippocampal neurons through increases in I(h)." Nat Neurosci **8**(11): 1542-1551.

Fawell, S., J. Seery, Y. Daikh, C. Moore, L. L. Chen, B. Pepinsky and J. Barsoum (1994). "Tat-mediated delivery of heterologous proteins into cells." Proc Natl Acad Sci U S A **91**(2): 664-668.

Feliciangeli, S., S. Bendahhou, G. Sandoz, P. Gounon, M. Reichold, R. Warth, M. Lazdunski, J. Barhanin and F. Lesage (2007). "Does sumoylation control K2P1/TWIK1 background K+ channels?" Cell **130**(3): 563-569.

Feligioni, M., A. Nishimune and J. M. Henley (2009). "Protein SUMOylation modulates calcium influx and glutamate release from presynaptic terminals." Eur J Neurosci **29**(7): 1348-1356.

Floresco, S. B., C. L. Todd and A. A. Grace (2001). "Glutamatergic afferents from the hippocampus to the nucleus accumbens regulate activity of ventral tegmental area dopamine neurons." J Neurosci **21**(13): 4915-4922.

Floresco, S. B., A. R. West, B. Ash, H. Moore and A. A. Grace (2003). "Afferent modulation of dopamine neuron firing differentially regulates tonic and phasic dopamine transmission." Nat Neurosci **6**(9): 968-973.

Flotho, A. and F. Melchior (2013). "Sumoylation: a regulatory protein modification in health and disease." Annu Rev Biochem **82**: 357-385.

Frey, U., H. Matthies, K. G. Reymann and H. Matthies (1991). "The effect of dopaminergic D1 receptor blockade during tetanization on the expression of long-term potentiation in the rat CA1 region in vitro." Neurosci Lett **129**(1): 111-114.

Fukuda, I., A. Ito, G. Hirai, S. Nishimura, H. Kawasaki, H. Saitoh, K. Kimura, M. Sodeoka and M. Yoshida (2009). "Ginkgolic acid inhibits protein SUMOylation by blocking formation of the E1-SUMO intermediate." Chem Biol **16**(2): 133-140.

Furst, O. and N. D'Avanzo (2015). "Isoform dependent regulation of human HCN channels by cholesterol." Sci Rep **5**: 14270.

Girach, F., T. J. Craig, D. L. Rocca and J. M. Henley (2013). "RIM1alpha SUMOylation is required for fast synaptic vesicle exocytosis." Cell Rep **5**(5): 1294-1301.

Goaillard, J. M., A. L. Taylor, D. J. Schulz and E. Marder (2009). "Functional consequences of animal-to-animal variation in circuit parameters." Nat Neurosci **12**(11): 1424-1430.

Goeritz, M. L., Q. Ouyang and R. M. Harris-Warrick (2011). "Localization and function of Ih channels in a small neural network." J Neurophysiol **106**(1): 44-58.

Golowasch, J. (2014). "Ionic Current Variability and Functional Stability in the Nervous System." Bioscience **64**(7): 570-580.

Golowasch, J., M. Casey, L. F. Abbott and E. Marder (1999). "Network stability from activity-dependent regulation of neuronal conductances." Neural Comput **11**(5): 1079-1096.

Goto, Y., S. Otani and A. A. Grace (2007). "The Yin and Yang of dopamine release: a new perspective." Neuropharmacology **53**(5): 583-587.

Grace, A. A. (1991). "Phasic versus tonic dopamine release and the modulation of dopamine system responsivity: a hypothesis for the etiology of schizophrenia." Neuroscience **41**(1): 1-24.

Grace, A. A. (2000). "The tonic/phasic model of dopamine system regulation and its implications for understanding alcohol and psychostimulant craving." Addiction **95 Suppl 2**: S119-128.

Grace, A. A. (2016). "Dysregulation of the dopamine system in the pathophysiology of schizophrenia and depression." Nat Rev Neurosci **17**(8): 524-532.

Grace, A. A. and B. S. Bunney (1983). "Intracellular and extracellular electrophysiology of nigral dopaminergic neurons--1. Identification and characterization." Neuroscience **10**(2): 301-315.

Grace, A. A. and B. S. Bunney (1984). "The control of firing pattern in nigral dopamine neurons: single spike firing." J Neurosci **4**(11): 2866-2876.

Guerra de Souza, A. C., R. D. Prediger and H. Cimarosti (2016). "SUMO-regulated mitochondrial function in Parkinson's disease." J Neurochem **137**(5): 673-686.

Gurden, H., M. Takita and T. M. Jay (2000). "Essential role of D1 but not D2 receptors in the NMDA receptor-dependent long-term potentiation at hippocampal-prefrontal cortex synapses in vivo." J Neurosci **20**(22): RC106.

Gurden, H., J. P. Tassin and T. M. Jay (1999). "Integrity of the mesocortical dopaminergic system is necessary for complete expression of in vivo hippocampal-prefrontal cortex long-term potentiation." Neuroscience **94**(4): 1019-1027.

Hammond, C., H. Bergman and P. Brown (2007). "Pathological synchronization in Parkinson's disease: networks, models and treatments." Trends Neurosci **30**(7): 357-364.

Han, Y., Y. Noam, A. S. Lewis, J. J. Gallagher, W. J. Wadman, T. Z. Baram and D. M. Chetkovich (2011). "Trafficking and gating of hyperpolarization-activated cyclic nucleotide-gated channels are regulated by interaction with tetratricopeptide repeat-containing Rab8b-interacting protein (TRIP8b) and cyclic AMP at distinct sites." J Biol Chem **286**(23): 20823-20834.

Hardel, N., N. Harmel, G. Zolles, B. Fakler and N. Klocker (2008). "Recycling endosomes supply cardiac pacemaker channels for regulated surface expression." Cardiovasc Res **79**(1): 52-60.

Harris-Warrick, R. M., L. M. Coniglio, R. M. Levini, S. Gueron and J. Guckenheimer (1995). "Dopamine modulation of two subthreshold currents produces phase shifts in activity of an identified motoneuron." J Neurophysiol **74**(4): 1404-1420.

Harris-Warrick, R. M., B. R. Johnson, J. H. Peck, P. Kloppenburg, A. Ayali and J. Skarbinski (1998). "Distributed effects of dopamine modulation in the crustacean pyloric network." Ann N Y Acad Sci **860**: 155-167.

Hay, R. T. (2005). "SUMO: a history of modification." Mol Cell **18**(1): 1-12.

Hay, R. T. (2013). "Decoding the SUMO signal." Biochem Soc Trans **41**(2): 463-473.

He, C., F. Chen, B. Li and Z. Hu (2014). "Neurophysiology of HCN channels: from cellular functions to multiple regulations." Prog Neurobiol **112**: 1-23.

Heckers, S. (2001). "Neuroimaging studies of the hippocampus in schizophrenia." Hippocampus **11**(5): 520-528.

Hedrich, U. B., F. Diehl and W. Stein (2011). "Gastric and pyloric motor pattern control by a modulatory projection neuron in the intact crab Cancer pagurus." J Neurophysiol **105**(4): 1671-1680.

Hendriks, I. A., R. C. D'Souza, J. G. Chang, M. Mann and A. C. Vertegaal (2015). "System-wide identification of wild-type SUMO-2 conjugation sites." Nat Commun **6**: 7289.

Hendriks, I. A. and A. C. Vertegaal (2016). "A comprehensive compilation of SUMO proteomics." Nat Rev Mol Cell Biol **17**(9): 581-595.

Henley, J. M., T. J. Craig and K. A. Wilkinson (2014). "Neuronal SUMOylation: mechanisms, physiology, and roles in neuronal dysfunction." Physiol Rev **94**(4): 1249-1285.

Hickey, C. M., N. R. Wilson and M. Hochstrasser (2012). "Function and regulation of SUMO proteases." Nat Rev Mol Cell Biol **13**(12): 755-766.

Hietakangas, V., J. Anckar, H. A. Blomster, M. Fujimoto, J. J. Palvimo, A. Nakai and L. Sistonen (2006). "PDSM, a motif for phosphorylation-dependent SUMO modification." Proc Natl Acad Sci U S A **103**(1): 45-50.

Hoppe, J. B., C. G. Salbego and H. Cimarosti (2015). "SUMOylation: Novel Neuroprotective Approach for Alzheimer's Disease?" Aging Dis **6**(5): 322-330.

Huang, Y. Y., E. Simpson, C. Kellendonk and E. R. Kandel (2004). "Genetic evidence for the bidirectional modulation of synaptic plasticity in the prefrontal cortex by D1 receptors." Proc Natl Acad Sci U S A **101**(9): 3236-3241.

Hudson, A. E. and A. A. Prinz (2010). "Conductance ratios and cellular identity." PLoS Comput Biol **6**(7): e1000838.

Hutcheon, B. and Y. Yarom (2000). "Resonance, oscillation and the intrinsic frequency preferences of neurons." Trends Neurosci **23**(5): 216-222.

Ishikawa, M., P. Mu, J. T. Moyer, J. A. Wolf, R. M. Quock, N. M. Davies, X. T. Hu, O. M. Schluter and Y. Dong (2009). "Homeostatic synapse-driven membrane plasticity in nucleus accumbens neurons." J Neurosci **29**(18): 5820-5831.

Ito, K., T. Haga, J. Lameh and W. Sadee (1999). "Sequestration of dopamine D2 receptors depends on coexpression of G-protein-coupled receptor kinases 2 or 5." Eur J Biochem **260**(1): 112-119.

Jaafari, N., F. A. Konopacki, T. F. Owen, S. Kantamneni, P. Rubin, T. J. Craig, K. A. Wilkinson and J. M. Henley (2013). "SUMOylation is required for glycine-induced increases in AMPA receptor surface expression (ChemLTP) in hippocampal neurons." PLoS One **8**(1): e52345.

Jentsch, S. and I. Psakhye (2013). "Control of nuclear activities by substrate-selective and protein-group SUMOylation." Annu Rev Genet **47**: 167-186.

Johnson, B. R., J. M. Brown, M. D. Kvarta, J. Y. Lu, L. R. Schneider, F. Nadim and R. M. Harris-Warrick (2011). "Differential modulation of synaptic strength and timing regulate synaptic efficacy in a motor network." J Neurophysiol **105**(1): 293-304.

Johnson, B. R. and R. M. Harris-Warrick (1997). "Amine modulation of glutamate responses from pyloric motor neurons in lobster stomatogastric ganglion." J Neurophysiol **78**(6): 3210-3221.

Johnson, B. R., P. Kloppenburg and R. M. Harris-Warrick (2003). "Dopamine modulation of calcium currents in pyloric neurons of the lobster stomatogastric ganglion." J Neurophysiol **90**(2): 631-643.

Johnson, B. R., J. H. Peck and R. M. Harris-Warrick (1995). "Distributed amine modulation of graded chemical transmission in the pyloric network of the lobster stomatogastric ganglion." J Neurophysiol **74**(1): 437-452.

Jung, S., L. N. Warner, J. Pitsch, A. J. Becker and N. P. Poolos (2011). "Rapid loss of dendritic HCN channel expression in hippocampal pyramidal neurons following status epilepticus." J Neurosci **31**(40): 14291-14295.

Justice, J. B., Jr. (1993). "Quantitative microdialysis of neurotransmitters." J Neurosci Methods **48**(3): 263-276.

Kamitani, T., H. P. Nguyen, K. Kito, T. Fukuda-Kamitani and E. T. Yeh (1998). "Covalent modification of PML by the sentrin family of ubiquitin-like proteins." J Biol Chem **273**(6): 3117-3120.

Kase, D. and K. Imoto (2012). "The Role of HCN Channels on Membrane Excitability in the Nervous System." J Signal Transduct **2012**: 619747.

Keefe, K. A., M. J. Zigmond and E. D. Abercrombie (1993). "In vivo regulation of extracellular dopamine in the neostriatum: influence of impulse activity and local excitatory amino acids." J Neural Transm Gen Sect **91**(2-3): 223-240.

Khorkova, O. and J. Golowasch (2007). "Neuromodulators, not activity, control coordinated expression of ionic currents." J Neurosci **27**(32): 8709-8718.

Kiehn, O. and R. M. Harris-Warrick (1992). "5-HT modulation of hyperpolarization-activated inward current and calcium-dependent outward current in a crustacean motor neuron." J Neurophysiol **68**(2): 496-508.

Kim, E. Z., J. Vienne, M. Rosbash and L. C. Griffith (2017). "Nonreciprocal homeostatic compensation in Drosophila potassium channel mutants." J Neurophysiol **117**(6): 2125-2136.

Kim, K. M., K. J. Valenzano, S. R. Robinson, W. D. Yao, L. S. Barak and M. G. Caron (2001). "Differential regulation of the dopamine D2 and D3 receptors by G protein-coupled receptor kinases and beta-arrestins." J Biol Chem **276**(40): 37409-37414.

Kimura, K., J. Kitano, Y. Nakajima and S. Nakanishi (2004). "Hyperpolarization-activated, cyclic nucleotide-gated HCN2 cation channel forms a protein assembly with multiple neuronal scaffold proteins in distinct modes of protein-protein interaction." Genes Cells **9**(7): 631-640.

Kirchheim, F., S. Tinnes, C. A. Haas, M. Stegen and J. Wolfart (2013). "Regulation of action potential delays via voltage-gated potassium Kv1.1 channels in dentate granule cells during hippocampal epilepsy." Front Cell Neurosci **7**: 248.

Kloppenburg, P., R. M. Levini and R. M. Harris-Warrick (1999). "Dopamine modulates two potassium currents and inhibits the intrinsic firing properties of an identified motor neuron in a central pattern generator network." J Neurophysiol **81**(1): 29-38.

Kloppenburg, P., W. R. Zipfel, W. W. Webb and R. M. Harris-Warrick (2007). "Heterogeneous effects of dopamine on highly localized, voltage-induced Ca2+ accumulation in identified motoneurons." J Neurophysiol **98**(5): 2910-2917.

Konopacki, F. A., N. Jaafari, D. L. Rocca, K. A. Wilkinson, S. Chamberlain, P. Rubin, S. Kantamneni, J. R. Mellor and J. M. Henley (2011). "Agonist-induced PKC phosphorylation regulates GluK2 SUMOylation and kainate receptor endocytosis." Proc Natl Acad Sci U S A **108**(49): 19772-19777.

Krenz, W. D., R. M. Hooper, A. R. Parker, A. A. Prinz and D. J. Baro (2013). "Activation of high and low affinity dopamine receptors generates a closed loop that maintains a conductance ratio and its activity correlate." Front Neural Circuits **7**: 169.

Krenz, W. D., A. R. Parker, E. Rodgers and D. J. Baro (2015). "Monoaminergic tone supports conductance correlations and stabilizes activity features in pattern generating neurons of the lobster, Panulirus interruptus." Front Neural Circuits **9**: 63.

Krenz, W. D., A. R. Parker, E. W. Rodgers and D. J. Baro (2014). "Dopaminergic tone persistently regulates voltage-gated ion current densities through the D1R-PKA axis, RNA polymerase II transcription, RNAi, mTORC1, and translation." Front Cell Neurosci **8**: 39.

Krenz, W. D., E. W. Rodgers and D. J. Baro (2015). "Tonic 5nM DA stabilizes neuronal output by enabling bidirectional activity-dependent regulation of the hyperpolarization activated current via PKA and calcineurin." PLoS One **10**(2): e0117965.

Kroener, S., L. J. Chandler, P. E. Phillips and J. K. Seamans (2009). "Dopamine modulates persistent synaptic activity and enhances the signal-to-noise ratio in the prefrontal cortex." PLoS One **4**(8): e6507.

Lane, B. J., P. Samarth, J. L. Ransdell, S. S. Nair and D. J. Schulz (2016). "Synergistic plasticity of intrinsic conductance and electrical coupling restores synchrony in an intact motor network." Elife **5**.

Lee, J., Y. Lee, M. J. Lee, E. Park, S. H. Kang, C. H. Chung, K. H. Lee and K. Kim (2008). "Dual modification of BMAL1 by SUMO2/3 and ubiquitin promotes circadian activation of the CLOCK/BMAL1 complex." Mol Cell Biol **28**(19): 6056-6065.

Lee, L., E. Dale, A. Staniszewski, H. Zhang, F. Saeed, M. Sakurai, M. Fa, I. Orozco, F. Michelassi, N. Akpan, H. Lehrer and O. Arancio (2014). "Regulation of synaptic plasticity and cognition by SUMO in normal physiology and Alzheimer's disease." Sci Rep **4**: 7190.

LeMasson, G., E. Marder and L. F. Abbott (1993). "Activity-dependent regulation of conductances in model neurons." Science **259**(5103): 1915-1917.

Lewis, A. S., E. Schwartz, C. S. Chan, Y. Noam, M. Shin, W. J. Wadman, D. J. Surmeier, T. Z. Baram, R. L. Macdonald and D. M. Chetkovich (2009). "Alternatively spliced isoforms of TRIP8b differentially control h channel trafficking and function." J Neurosci **29**(19): 6250-6265.

Lin, C. H., S. Y. Liu and E. H. Lee (2016). "SUMO modification of Akt regulates global SUMOylation and substrate SUMOylation specificity through Akt phosphorylation of Ubc9 and SUMO1." Oncogene **35**(5): 595-607.

Linsdell, P. and W. J. Moody (1994). "Na+ channel mis-expression accelerates K+ channel development in embryonic Xenopus laevis skeletal muscle." J Physiol **480 (Pt 3)**: 405-410.

Lisman, J., A. A. Grace and E. Duzel (2011). "A neoHebbian framework for episodic memory; role of dopamine-dependent late LTP." Trends Neurosci **34**(10): 536-547.

Lodge, D. J. and A. A. Grace (2006). "The hippocampus modulates dopamine neuron responsivity by regulating the intensity of phasic neuron activation." Neuropsychopharmacology **31**(7): 1356-1361.

Lokwan, S. J., P. G. Overton, M. S. Berry and D. Clark (1999). "Stimulation of the pedunculopontine tegmental nucleus in the rat produces burst firing in A9 dopaminergic neurons." Neuroscience **92**(1): 245-254.

Loriol, C., F. Casse, A. Khayachi, G. Poupon, M. Chafai, E. Deval, C. Gwizdek and S. Martin (2014). "mGlu5 receptors regulate synaptic sumoylation via a transient PKC-dependent diffusional trapping of Ubc9 into spines." Nat Commun **5**: 5113.

Loriol, C., A. Khayachi, G. Poupon, C. Gwizdek and S. Martin (2013). "Activity-dependent regulation of the sumoylation machinery in rat hippocampal neurons." Biol Cell **105**(1): 30-45.

Lu, H., B. Liu, S. You, Q. Xue, F. Zhang, J. Cheng and B. Yu (2009). "The activity-dependent stimuli increase SUMO modification in SHSY5Y cells." Biochem Biophys Res Commun **390**(3): 872-876.

Ludwig, A., T. Budde, J. Stieber, S. Moosmang, C. Wahl, K. Holthoff, A. Langebartels, C. Wotjak, T. Munsch, X. Zong, S. Feil, R. Feil, M. Lancel, K. R. Chien, A. Konnerth, H. C. Pape, M. Biel and F. Hofmann (2003). "Absence epilepsy and sinus dysrhythmia in mice lacking the pacemaker channel HCN2." EMBO J **22**(2): 216-224.

Luo, J., E. Ashikaga, P. P. Rubin, M. J. Heimann, K. L. Hildick, P. Bishop, F. Girach, F. Josa-Prado, L. T. Tang, R. E. Carmichael, J. M. Henley and K. A. Wilkinson (2013). "Receptor trafficking and the regulation of synaptic plasticity by SUMO." Neuromolecular Med **15**(4): 692-706.

MacLean, J. N., Y. Zhang, M. L. Goeritz, R. Casey, R. Oliva, J. Guckenheimer and R. M. Harris-Warrick (2005). "Activity-independent coregulation of IA and Ih in rhythmically active neurons." J Neurophysiol **94**(5): 3601-3617.

MacLean, J. N., Y. Zhang, B. R. Johnson and R. M. Harris-Warrick (2003). "Activity-independent homeostasis in rhythmically active neurons." Neuron **37**(1): 109-120.

Mahajan, R., C. Delphin, T. Guan, L. Gerace and F. Melchior (1997). "A small ubiquitin-related polypeptide involved in targeting RanGAP1 to nuclear pore complex protein RanBP2." Cell **88**(1): 97-107.

Makhnevych, T., Y. Sydorskyy, X. Xin, T. Srikumar, F. J. Vizeacoumar, S. M. Jeram, Z. Li, S. Bahr, B. J. Andrews, C. Boone and B. Raught (2009). "Global map of SUMO function revealed by protein-protein interaction and genetic networks." Mol Cell **33**(1): 124-135.

Marder, E. and D. Bucher (2007). "Understanding circuit dynamics using the stomatogastric nervous system of lobsters and crabs." Annu Rev Physiol **69**: 291-316.

Marder, E., M. L. Goeritz and A. G. Otopalik (2015). "Robust circuit rhythms in small circuits arise from variable circuit components and mechanisms." Curr Opin Neurobiol **31**: 156-163.

Martin, S., A. Nishimune, J. R. Mellor and J. M. Henley (2007). "SUMOylation regulates kainate-receptor-mediated synaptic transmission." Nature **447**(7142): 321-325.

Matsuda, Y., A. Marzo and S. Otani (2006). "The presence of background dopamine signal converts long-term synaptic depression to potentiation in rat prefrontal cortex." J Neurosci **26**(18): 4803-4810.

Matunis, M. J., E. Coutavas and G. Blobel (1996). "A novel ubiquitin-like modification modulates the partitioning of the Ran-GTPase-activating protein RanGAP1 between the cytosol and the nuclear pore complex." J Cell Biol **135**(6 Pt 1): 1457-1470.

Medoff, D. R., H. H. Holcomb, A. C. Lahti and C. A. Tamminga (2001). "Probing the human hippocampus using rCBF: contrasts in schizophrenia." Hippocampus **11**(5): 543-550.

Mendes, A. V., C. P. Grou, J. E. Azevedo and M. P. Pinto (2016). "Evaluation of the activity and substrate specificity of the human SENP family of SUMO proteases." Biochim Biophys Acta **1863**(1): 139-147.

Mitchell, G. S. and S. M. Johnson (2003). "Neuroplasticity in respiratory motor control." J Appl Physiol (1985) **94**(1): 358-374.

Much, B., C. Wahl-Schott, X. Zong, A. Schneider, L. Baumann, S. Moosmang, A. Ludwig and M. Biel (2003). "Role of subunit heteromerization and N-linked glycosylation in the formation of functional hyperpolarization-activated cyclic nucleotide-gated channels." J Biol Chem **278**(44): 43781-43786.

Mukhopadhyay, D. and M. Dasso (2007). "Modification in reverse: the SUMO proteases." Trends Biochem Sci **32**(6): 286-295.

Nair, R. R., S. Patil, A. Tiron, T. Kanhema, D. Panja, L. Schiro, K. Parobczak, G. Wilczynski and C. R. Bramham (2017). "Dynamic Arc SUMOylation and Selective Interaction with F-Actin-Binding Protein Drebrin A in LTP Consolidation In Vivo." Front Synaptic Neurosci **9**: 8.

Nakamura, Y., X. Shi, T. Numata, Y. Mori, R. Inoue, C. Lossin, T. Z. Baram and S. Hirose (2013). "Novel HCN2 mutation contributes to febrile seizures by shifting the channel's kinetics in a temperature-dependent manner." PLoS One **8**(12): e80376.

Nayak, A. and S. Muller (2014). "SUMO-specific proteases/isopeptidases: SENPs and beyond." Genome Biol **15**(7): 422.

Nazzari, H., D. Angoli, S. S. Chow, G. Whitaker, L. Leclair, E. McDonald, V. Macri, K. Zahynacz, V. Walker and E. A. Accili (2008). "Regulation of cell surface expression of functional pacemaker channels by a motif in the B-helix of the cyclic nucleotide-binding domain." Am J Physiol Cell Physiol **295**(3): C642-652.

Nirogi, R., P. Komarneni, V. Kandikere, R. Boggavarapu, G. Bhyrapuneni, V. Benade and S. Gorentla (2013). "A sensitive and selective quantification of catecholamine neurotransmitters in rat microdialysates by pre-column dansyl chloride derivatization using liquid chromatography-tandem mass spectrometry." J Chromatogr B Analyt Technol Biomed Life Sci **913-914**: 41-47.

Noam, Y., Q. Zha, L. Phan, R. L. Wu, D. M. Chetkovich, W. J. Wadman and T. Z. Baram (2010). "Trafficking and surface expression of hyperpolarization-activated cyclic nucleotide-gated channels in hippocampal neurons." J Biol Chem **285**(19): 14724-14736.

O'Brien, R. J., S. Kamboj, M. D. Ehlers, K. R. Rosen, G. D. Fischbach and R. L. Huganir (1998). "Activity-dependent modulation of synaptic AMPA receptor accumulation." Neuron **21**(5): 1067-1078.

O'Leary, T., M. C. van Rossum and D. J. Wyllie (2010). "Homeostasis of intrinsic excitability in hippocampal neurones: dynamics and mechanism of the response to chronic depolarization." J Physiol **588**(Pt 1): 157-170.

O'Leary, T., A. H. Williams, J. S. Caplan and E. Marder (2013). "Correlations in ion channel expression emerge from homeostatic tuning rules." Proc Natl Acad Sci U S A **110**(28): E2645-2654.

O'Leary, T., A. H. Williams, A. Franci and E. Marder (2014). "Cell types, network homeostasis, and pathological compensation from a biologically plausible ion channel expression model." Neuron **82**(4): 809-821.

O'Leary, T. and D. J. Wyllie (2011). "Neuronal homeostasis: time for a change?" J Physiol **589**(Pt 20): 4811-4826.

Ochaba, J., A. M. Monteys, J. G. O'Rourke, J. C. Reidling, J. S. Steffan, B. L. Davidson and L. M. Thompson (2016). "PIAS1 Regulates Mutant Huntingtin Accumulation and Huntington's Disease-Associated Phenotypes In Vivo." Neuron **90**(3): 507-520.

Oginsky, M. F., E. W. Rodgers, M. C. Clark, R. Simmons, W. D. Krenz and D. J. Baro (2010). "D(2) receptors receive paracrine neurotransmission and are consistently targeted to a subset of synaptic structures in an identified neuron of the crustacean stomatogastric nervous system." J Comp Neurol **518**(3): 255-276.

Olypher, A. V. and A. A. Prinz (2010). "Geometry and dynamics of activity-dependent homeostatic regulation in neurons." J Comput Neurosci **28**(3): 361-374.

Otani, S., N. Auclair, J. M. Desce, M. P. Roisin and F. Crepel (1999). "Dopamine receptors and groups I and II mGluRs cooperate for long-term depression induction in rat prefrontal cortex through converging postsynaptic activation of MAP kinases." J Neurosci **19**(22): 9788-9802.

Otani, S., J. Bai and K. Blot (2015). "Dopaminergic modulation of synaptic plasticity in rat prefrontal neurons." Neurosci Bull **31**(2): 183-190.

Otani, S., O. Blond, J. M. Desce and F. Crepel (1998). "Dopamine facilitates long-term depression of glutamatergic transmission in rat prefrontal cortex." Neuroscience **85**(3): 669-676.

Ouyang, Q., M. Goeritz and R. M. Harris-Warrick (2007). "Panulirus interruptus Ih-channel gene PIIH: modification of channel properties by alternative splicing and role in rhythmic activity." J Neurophysiol **97**(6): 3880-3892.

Owesson-White, C. A., M. F. Roitman, L. A. Sombers, A. M. Belle, R. B. Keithley, J. L. Peele, R. M. Carelli and R. M. Wightman (2012). "Sources contributing to the average extracellular concentration of dopamine in the nucleus accumbens." J Neurochem **121**(2): 252-262.

Parker, A. R., M. A. Welch, L. A. Forster, S. M. Tasneem, J. A. Dubhashi and D. J. Baro (2016). "SUMOylation of the Hyperpolarization-Activated Cyclic Nucleotide-Gated Channel 2 Increases Surface Expression and the Maximal Conductance of the Hyperpolarization-Activated Current." Front Mol Neurosci **9**: 168.

Peck, J. H., E. Gaier, E. Stevens, S. Repicky and R. M. Harris-Warrick (2006). "Amine modulation of Ih in a small neural network." J Neurophysiol **96**(6): 2931-2940.

Peck, J. H., S. T. Nakanishi, R. Yaple and R. M. Harris-Warrick (2001). "Amine modulation of the transient potassium current in identified cells of the lobster stomatogastric ganglion." J Neurophysiol **86**(6): 2957-2965.

Peng, I. F. and C. F. Wu (2007). "Drosophila cacophony channels: a major mediator of neuronal Ca2+ currents and a trigger for K+ channel homeostatic regulation." J Neurosci **27**(5): 1072-1081.

Plant, L. D., E. J. Dowdell, I. S. Dementieva, J. D. Marks and S. A. Goldstein (2011). "SUMO modification of cell surface Kv2.1 potassium channels regulates the activity of rat hippocampal neurons." J Gen Physiol **137**(5): 441-454.

Plant, L. D., J. D. Marks and S. A. Goldstein (2016). "SUMOylation of NaV1.2 channels mediates the early response to acute hypoxia in central neurons." Elife **5**.

Pozzi, D., G. Lignani, E. Ferrea, A. Contestabile, F. Paonessa, R. D'Alessandro, P. Lippiello, D. Boido, A. Fassio, J. Meldolesi, F. Valtorta, F. Benfenati and P. Baldelli (2013). "REST/NRSF-mediated intrinsic homeostasis protects neuronal networks from hyperexcitability." EMBO J **32**(22): 2994-3007.

Proenza, C., N. Tran, D. Angoli, K. Zahynacz, P. Balcar and E. A. Accili (2002). "Different roles for the cyclic nucleotide binding domain and amino terminus in assembly and expression of hyperpolarization-activated, cyclic nucleotide-gated channels." J Biol Chem **277**(33): 29634-29642.

Qi, Y., J. Wang, V. C. Bomben, D. P. Li, S. R. Chen, H. Sun, Y. Xi, J. G. Reed, J. Cheng, H. L. Pan, J. L. Noebels and E. T. Yeh (2014). "Hyper-SUMOylation of the Kv7 potassium channel diminishes the M-current leading to seizures and sudden death." Neuron **83**(5): 1159-1171.

Ransdell, J. L., S. Temporal, N. L. West, M. L. Leyrer and D. J. Schulz (2013). "Characterization of inward currents and channels underlying burst activity in motoneurons of crab cardiac ganglion." J Neurophysiol **110**(1): 42-54.

Reynolds, J. N., B. I. Hyland and J. R. Wickens (2001). "A cellular mechanism of reward-related learning." Nature **413**(6851): 67-70.

Rice, M. E., J. C. Patel and S. J. Cragg (2011). "Dopamine release in the basal ganglia." Neuroscience **198**: 112-137.

Robinson, B. G., J. R. Bunzow, J. B. Grimm, L. D. Lavis, J. T. Dudman, J. Brown, K. A. Neve and J. T. Williams (2017). "Desensitized D2 autoreceptors are resistant to trafficking." Sci Rep **7**(1): 4379.

Robinson, R. B. and S. A. Siegelbaum (2003). "Hyperpolarization-activated cation currents: from molecules to physiological function." Annu Rev Physiol **65**: 453-480.

Rodgers, E. W., J. J. Fu, W. D. Krenz and D. J. Baro (2011). "Tonic nanomolar dopamine enables an activity-dependent phase recovery mechanism that persistently alters the maximal conductance of the hyperpolarization-activated current in a rhythmically active neuron." J Neurosci **31**(45): 16387-16397.

Rodgers, E. W., W. D. Krenz and D. J. Baro (2011). "Tonic dopamine induces persistent changes in the transient potassium current through translational regulation." J Neurosci **31**(37): 13046-13056.

Rodgers, E. W., W. D. Krenz, X. Jiang, L. Li and D. J. Baro (2013). "Dopaminergic tone regulates transient potassium current maximal conductance through a translational mechanism requiring D1Rs, cAMP/PKA, Erk and mTOR." BMC Neurosci **14**: 143.

Rodriguez, M. S., C. Dargemont and R. T. Hay (2001). "SUMO-1 conjugation in vivo requires both a consensus modification motif and nuclear targeting." J Biol Chem **276**(16): 12654-12659.

Sampson, D. A., M. Wang and M. J. Matunis (2001). "The small ubiquitin-like modifier-1 (SUMO-1) consensus sequence mediates Ubc9 binding and is essential for SUMO-1 modification." J Biol Chem **276**(24): 21664-21669.

Santoro, B., B. J. Wainger and S. A. Siegelbaum (2004). "Regulation of HCN channel surface expression by a novel C-terminal protein-protein interaction." J Neurosci **24**(47): 10750-10762.

Schorova, L. and S. Martin (2016). "Sumoylation in Synaptic Function and Dysfunction." Front Synaptic Neurosci **8**: 9.

Schultz, W. (2007). "Multiple dopamine functions at different time courses." Annu Rev Neurosci **30**: 259-288.

Schulz, D. J., J. M. Goaillard and E. E. Marder (2007). "Quantitative expression profiling of identified neurons reveals cell-specific constraints on highly variable levels of gene expression." Proc Natl Acad Sci U S A **104**(32): 13187-13191.

Seifert, A., P. Schofield, G. J. Barton and R. T. Hay (2015). "Proteotoxic stress reprograms the chromatin landscape of SUMO modification." Sci Signal **8**(384): rs7.

Shah, M. M. (2014). "Cortical HCN channels: function, trafficking and plasticity." J Physiol **592**(13): 2711-2719.

Shah, M. M., A. E. Anderson, V. Leung, X. Lin and D. Johnston (2004). "Seizure-induced plasticity of h channels in entorhinal cortical layer III pyramidal neurons." Neuron **44**(3): 495-508.

Sikstrom, S. and G. Soderlund (2007). "Stimulus-dependent dopamine release in attention-deficit/hyperactivity disorder." Psychol Rev **114**(4): 1047-1075.

Smith, T., M. Al Otaibi, J. Sathish and L. Djouhri (2015). "Increased expression of HCN2 channel protein in L4 dorsal root ganglion neurons following axotomy of L5- and inflammation of L4-spinal nerves in rats." Neuroscience **295**: 90-102.

Soofi, W., S. Archila and A. A. Prinz (2012). "Co-variation of ionic conductances supports phase maintenance in stomatogastric neurons." J Comput Neurosci **33**(1): 77-95.

Steinert, J. R., S. W. Robinson, H. Tong, M. D. Haustein, C. Kopp-Scheinpflug and I. D. Forsythe (2011). "Nitric oxide is an activity-dependent regulator of target neuron intrinsic excitability." Neuron **71**(2): 291-305.

Su, Y. F., T. Yang, H. Huang, L. F. Liu and J. Hwang (2012). "Phosphorylation of Ubc9 by Cdk1 enhances SUMOylation activity." PLoS One **7**(4): e34250.

Sun, H., L. Lu, Y. Zuo, Y. Wang, Y. Jiao, W. Z. Zeng, C. Huang, M. X. Zhu, G. W. Zamponi, T. Zhou, T. L. Xu, J. Cheng and Y. Li (2014). "Kainate receptor activation induces glycine receptor endocytosis through PKC deSUMOylation." Nat Commun **5**: 4980.

Suzuki, T., A. Ichiyama, H. Saitoh, T. Kawakami, M. Omata, C. H. Chung, M. Kimura, N. Shimbara and K. Tanaka (1999). "A new 30-kDa ubiquitin-related SUMO-1 hydrolase from bovine brain." J Biol Chem **274**(44): 31131-31134.

Swensen, A. M. and B. P. Bean (2005). "Robustness of burst firing in dissociated purkinje neurons with acute or long-term reductions in sodium conductance." J Neurosci **25**(14): 3509-3520.

Temporal, S., M. Desai, O. Khorkova, G. Varghese, A. Dai, D. J. Schulz and J. Golowasch (2012). "Neuromodulation independently determines correlated channel expression and conductance levels in motor neurons of the stomatogastric ganglion." J Neurophysiol **107**(2): 718-727.

Temporal, S., K. M. Lett and D. J. Schulz (2014). "Activity-dependent feedback regulates correlated ion channel mRNA levels in single identified motor neurons." Curr Biol **24**(16): 1899-1904.

Tierney, A. J. and R. M. Harris-Warrick (1992). "Physiological role of the transient potassium current in the pyloric circuit of the lobster stomatogastric ganglion." J Neurophysiol **67**(3): 599-609.

Tran, N., C. Proenza, V. Macri, F. Petigara, E. Sloan, S. Samler and E. A. Accili (2002). "A conserved domain in the NH2 terminus important for assembly and functional expression of pacemaker channels." J Biol Chem **277**(46): 43588-43592.

Turrigiano, G. (2011). "Too many cooks? Intrinsic and synaptic homeostatic mechanisms in cortical circuit refinement." Annu Rev Neurosci **34**: 89-103.

Turrigiano, G., L. F. Abbott and E. Marder (1994). "Activity-dependent changes in the intrinsic properties of cultured neurons." Science **264**(5161): 974-977.

Ulens, C. and S. A. Siegelbaum (2003). "Regulation of hyperpolarization-activated HCN channels by cAMP through a gating switch in binding domain symmetry." Neuron **40**(5): 959-970.

Um, J. W. and K. C. Chung (2006). "Functional modulation of parkin through physical interaction with SUMO-1." J Neurosci Res **84**(7): 1543-1554.

van Welie, I., J. A. van Hooft and W. J. Wadman (2004). "Homeostatic scaling of neuronal excitability by synaptic modulation of somatic hyperpolarization-activated Ih channels." Proc Natl Acad Sci U S A **101**(14): 5123-5128.

van Zessen, R., J. L. Phillips, E. A. Budygin and G. D. Stuber (2012). "Activation of VTA GABA neurons disrupts reward consumption." Neuron **73**(6): 1184-1194.

Wahl-Schott, C. and M. Biel (2009). "HCN channels: structure, cellular regulation and physiological function." Cell Mol Life Sci **66**(3): 470-494.

Wang, J., S. Chen and S. A. Siegelbaum (2001). "Regulation of hyperpolarization-activated HCN channel gating and cAMP modulation due to interactions of COOH terminus and core transmembrane regions." J Gen Physiol **118**(3): 237-250.

Watts, F. Z. (2013). "Starting and stopping SUMOylation. What regulates the regulator?" Chromosoma **122**(6): 451-463.

Weaver, A. L. and S. L. Hooper (2003). "Follower neurons in lobster (Panulirus interruptus) pyloric network regulate pacemaker period in complementary ways." J Neurophysiol **89**(3): 1327-1338.

Welch, M. A., L. A. Forster and D. J. Baro SUMOylation of the mouse voltage-gated potassium channel Kv4.2 decreases the maximal conductance of the A-type potassium current, IA. Washinton, DC: Society for Neuroscience, Program No. 375.11, 2017 Neuroscience Meeting Planner. **Online**.

Yasugi, T. and P. M. Howley (1996). "Identification of the structural and functional human homolog of the yeast ubiquitin conjugating enzyme UBC9." Nucleic Acids Res **24**(11): 2005-2010.

Yeh, E. T. (2009). "SUMOylation and De-SUMOylation: wrestling with life's processes." J Biol Chem **284**(13): 8223-8227.

Zagotta, W. N., N. B. Olivier, K. D. Black, E. C. Young, R. Olson and E. Gouaux (2003). "Structural basis for modulation and agonist specificity of HCN pacemaker channels." Nature **425**(6954): 200-205.

Zenke, F., W. Gerstner and S. Ganguli (2017). "The temporal paradox of Hebbian learning and homeostatic plasticity." Curr Opin Neurobiol **43**: 166-176.

Zha, Q., A. L. Brewster, C. Richichi, R. A. Bender and T. Z. Baram (2008). "Activity-dependent heteromerization of the hyperpolarization-activated, cyclic-nucleotide gated (HCN) channels: role of N-linked glycosylation." J Neurochem **105**(1): 68-77.

Zhang, H., E. W. Rodgers, W. D. Krenz, M. C. Clark and D. J. Baro (2010). "Cell specific dopamine modulation of the transient potassium current in the pyloric network by the canonical D1 receptor signal transduction cascade." J Neurophysiol **104**(2): 873-884.

Zhang, Y., R. Oliva, G. Gisselmann, H. Hatt, J. Guckenheimer and R. M. Harris-Warrick (2003). "Overexpression of a hyperpolarization-activated cation current (Ih) channel gene modifies the firing activity of identified motor neurons in a small neural network." J Neurosci **23**(27): 9059-9067.

Zhao, S. and J. Golowasch (2012). "Ionic current correlations underlie the global tuning of large numbers of neuronal activity attributes." J Neurosci **32**(39): 13380-13388.

Zhou, L., N. B. Olivier, H. Yao, E. C. Young and S. A. Siegelbaum (2004). "A conserved tripeptide in CNG and HCN channels regulates ligand gating by controlling C-terminal oligomerization." Neuron **44**(5): 823-834.

APPENDICES

Curriculum Vitae

Research Interests

1 – Homeostatic mechanisms regulating ionic currents
2 – The role of tonic DA in neuronal network stabilization
3 – SUMO regulation of ion channels

Methods of Independent Expertise

Tissue culture and transfection, whole cell patch clamping, western blotting, immunoprecipitation, Stomatogastric Ganglion (STG) dissection and isolation from lobster, Two Electrode Voltage Clamp (TEVC) recordings, dye filling and immunohistochemistry of STG whole mount preparation, confocal imaging, molecular cloning, peptide synthesis

Education

Degree: Doctorate of Philosophy: **Advisor: Deborah Baro**	Biology	Georgia State University	(2010-2017)
Degree: Bachelor of Science: **Advisor: Bagie George**	Biology	Georgia Gwinnett College	(2007-2010)

Primary Publications

Parker, A. R., Welch, M. A., Forster, L. A., Tasneem, S. M., J. A. Dubhashi, J. A. and Baro, D. J. (2016). "SUMOylation of the Hyperpolarization-Activated Cyclic Nucleotide-Gated Channel 2 Increases Surface Expression and the Maximal Conductance of the Hyperpolarization-Activated Current." Front Mol Neurosci 9: 168.

Krenz, W. D., **Parker, A. R.**, Rodgers, E. W. and Baro, D. J. (2015). "Monoaminergic tone supports conductance correlations and stabilizes activity features in pattern generating neurons of the lobster, Panulirus interruptus." Front Neural Circuits 9: 63.

Krenz, W. D., **Parker, A. R.**, Rodgers, E. W. and Baro, D. J. (2014). "Dopaminergic tone persistently regulates voltage-gated ion current densities through the D1R-PKA axis, RNA polymerase II transcription, RNAi, mTORC1, and translation." Front Cell Neurosci 8: 39.

Krenz, W. D., Hooper, R. M., **Parker, A. R.**, Prinz A. A. and Baro D. J. (2013). "Activation of high and low affinity dopamine receptors generates a closed loop that maintains a conductance ratio and its activity correlate." Front Neural Circuits 7: 169.

Posters and Presentations

Welch, M. A., Forster, L. A., **Parker, A. R.**, Baro, D. J. "Regulation of mouse HCN2 channel surface expression through SUMO post-translational modification" Brains and Behavior Retreat, Atlanta, Ga. 2017

Parker, A. R., Baro, D. J. "Tonic 5nM dopamine (DA) permits and abolishes activity-dependent regulation of the hyperpolarization-activated (I_h) and transient potassium (I_A) currents, respectively, in the lateral pyloric neuron (LP), a component of the pyloric circuit of the spiny lobster, *Panulirus interruptus*" Brains and Behavior Retreat, Atlanta, Ga. 2017

Welch, M. A., Forster, L. A., **Parker, A. R.**, Baro, D. J. "Regulation of mouse HCN2 channel surface expression through SUMO post-translational modification" Society for Neuroscience Conference, San Diego, CA. 2016

Parker, A. R., Baro, D. J. "Tonic 5nM dopamine (DA) permits and abolishes activity-dependent regulation of the hyperpolarization-activated (I_h) and transient potassium (I_A) currents, respectively, in the lateral pyloric neuron (LP), a component of the pyloric circuit of the spiny lobster, *Panulirus interruptus*" Society for Neuroscience Conference, San Diego, CA. 2016

Parker, A. R., Baro, D. J. "SUMOylation mediates dopamine (DA)-enabled, activity-dependent regulation of the hyperpolarization-activated current (I_h)" Brains and Behavior Retreat, Atlanta, Ga. 2016

Parker, A. R., Baro, D. J. "SUMOylation mediates dopamine (DA)-enabled, activity-dependent regulation of the hyperpolarization-activated current (I_h)" Society for Neuroscience Conference, Chicago, IL. 2015

Parker, A. R., Krenz, W.-D. C., Baro, D. J. "Dopamine enabled, activity-dependent, bi-directional regulation of the hyperpolarization-activated current by protein kinase A (PKA) and calcineurin" Brains and Behavior Retreat, Atlanta, Ga. 2015

Parker, A. R., Krenz, W.-D. C., Baro, D. J. "Dopamine enabled, activity-dependent, bi-directional regulation of the hyperpolarization-activated current by protein kinase A (PKA) and calcineurin" Society for Neuroscience, Washington D.C. 2014

Parker A. R., Krenz W.-D.C., Rodgers E. W., and Baro D. J. "Dopamine-Enabled Homeostats Act to Maintain Conductance Ratios" Brains and Behavior Retreat, Atlanta, Ga. 2014
Fu, J. J., Krenz, W.-D. C., **Parker, A.R.**, Rodgers E. W., Baro D. J. "Distinct Functions of Tonic and Phasic Dopamine Modulation", Brains and Behavior Retreat, Atlanta, GA, 2013

Fu, J. J., Krenz, W.-D. C., **Parker, A.R.**, Rodgers E. W., Baro D. J. A Potential "Role for miRNA in a Dopamine Enabled Homeostatic Mechanism", Brains and Behavior Retreat, Atlanta, GA, 2012

Awards

Brains & Behavior Fellowship. *Georgia State University*. 2014- present

Teaching

BIO 1104: Introductory Biology Lab. *Georgia State University*. 2013-present